

DEVELOPMENT OF HIGH TEMPERATURE VACUUM BRAZED WC-Co-NiP FUNCTIONAL COMPOSITE COATINGS

Teză destinată obținerii
titlului științific de doctor inginer
la
Universitatea Politehnica Timișoara
în domeniul INGINERIA MATERIALELOR
de către

Ing. Dragoș Toader Pascal

Conducători științifici: prof.univ.dr.ing. Viorel Aurel Șerban
prof.univ.dr.ing. Waltraut Brandl
Referenți științifici: prof.univ.dr.ing. Ioan Vida-Simiti
prof.univ.dr.ing. Corneliu Munteanu
prof.univ.dr.ing. Ion Mitelea

Ziua susținerii tezei: 14.06.2017

Seriile Teze de doctorat ale UPT sunt:

- | | |
|---|--|
| 1. Automatică | 10. Știința Calculatoarelor |
| 2. Chimie | 11. Știința și Ingineria Materialelor |
| 3. Energetică | 12. Ingineria sistemelor |
| 4. Ingineria Chimică | 13. Inginerie energetică |
| 5. Inginerie Civilă | 14. Calculatoare și tehnologia informației |
| 6. Inginerie Electrică | 15. Ingineria materialelor |
| 7. Inginerie Electronică și Telecomunicații | 16. Inginerie și Management |
| 8. Inginerie Industrială | 17. Arhitectură |
| 9. Inginerie Mecanică | 18. Inginerie civilă și instalații |

Universitatea Politehnică Timișoara a inițiat seriile de mai sus în scopul diseminării expertizei, cunoștințelor și rezultatelor cercetărilor întreprinse în cadrul Școlii doctorale a universității. Seriile conțin, potrivit H.B.Ex.S Nr. 14 / 14.07.2006, tezele de doctorat susținute în universitate începând cu 1 octombrie 2006.

Copyright © Editura Politehnică – Timișoara, 2017

Această publicație este supusă prevederilor legii dreptului de autor. Multiplicarea acestei publicații, în mod integral sau în parte, traducerea, tipărirea, reutilizarea ilustrațiilor, expunerea, radiodifuzarea, reproducerea pe microfilme sau în orice altă formă este permisă numai cu respectarea prevederilor Legii române a dreptului de autor în vigoare și permisiunea pentru utilizare obținută în scris din partea Universității Politehnice Timișoara. Toate încălcările acestor drepturi vor fi penalizate potrivit Legii române a drepturilor de autor.

România, 300159 Timișoara, Bd. Republicii 9,
Tel./fax 0256 403823
e-mail: editura@edipol.upt.ro

Foreword

The present thesis was elaborated based on the scientific work conducted in the Department of Materials Science and Engineering from the Faculty of Mechanics, at the Polytechnic University of Timișoara, Romania in cooperation with the Department of Materials Science and Testing from Westphalian University of Applied Sciences, Gelsenkirchen, Germany.

This work deals with the development of *HIGH TEMPERATURE VACUUM BRAZED WC-Co-NiP FUNCTIONAL COMPOSITE COATINGS* deposited on top of iron based metallic substrates for protection against wear and corrosion.

During these last three years, it would have been impossible for me to accomplish this work without the help, encouragement and support of coordinating professors, colleagues, friends and family.

First and foremost, I would like to express my sincere gratitude to Prof. Dr. Eng. Viorel Aurel Șerban from Polytechnic University of Timișoara, for giving me the possibility to study an interesting subject under his academic guidance and support and for his invaluable help throughout my PhD study. The same level of appreciation goes to Prof. Dr. Eng. Waltraut Brandl from Westphalian University of Applied Sciences, Gelsenkirchen, for all the support, valuable scientific advices and for offering me the opportunity to conduct my research in an international environment.

Special thanks to Prof. Dr. Eng. Gabriela Mărginean from Westphalian University of Applied Sciences, Gelsenkirchen, for her permanent help, for always having time to offer me advices and to teach me and for giving me a lot of opportunities to learn new things.

Furthermore, I would like to thank Prof. Dr. Eng. Ion Mitelea, Assoc. Prof. Dr. Eng. Bogdan Radu, Assoc. Prof. Dr. Eng. Ion Dragoș Uțu and Assoc. Prof. Dr. Eng. Cosmin Codrean from Polytechnic University of Timișoara for being part of my guidance committee and for their countless suggestions and advices regarding my scientific research.

Many thanks to my colleagues and friends from Gelsenkirchen and Timișoara, namely Dr. Eng. Roxana Muntean, M.Sc. Markus Kiryc, M.Sc. Norbert Kazamer, M.Sc. Petru Vălean, Dr. Eng. Ioan Secoșan, Dr. Eng. Iosif Hulka for the constructive discussions, their moral support, advices and friendship.

Last but definitely not least, I am extremely grateful to my family for their unconditional support, for trusting me and encouraging me to make important steps in my life.

Timișoara, June 2017

Eng. Dragoș PASCAL

Pascal, Dragoş Toader

DEVELOPMENT OF HIGH TEMPERATURE VACUUM BRAZED WC-Co-NiP FUNCTIONAL COMPOSITE COATINGS

Teze de doctorat ale UPT, Seria 15, Nr. 24, Editura Politehnica, 2017, 128 pagini, 65 figuri, 12 tabele.

ISSN: 2285-1720

ISSN-L: 2285-1720

ISBN: 978-606-35-0155-5

Keywords: WC-Co-NiP, vacuum brazing, composite coatings, wear and corrosion resistance.

Abstract,

The present thesis deals with a current topic, namely the development and characterization of functional composite coatings (WC-Co-NiP) deposited on steel substrate. In this regard the coatings characteristics like morphology, microstructure, chemical composition and the appearance of the interface with the substrate have been analyzed. Tribological behavior is assessed with the aid of a tribometer utilizing a pin-on-disk testing arrangement. Corrosion resistance is appraised using the potentiodynamic polarization method in a three-electrode cell configuration. It was determined that this coating technology makes possible the deposition of high quality hardfacings, with minimal influence on metallic substrate. It was found that the wear rate of the coating is significantly lower than that of the unprotected substrate material. The electrochemical measurements performed on the coated samples resulted in a lower corrosion current density, correlated with a significant improvement in corrosion performance, compared to the unprotected substrate.

Cuvinte cheie: WC-Co-NiP, brazare în vid, straturi compozite, rezistență la uzare și coroziune.

Rezumat,

Prezenta teză abordează un subiect de actualitate, și anume dezvoltarea și caracterizarea straturilor compozite funcționale (WC-Co-NiP) depuse pe substrat de oțel. În acest sens au fost analizate unele caracteristici și proprietăți ale acoperirilor, cum ar fi morfologia, microstructura, compoziția chimică și aspectul interfeței cu substratul metalic (16MnCr5). Comportamentul tribologic este evaluat cu ajutorul unui tribometru utilizând un aranjament de testare pin-on-disc. Rezistența la coroziune este evaluată utilizând metoda de polarizare potențiodinamică într-o configurație de celulă cu trei electrozi. S-a stabilit că această tehnologie de acoperire face posibilă depunerea de straturi funcționale de înaltă calitate, cu influență minimă asupra substratului metalic. S-a constatat că rata de uzare a acoperirii este substanțial mai mică decât cea a materialului substrat neprotejat. Măsurătorile electrochimice realizate pe strat au afișat o densitate a curentului de coroziune mai mică, corelată cu o îmbunătățire semnificativă a performanței la coroziune, în comparație cu cea a substratului neprotejat.

Content

Abstract	7
Abbreviations	9
1 INTRODUCTION	11
1.1 Background and Motivation	11
1.2 Aim of the Work	13
2 STATE OF THE ART	15
2.1 Theoretical Aspects Regarding Functional Coatings	15
2.1.1 Tribological Behavior	18
2.1.1.1 Friction	18
2.1.1.2 Wear	20
2.1.2 Corrosion Behavior	24
2.2 Fundamentals of Brazing and Braze Coatings	26
2.2.1 Capillary Attraction, Wetting, Spreading and Diffusion	26
2.2.2 Temperature and Time	29
2.2.3 Surface Preparation	29
2.2.4 Influence of the Brazing Atmosphere	30
2.2.5 Materials	32
2.2.5.1 Base Metals (BMs)	32
2.2.5.2 Filler Materials (BFMs)	33
2.2.5.3 Reinforcing Materials	38
2.2.5.4 Polymeric Binders	43
2.3 Applications of Braze Coatings	44
3 METHODOLOGY AND EQUIPMENT	46
3.1 Equipment and Materials	46
3.2 Brazing Equipment	47
3.2.1 Mixing, Rolling and Tape Preparation	47
3.2.2 High Temperature Vacuum Brazing	47
3.3 Physical Characterization	47
3.3.1 Metallographic Preparation	47
3.3.2 Scanning Electron Microscopy (SEM)	48
3.3.3 Energy Dispersive X-ray Spectroscopy (EDX)	48
3.3.4 Confocal Laser Scanning Microscopy (CLSM)	49
3.3.5 X-ray Diffraction (XRD)	50
3.3.6 Thermogravimetric Analysis (TGA)	51
3.4 Mechanical Testing	51
3.4.1 Micro Vickers Hardness Tester	51
3.4.2 Universal Testing Machine	52
3.4.3 Wear Testing and Wear Measurement	52
3.5 Corrosion Investigation	53
4 EXPERIMENTAL PROGRAM	54
4.1 Materials	55
4.1.1 Substrate Material	55
4.1.2 Filler Alloy	56
4.1.3 Reinforcing Material	60

4.1.4	Organic Binder	63
4.2	Manufacturing of Flexible Tapes	64
4.3	Brazing Process Optimization	66
4.3.1	Influence of Vacuum Quality	71
4.4	Characteristics and Properties of the Brazed Coatings	72
4.4.1	Microstructure	72
4.4.2	Phase Composition	75
4.4.3	Mechanical Properties	78
4.4.3.1	Hardness	78
4.4.3.2	Tensile Adhesive Strength	81
4.4.4	Tribological Behavior	84
4.4.5	Corrosion Resistance	95
5	CONCLUSIONS	101
	Outlook	105
	References	106
	Appendix	113

Abstract

The main goal of the present study was to develop and characterize high temperature vacuum brazed WC-Co-NiP coatings deposited on steel substrates.

The thesis has been structured into 5 chapters:

Chapter 1 presents the background and motivation of the chosen topic.

Chapter 2 deals with the state of the art in the field of brazing, presenting some theoretical aspects regarding, methods, current materials, classification and applications. Moreover, an introduction in the tribological and corrosion behavior of brazed coatings is made. Main advantages and limitations compared to other coating technologies are also discussed.

Chapter 3 describes the methodology and equipment used to achieve the experimental study. This chapter offers an outline concerning the applied investigation methods and presents different experimental techniques, which can provide important information on the quality and performance of high temperature vacuum brazed coatings.

Chapter 4 presents the experimental program concerning the infiltration hardfacing process, the results obtained during this study and highlights the most important aspects.

Chapter 5 points out the conclusions of this study and the personal contributions accomplished through this work.

In the current state of the art, tape brazing involves the use of flexible cloths rolled from mixtures of hard phase powders, filler metal powder and appropriate polymeric binders. The mats can be easily manufactured under diverse chemical compositions of base and filler metal powder, and formed to size and shape by cutting or stamping. After forming, the cloths are overlaid on top of the metallic substrate and fixed in place often with a small amount from the same polymeric binder. The coating process actually takes place at temperatures usually slightly above the liquidus temperature of the filler alloy, in vacuum or under protective atmosphere, with the aid of a furnace. During the brazing process, filler metal reaches liquid state and infiltrates the spaces between the hard phase particles wetting and enveloping them. Metallurgical interactions governed by diffusion and alloying appear among base powder and brazing alloy, as well as at the coating/metallic substrate interface, resulting in a strong metallurgical bond.

No universal reference for the brazing temperatures and holding times exists, because the values depend strongly on the chemical composition of the substrate material, reinforcing powder and filler metal, their ratio in the mixture and the metallurgical interactions. Considering that the majority of substrate materials are iron, nickel, chromium or cobalt alloys, base powders are usually ceramics or cermets and the metal matrix consists typically of self-fluxing nickel base alloys, the furnace brazing temperature is approximately 1100°C. Brazed overlays with a thickness range of 150 µm to 20 mm have been successfully deposited, with theoretical possibilities of an even greater thickness interval. Due to the common high amount of hard phases (up to 70% or more in some cases), associated with the Ni-base matrix alloy, and

generally a low porosity ($\approx 1\%$), these coatings can offer high wear and corrosion resistance under severe working conditions. The major limitation of this coating technique is the requirement to treat the whole substrate to the necessary high brazing temperature. This process can have a negative effect on the substrate material, leading to undesired grain growth or phase transformations. Another current disadvantage of this method is the use of potentially harmful chemical compounds in the polymeric binders, which need to be filtered, contained and neutralized.

The present study assessed the possibility of overcoming the aforementioned limitations of the high temperature vacuum braze coating technique.

The **personal contributions** of this study refer to the possibility of utilizing vacuum brazing as a non-conventional coating method in order to obtain WC-Co-NiP functional hardfacings with superior wear and corrosion resistance. In this regard, it was explored the possibility of combining recycled WC-Co powder as reinforcing phase with NiP brazing filler metal as metallic matrix, to develop vacuum brazed composite coatings. A careful selection of feedstock materials in order to favorably combine a manufacturing process as accessible, economic, and environmentally friendly as possible, with the production of coatings with superior characteristics was also carried out. The successful employment of water-base fugitive glue as organic binder for the manufacturing of flexible cloths, which is safe to handle and harmless to the environment, and at the same time offers adequate flexibility and long shelf life was highlighted. The usage of BNi6 (NiP alloy) brazing filler metal as metallic matrix decreased the maximum temperature of the brazing process down to 1000°C, thus reducing production costs and thermal influence on the substrate material. Studies on the deposition mechanism, as well as investigations on the influence of the thermal cycle parameters on the morphology of the coatings have been accomplished. Consequently, the optimization of the brazing process parameters for the studied chemical composition was successfully performed. Experimental investigations revealed noteworthy characteristics and properties of the high temperature vacuum brazed WC-Co-NiP functional composite coatings (including wear and corrosion resistance).

Accordingly, the method presented in this thesis leads to a facile and cost effective way to develop metallurgically bonded functional coatings with improved wear and corrosion resistance, due to the dense, composite microstructure.

Abbreviations

AS	Arc Spraying
ASM	American Society for Metals
ASTM	American Standard Test Method
BCC	Body-Centered Cubic
BCT	Body-Centered Tetragonal
BFM	Brazing Filler Metal
BM	Base Material
BSE	Backscattered Electrons
CE	Counter Electrode
CLSM	Confocal Laser Scanning Microscopy
CTE	Coefficient of Thermal Expansion
CVD	Chemical Vapor Deposition
ΔG_0	Gibbs Free Energy
D-GUN	Detonation Gun
DIN	Deutsches Institut für Normung
DTA	Differential Thermal Analysis
E_{corr}	Corrosion Potential
EDX	Energy Dispersive X-ray Spectroscopy
EN	European Standard (Norm)
FCC	Face-Centered Cubic
F_N	Normal Force
FS	Flame Spraying
GDP	Gross Domestic Product
HCP	Hexagonal Close-Packed
HV	Hardness Vickers
HVOF	High Velocity Oxygen Fuel
IBTCC	Infiltration Brazed Tungsten Carbide Claddings
I_{corr}	Corrosion Current Density
ISO	International Organization for Standardization
K	Wear Rate
K_{ic}	Fracture Toughness
μ_k	Coefficient of Kinetic Friction
μ_s	Coefficient of Static Friction
NACE	National Association of Corrosion Engineers
NASA	National Aeronautics and Space Administration
OEM	Original Equipment Manufacturer
PEO	Polyethylene Oxide
POD	Pin-On-Disk
PS	Plasma Spraying
PTFE	Polytetrafluoroethylene
PVA	Polyvinyl Acetate
PVD	Physical Vapor Deposition
RE	Reference Electrode
RCF	Rolling Contact Fatigue
s	Sliding Distance

SCE	Saturated Calomel Electrode
SE	Secondary Electrons
SEM	Scanning Electron Microscopy
θ	Contact Angle
TGA	Thermogravimetric Analysis
WE	Working Electrode
W_v	Wear Volume
XRD	X-ray Diffraction

1 Introduction

*"Everything should be made as simple as possible,
but not simpler."*

- Albert Einstein

1.1 Background and Motivation

In the 15th century, one of Leonardo da Vinci's main interests in his work as an engineer and inventor was with friction and its effect on the movement of his mechanical devices. Friction persisted to dictate studies of mechanical systems for the next three centuries. Wear of materials developed into a very important subject in the mid-20th century. In 1966 Peter Jost conducted a study, summarized in a report that gave a big boost to the subject of *tribology*, a term coined by Jost, derived from the Greek word *tribos* meaning "rubbing". This report led the evolution of the discipline from a study of mere friction to the science and technology of friction, wear and lubrication of interacting surfaces in relative motion.

According to the ASM publication "*Green Tribology, Green Surface Engineering, and Global Warming (2014)*", the effects of wear bleed billions of dollars each year from the industrial economy. Exclusively in the United States, industries lose annually 200 billion dollars due to wear and 300 billion dollars due to corrosion. Therefore, surface engineering plays a crucial role in mitigating the massive losses caused by tribological failure. Starting with the 1970s, extraordinary breakthroughs have been made in both triboscience and surface engineering to support innovative solutions for diminishing the wear effect in advanced equipment and machinery exploited in hostile environments [1].

Unquestionably, one of the major challenges of material scientists and mechanical engineers is to deal with the demand for longer lasting and more predictable systems in all markets and for all applications. The added consumption of energy caused by friction and the limits of endurance by wear should be overcome with better engineered materials and surfaces. Even though the once primitive knowledge on the mechanisms of friction and wear has evolved extraordinarily during the last five decades, numerous technical solutions still follow the "trial and error" process. But any accurate selection of the most suitable surface engineering processes, materials, optimal topography, and the correct chemical composition in combination with productional and structural properties necessitate a systematic approach and a profound understanding of the acting mechanisms. Hence friction, wear, and wear protection are actually interdisciplinary research areas that must integrate scientists from theoretical and applied science as well as engineering [2, 3].

Cost of Friction and Wear: Friction gives rise to both added costs and emissions. It has been estimated that as much 30% of production in the industrialized countries goes to replacing worn-out parts. More than one third of the world's energy is used to overcome friction. The costs caused by friction and wear are very high worldwide. The VTT Technical Research Center of Finland announces that several surveys carried out in different countries concluded that the economic impact resulting from friction and wear is 1%-2% of the global Gross Domestic Product GDP. For

example, in the United States alone, reducing friction and wear in engines and transmissions would save 120 billion dollars per year. Friction and the resulting wear and failure of active components can stop entire manufacturing plants for long periods of time. It was assessed that the costs arising from the shutdown of a European coal-fired power plant are 800 000 euros per week, of a paper and pulp mill 1.5 million euros, and of a nuclear power plant 2.2 million euros. Increased friction and wear translate in higher energy consumption, consequently, they are major sources of emissions causing climate change. It is considered to be possible to reduce CO₂ emissions from traffic and industry by 2%-10%, alone by means of new technological friction solutions. In the case of fossil fuel powered vehicle rolling resistance itself makes up 20% of the fuel consumption [4]. A study performed by the University of Southampton declares that UK loses 24 billion pound every year because of problems with friction, wear and lubrication. This figure represents up to 1.6 percent of the country's GDP [5].

There are technological answers to overcome the problems caused by friction and wear, through which energy loss can be prevented and material endurance improved. Friction and wear of components can be controlled by means of films or coatings. Friction and wear are not purely material properties that can be solved by simply selecting a harder material, for example. They emerge from the contact interaction between moving parts, that in turn is influenced by many factors, such as contact, load, speed, surface and base material hardness, elasticity, toughness, chemical reactions and lubrication, and also the dominant environmental factors, including temperature, humidity, impurities, and radiation. Some deficiencies causing friction and wear can be addressed rather easily, while other are more complicated to solve. The lifetime of consumer products can be extended by means of optimal material selection and wear-resistant coatings. Friction and wear in factory conveyors, mineral processing, mixers, extruders, blowers, pumps, and regulating valves can be reduced by efficient lubrication, anti-friction or low-friction coatings, and the correct selection of materials [4].

Cost of Corrosion: In nearly every area of industry, wear and corrosion are phenomena of paramount concern. Corrosion has been the subject of scientific study for more than 150 years. It is a naturally occurring phenomenon commonly defined as the deterioration of a material (usually a metal) or its properties because of electrochemical reactions with its environment.

The global cost of corrosion was estimated in 2013 to be 2.5 trillion dollars, which is equivalent to 3.4% of the global GDP. With total annual corrosion costs in the US alone rising above 1 trillion dollars in the middle of 2013, illustrated the extensive and expensive challenge that corrosion presents to equipment and materials. It is estimated that the costs of corrosion in the US will surpass 1.1 trillion dollars for 2016. These estimations are based on a landmark study by NACE International, that also estimated that direct corrosion costs were 276 billion dollars in 1998 (as reported in the NACE Corrosion Costs Study) [6, 7].

Recent surveys express that the worldwide (direct) cost of corrosion is between 1.3 and 1.4 trillion dollars, that is 3.1% to 3.5% of a developed country' annual GDP. These figures represent only the direct costs of corrosion basically materials, equipment, and services involved with repair, maintenance, and replacement. They do not comprise the environmental damage, waste of resources, loss of production, or personal injury caused by corrosion. Both NACE and NASA corrosion experts have determined that a net of 15% to 35% of the annual corrosion-related expense can be reclaimed by applying presently available corrosion control practices [8, 9, 10, 11].

Even though corrosion is a natural process, thus it cannot be completely stopped, according to ASM International, five primary techniques can be applied in order to control it. These methods are: material selection, coatings, inhibitors, cathodic protection and design [12].

1.2 Aim of the Work

Surface degradation of structural and active components is a continuous concern of modern engineering. Recently, various technologies, including thermal spraying, laser cladding, welding and high temperature vacuum brazing have been implemented with the purpose of depositing thick wear and corrosion resistant coatings. Considering the present knowledge in the field of surface engineering, the main goal of this study was to develop, investigate and characterize infiltration braze claddings, deposited from Ni-base self-fluxing alloys reinforced with WC-based cermets. Nickel based coatings, are being successfully applied onto metallic substrates and show superior characteristics that make them more attractive compared to other types of coatings. Besides de large variety of technologies able to deposit WC reinforced hardfacings, infiltration braze coating is being noted as an effective method to overlay composite coatings with high density and superior bond strength, wear and corrosion resistance. Due to the vastness of possible chemical compositions, the properties of such coatings, obtained through high temperature vacuum brazing are still scarcely known. Therefore, this work aims to study the deposition process of functional composite coatings with metallic matrix based on NiP self-fluxing alloy reinforced with WC-based hard particles. Furthermore, it will investigate the influence of process parameters and the obtained coating characteristics like morphology, chemical and mechanical properties.

Several areas of application (components of pumps, mixers or extruders, mixing buckets, baffles and pipe bends) have been found to fit the particular properties and characteristics of brazed coatings.

Regarding the main limitations of the technique, fruitful means to overcome or at least mitigate them have been found, eliminating the use of hazardous organic binders and reducing the maximum process temperature. More than a few Ni-based self-fluxing alloy powders were considered and tested, and the initial nitrile-based glue was replaced with a nontoxic water-based fugitive binder. The flexible composite tapes have been placed on top of 16MnCr5 (1.7131) case hardening steel substrates and brazed with different parameters to finely optimize the thermal treatment.

Thermal behavior of the selected powders as well as organic binders was observed with the aid of Differential Thermal Analysis (DTA) and Thermogravimetric Analysis (TGA) respectively. The morphology, microstructure, chemical composition of the coatings and the quality of the interface with the substrate have been analyzed by means of Scanning Electron Microscopy (SEM) combined with Energy Dispersive X-ray Spectroscopy (EDX). Size, occurrence and distribution of pores and microcracks has been estimated using image processing of micrographs. Phase composition of the initial filler metal and reinforcing powders, and subsequent deposited coatings was determined using X-Ray Diffraction (XRD). Surface hardness and cross-section hardness profile was evaluated by Vickers indentation. Bond and adhesion/cohesion strength have been investigated through uniaxial tensile testing. To assess and compare the wear resistance of the composite coating to that of the base metal, tribological investigations were performed with a ball-on-disk testing arrangement.

The electrochemical corrosion behavior was evaluated by potentiodynamic polarization, employing a three-electrode cell.

All the aforementioned steps are performed with the purpose of eliminating fractures and crack initiation, reducing the degree of porosity, in order to produce high quality coatings. The present thesis also aims to answer several important questions regarding the development and characteristics of high temperature vacuum brazed coatings.

Accordingly, the thesis is structured into 5 chapters:

Chapter 1 presents the background and motivation of the chosen topic.

Chapter 2 deals with the state of the art in the field of brazing, presenting some theoretical aspects regarding, methods, current materials, classification and applications. Moreover, an introduction in the tribological and corrosion behavior of brazed coatings is made. Main advantages and limitations compared to other coating technologies are also discussed.

Chapter 3 describes the methodology and equipment used to achieve the experimental study. This chapter offers an outline concerning the applied investigation methods and presents different experimental techniques, which can provide important information on the quality and performance of high temperature vacuum brazed coatings.

Chapter 4 presents the experimental program concerning the infiltration hardfacing process, the results obtained during this study and highlight the most important aspects.

Chapter 5 points out the conclusions of this study and the personal contributions accomplished through this work.

2 State of the Art

2.1 Theoretical Aspects Regarding Functional Coatings

A coating is in an extremely general view, defined as a material which is applied onto a surface. Coatings are mainly overlaid on surfaces for decorative, protective, or functional reasons, but in nearly all situations, it is a combination of the afore mentioned.

The concept "functional coatings" defines structures which possess, beyond the classical properties of a coating (protection and decoration), other functionalities. These supplementary functionalities may be diverse, and rely upon the practical application of the coated substrate. Characteristic requirements of functional coatings comprise of durability, reproducibility, easy application and cost efficiency, tailored surface morphology and environmental friendliness [13, 14]. Functional coatings are essential in a wide range of applications, from food and agriculture to aerospace and nuclear industry. In numerous cases these coatings are composite materials consisting conventionally of a softer, more ductile component and a harder, wear resistant reinforcement.

With regards to the aforementioned aspects, several coating techniques (classified by thickness) that provide simultaneous protection against wear and corrosion are illustrated in Figure 2.1.

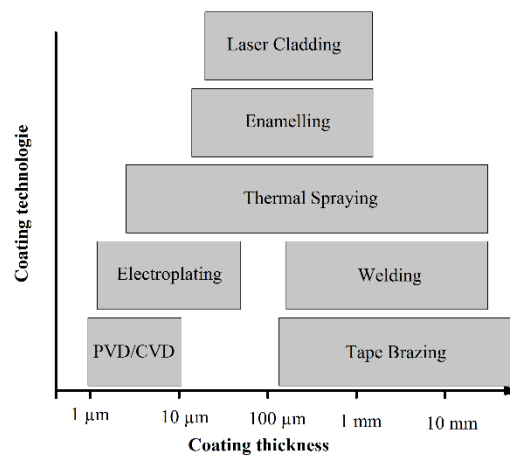


Figure 2.1 Coating techniques

Each of these processes can deposit functional coatings with different chemical compositions and variable thicknesses, appropriate to the working environment.

PVD and **CVD** usually generate thin, hard ceramic and/or metallic coatings from vapor-phase. The typical thickness is situated between 1 μm and 10 μm, and they are especially adequate to reduce sliding and low-stress abrasive wear, due to the low coefficient of friction. In consequence, they are extensively utilized for cutting

tools applications. Because of the restricted thickness such coatings have low fatigue strength and are susceptible to deterioration by contact fatigue. The CVD process temperature usually ranges between 500°C and 1500°C, making this technology limited only to materials that can withstand high temperatures. The PVD technique requires lower process temperature, between 100°C and 500°C, at sub-atmospheric pressure (10^{-4} Pa to 10^{-1} Pa). Because of the lower process temperatures, adhesion of PVD coatings to the substrate materials can be affected. PVD is further limited by the difficulty in coating holes deeper than their width. Furthermore, both technologies involve very complex equipment, requiring highly qualified personnel, and costly maintenance. Being mostly ceramic in nature, both PVD and CVD coatings are generally highly resistant to corrosion, but due to highly tensile thermal residual stresses induced by the different thermal expansion coefficients of the coating and substrate, thin films can easily detach, leaving the base material unprotected [15].

Electroless and **Electroplating** are versatile and powerful methods of coating surfaces in order to protect against wear and corrosion. Electroless techniques involve autocatalytic redox processes, whereas electrodeposition encompasses both an electrolyte bath and electrical current. Coatings of variable chemical composition (metals and/or alloys) can be deposited with both methods. For electroless deposition, the substrate to be coated plays the role of catalytic surface for the reaction between a reducing agent and cations of interest, and therefore the coating is initiated and grows onto it. In the case of electrodeposition, the material to be plated must be electrically conductive and embodies the cathode (negatively charged), while the electrolyte is positively charged with the aid of an anode. Coating thicknesses generally depend on the substrate material, deposition bath and/or current density, but usually vary from 3 μm to 80 μm (in some cases higher values can be achieved). Both procedures have the disadvantage of low efficiency (e.g. 20% efficiency is common in plating of chromium) and usage of hazardous chemical substances, that need to be handled carefully and neutralized after use. Moreover, the deposit properties depend vastly on surface finishing, pretreatment, bath composition, process conditions and age of the electrolyte, further complicating the process [16].

Thermal spraying processes allow coating material, initially as powders or wire to be feed into a combustion chamber where a fuel and oxidizing gas mixture is burned, bringing the materials into a molten or semi-molten state, propelling it under the form of a high-speed fluid spray. This method offers one of the most versatile way of depositing wear resistant materials, allowing rapid coating of various materials on different substrates. It has the capability to deposit thicknesses between 5 μm and 15 mm (depending on the technique, coating material and substrate) [17]. Chemical composition of the coatings can range from pure metals to alloys, cermets and/or ceramics [18]. Various thermal spraying techniques (FS, AS, PS, D-GUN, HVOF) are currently employed for deposition of functional coating to mitigate wear and corrosion. Major drawbacks of thermal sprayed coatings are the inhomogeneous microstructure, discontinuities such as pores, oxidized and/or incompletely molten particles, potentially having a negative impact on wear and corrosion resistance [19]. Furthermore, tensile adhesion (provided only by mechanical hooking) is greatly influenced by surface quality and restricted to a maximum of 100 MPa [20, 21, 22]. To alleviate these disadvantages, it is often necessary to subject as-sprayed coatings to post-spray treatments [18, 23, 24, 25, 26].

Enameling is performed primarily on components made of steel, cast iron and/or aluminum to improve appearance and to protect against wear and corrosion.

Porcelain enamels are mainly vitreous powder materials fused to a metallic substrate by firing at temperatures above 425°C. The base materials for porcelain enamel coatings are called frits, which are metallic oxides and complex borosilicate glasses that are manufactured by quenching molten glassy mixtures. Because enamels are typically engineered for precise applications, the chemical composition of the initial frits differ broadly. Coating characteristics and properties include chemical, weather and abrasion resistance, corrosion protection, specific mechanical and electrical properties, heat and thermal shock resistance. Thickness of enameled coatings is found usually in the interval 30 µm – 2 mm. Main disadvantages are related to limited variety of substrate material that can be coated and imperative defect (deep scratches, pits, open laminations) free surfaces [27].

Laser cladding utilizes a high-power laser beam to liquefy the powder or wire feedstock and a thin surface layer of the substrate to deposit a clad with minimal dilution. A metallurgical bond is thus formed between the coating and base material. The properties of the hardfacing can be adjusted in order to withstand service conditions. Therefore, this technology can be applied to improve wear and corrosion resistance. Coatings of 50 µm up to 2 mm thickness are usually produced with the aid of this process. Major limitations of laser cladding are very low surface coverage rates and high costs for equipment and maintenances [16, 28].

Welding provides the means to deposit hardfacings or weld overlays by applying layers of variable thicknesses and chemical compositions to a metallic substrate. Surface cladding and hardfacing involve the deposition of a relatively thick coating of more wear and/or corrosion resistant material. Welded coatings are essentially fusion welds and display a cast microstructure. The microstructure and properties of the coatings depend largely on feedstock, base metal and welding process. Dilution is accepted and normally required in order to achieve a metallurgical bond, but wear and corrosion resistance usually decrease with increased dilution and therefore it must be strictly controlled. Discrepancies in the coefficient of thermal expansion between coating and base material can produce thermal stress and lead to failure in service. Typical thickness of weld hardfacing is found in the range of 200 µm to 15 mm. Thicker coatings can be obtained utilizing multipass techniques. Costs are mostly directed towards labor and materials. Main disadvantages are related to distortion and residual stresses that lead to cracks in the coating of base material, defects (pores, microcracks and segregation) and difficulties in controlling the microstructure [16, 28].

Tape brazing involves the use of flexible cloths rolled from mixtures of hard phase powders, filler metal powder and appropriate polymeric binders. The mats can easily be manufactured under diverse chemical compositions of base and filler metal powder, and formed to size and shape by cutting or stamping. After forming, the cloths are overlaid on top of the metallic substrate and fixed in place often with a small amount from the same polymeric binder. The coating process actually takes place at temperatures usually slightly above the liquidus temperature of the filler alloy, in vacuum or under protective atmosphere, with the aid of a furnace. During the brazing process, filler metal reaches liquid state and infiltrates the spaces between the hard phase particles wetting and enveloping them. Metallurgical interactions governed by diffusion and alloying appear among base powder and brazing alloy, as well as at the coating - metallic substrate interface, resulting in a strong metallurgical bond. No universal reference for the brazing temperatures and holding times exists, because the values depend strongly on the chemical composition of the substrate

material, reinforcing powder and filler metal, their ratio in the mixture and the metallurgical interactions. Considering that the majority of substrate materials are iron, nickel, chromium or cobalt alloys, base powders are usually ceramics or cermets and the metal matrix consists typically of self-fluxing nickel base alloys the furnace brazing temperature is approximately 1100°C. Braze overlays with a thickness range of 150 µm to 20 mm have been successfully deposited, with theoretical possibilities of an even greater thickness interval. Due to the common high amount of hard phases (up to 70% or more in some cases), Ni-base matrix alloy, and generally low porosity (< 1%), these coatings can offer high wear and corrosion resistance under severe working conditions. The major limitation of this coating technique is the requirement to treat the whole workpiece to the necessary high brazing temperature. This process can have a negative effect on the substrate material, leading to undesired grain growth or phase transformations. Another current disadvantage of the method is the use of potentially harmful chemical compounds in the polymeric binders, which need to be filtered, contained and neutralized [29, 30].

2.1.1 Tribological Behavior

The term *tribology* is derived from the Greek word *tribos*, meaning friction, and was coined by Peter Jost in 1966. The tribological behavior of coatings is defined by the interaction between surfaces in relative motion, subjected to contact, friction and wear [31].

2.1.1.1 Friction

Friction is defined as the resistance to movement of one body over another. The very first effort to provide a scientific explanation for the phenomenon of friction is attributed to Leonardo da Vinci in the 16th century. His famous sketches inspired the later research of Guillaume Amontons (1700s), who formulated the first basic laws of friction:

- *the friction force is proportional to the normal applied load;*
- *the friction force is independent of the apparent contact area.*

In the 1780s, Charles-Augustin Coulomb noticed that these initial laws do not apply to very hard materials or materials with high elasticity. Furthermore, a behavior opposite to the first law was observed even in the case of metals, once the contact pressure is lower than the plastic flow threshold. Consequently, he introduced the distinction between static and dynamic coefficients of friction, formulating the third law of friction:

- *the friction coefficient is independent of the sliding speed.*

It must be taken into account that these rules are very general in nature, and although they have been applied successfully in many instances, they are not relevant to all materials under every working condition. For example, when a high sliding speed is present or the applied load is too large, the above-mentioned aspect is valid [32].

The *coefficient of static friction* μ_s relies on the pairing of contact materials, but, it displays nearly no dependence on contact area or roughness. The mathematical expression is given in Eq. 2.1.

$$\mu_s = \frac{F_s}{F_N} \quad (\text{Eq. 2.1})$$

where μ_s is the coefficient of static friction, F_s is the force of static friction and F_N is the normal force.

The *coefficient of kinetic friction* μ_k is proportional to the normal force and expresses no substantial dependence on contact area or surface roughness. The mathematical expression is given in Eq. 2.2.

$$\mu_k = \frac{F_R}{F_N} \quad (\text{Eq. 2.2})$$

where μ_k is the coefficient of kinetic friction, F_R is the force of kinetic friction and F_N is the normal force.

The coefficient of kinetic friction is approximately equal to the coefficient of static friction [31], as shown in Eq. 2.3:

$$\mu_k \approx \mu_s \quad (\text{Eq. 2.3})$$

A generally valid coefficient of friction-sliding distance curve generated under dry sliding conditions contains four basic stages. A conventional example for a metal/metal arrangement is displayed in Figure 2.2. It must be taken into consideration that Figure 2.2 shows a simplified, smoothed friction evolution, which in practice may well be overlapped by short-term fluctuations, friction peaks, or stick-slip effects.

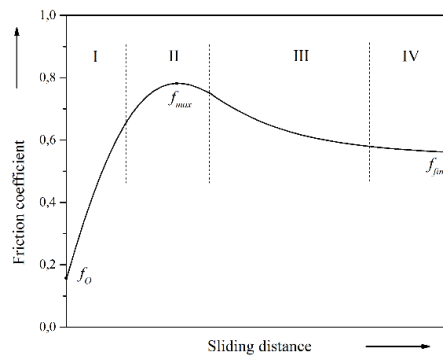


Figure 2.2 Friction-sliding distance typical curve

The early friction coefficient value of stage I, which is commonly around $f_0=0.1$, is reliant on low loads, F_N , and on the shear resistance of surface contaminants, but is mostly independent of material combinations, surface nature and environmental circumstances. Surface layer removal and an upsurge in adhesion due to the development of clean interfacial areas as well as increased asperity interactions and possible formation of third-body wear particles, entrapment leads to a steady intensification in the coefficient of friction. The stages of initial friction may differ in other situations, such as in systems where material transfer layers are generated, and interfacial friction is caused mainly by the collective effect of adhesion, asperity deformation, galling and ploughing.

Stage II, which generally produces the maximum value for the coefficient of friction (f_{\max} 0.3 to 1.0 for most metal pairs), is entered when maximum interfacial adhesion and asperity deformation takes place, and the third-body wear particles are entrapped in the tribo-system, between the sliding partners. As a consequence, higher wear rates can be observed.

In stage III, a reduction in the coefficient of friction can happen due to the formation of protective tribochemical oxide surface layers and thus a decrease in

asperity deformation, galling or plowing occurs. In some situations, for example when a very hard partner is slid against a softer specimen, the asperities of the hard surface are progressively removed, generating a mirror-like polished surface. Subsequently, the frictional force diminishes, due to the mitigation of asperity deformation.

Stage IV is characterized by steady-state interfacial tribological conditions leading ultimately to a nearly constant value for the coefficient of friction (f_{final}) [33].

In moving equipment, friction is accountable for dissipation and loss of large quantities of energy. In order to sustain sliding motion, an additional energy input must be constantly introduced to substitute the energy dissipated by friction.

Energy is dissipated in mechanical systems, mostly as heat, it can limit the parameters at which the equipment can be operated. In some circumstances, it must be removed by cooling to prevent degradation. Part of the energy is dissipated in several deformation processes, leading to wear of the sliding surfaces and subsequently breakdown. Wear of sliding components represents a substantial part of the economic impact of friction, because without sliding friction try-elements would not wear [34].

2.1.1.2 Wear

Wear is generally defined as the loss of material from one or both counterbodies due to tribological interaction in relative motion. This definition is incomplete, not including plastic deformation, when wear occurs without removal of material. According to DIN 50320, wear is not an intrinsic property of materials but rather a system one. Therefore, the wear performance of a material is dictated by the tribological system [1].

A large number of different wear mechanisms have been identified, each requiring a different approach to mitigate. DIN 50320 divides them into four main types:

- Adhesive wear;
- Abrasive wear;
- Tribochemical wear;
- Fatigue wear.

Adhesive wear occurs when the adhesion forces between the contacting asperities exert a predominant role in the formation of wear fragments. This mechanism was first described by Archard's theory, even if the current interpretation has been improved, due to developments and better understanding the involved phenomena.

In ductile materials (majority of metals), adhesion takes place at junctions that in some circumstances might have higher resistance than the bulk. This will result in a worn material fragment to be transferred from one surface to another.

Frequently, other phenomena, of higher importance appear at the contact areas influencing the friction and wear behavior and further complicating the process. Every so often material fragments remain captive at the interface of the contacting surfaces before exiting the tribological system. Consequently, they can transfer on to the counterface, forming tribo-layers. In these instances, friction and resulting wear are changed.

In the case of brittle materials (ceramics), a special form of adhesive wear might take place. The adhesive interaction at the contacting asperities induces the appearance of a surface tensile stress during sliding. Such a stress can induce the formation of a wear fragment by brittle contact, if the material has low fracture

toughness. The corresponding value of wear rate and coefficient of friction are fairly large. If the applied pressure is lower than the critical fracture toughness, the fragmentation is restricted to the asperities, and the fragments are compressed and produce scales able to carry the applied load. Therefore, both wear rate and coefficient of friction are considerably lower [35].

A sketch of the adhesive wear mechanism is shown in Figure 2.3.

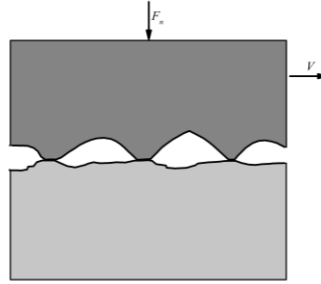


Figure 2.3 Adhesive wear mechanism

Abrasive wear occurs frequently when a hard material is put into contact with a softer one. It often causes scratches, wear grooves and leads to material removal. Abrasion is generally classified based on the type of interaction and contact environment. The types of contact lead to two-body and three-body wear. The first one appears when abrasive particles or protuberances slide along a surface, second one occurs when an abrasive is situated between the complementary surfaces. In the latter situation, the hard particles are quite free to move, thus, their action is limited. Two-body abrasion wear is a very severe form of material degradation. Contact environments are categorized as open (free) and closed (constrained) systems. Abrasion is often additionally divided into low stress, high stress and gouging. In low-stress abrasion the abrasive particles remain fairly intact. High-stress abrasion occurs once the abrasive bodies are crushed. In the case of gouging abrasion, a rather large abrasive particle or protuberance will cut into materials that are not hard enough to withstand the stress [34].

In ductile materials, abrasive wear manifests itself under three modes, namely plowing, wedge formation and cutting. It was observed that the amount of penetration was decisive in the transition from plowing and wedge formation to cutting.

In the case of brittle materials, the supplementary mechanism, namely, microcracking is frequently observed. Microfractures manifest when loads applied by the abrasive particles or protuberances surpass the fracture toughness of the stressed material. This is often the principal mechanism of severe wear encountered in hard metallic materials and ceramic [34].

A basic illustration of the abrasive wear mechanism is displayed in Figure 2.4.

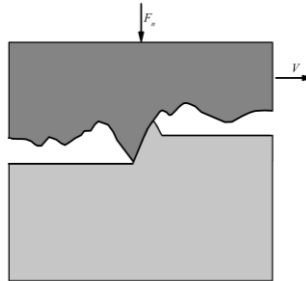


Figure 2.4 Abrasive wear mechanism

Tribochemical wear is a surface damaging mechanism that mostly involves the development of a film generated by chemical interactions between sliding surfaces, usually in unlubricated conditions, and the surrounding environment.

One of the most frequent types of tribochemical wear is tribo-oxidation. The relatively high temperature generated by friction encourages the growth of an oxide layer which, undesirably, in many cases separates from the surface when it overgrows a critical thickness. The resulted debris can be further involved in the wear process or they can be evacuated from the tribosystem.

Often, tribological oxidation will reduce the wear rate by two orders of magnitude, in comparison to the wear of the equivalent material under an inert atmosphere. However, improvement of the wear rate will only happen if the oxide films are stable under service conditions.

Tribochemical wear might occasionally appear in lubricated sliding situations, when the oil film thickness is less than the combined surface roughness of the tribo-pair. Tribo-oxidation is a protection mechanism of boundary lubricated metallic triboelements against scuffing. Moreover, this phenomenon is also the only protection that some of the recently developing ceramic tribosystems possess against breakdown in high temperature working environments [34].

Figure 2.5 exemplifies the tribochemical wear mechanism.

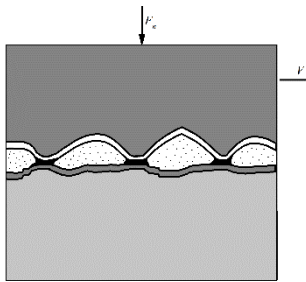


Figure 2.5 Tribochemical wear mechanism

Fatigue wear is a phenomenon characterized by surface deterioration of a component exposed to cyclical stress. This occurs because of strain induced in the superficial layers of the material, generating cracks parallel to the surface within the material. After they reach a critical size, they produce flake-like fragments. This process is also denoted as delamination wear. In majority of cases, wear by contact fatigue occurs in non-conformal contacts, when at least one of the two components

rolls over the other. In such situations, this wear mechanism is referred to as rolling contact fatigue (RCF).

In the case of ductile materials, fatigue failure happens by crack nucleation, followed by crack propagation, and ultimately fracture. Because of the cyclic loading, a crack underneath the surface nucleates after a given number of cycles. Nucleation generally arises in areas with high stress concentration. After nucleation, the cracks beneath the surface propagate driven by the contact stresses. Finally, they spread until the ligament between their tip and the surface fractures by plastic collapse. The crack can subsequently reach the surface, producing a wear fragment.

In brittle materials, the process differs slightly. In this case the material matrix in the vicinity of a defect possesses low fracture toughness. Consequently, microstructural defects, for instance pores, could be considered as pre-existing cracks that are capable to propagate very fast if the applied stress intensity factor is superior to a critical threshold.

It is a particularly dangerous form of wear, because it is frequently problematic to notice in its initial stages. The precursor defects can be concealed from detection as they propagate beneath the contact surface. By the time cracks grow substantially enough to appear at the surface and generate wear particles or delamination, these particles can become large spalls or flakes, leading to immediate component loss of function or efficiency [35].

Figure 2.6 shows a schematic representation of the fatigue wear mechanism.

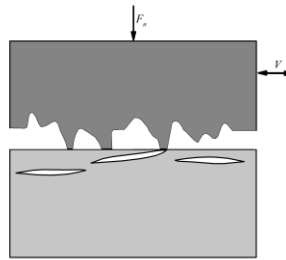


Figure 2.6 Fatigue wear mechanism

The general form of the **wear equation** is grounded on the relationship developed by *J. F. Archard* (1953) [36], in which, the wear volume (W_v) is directly proportional to the sliding distance (s) and the applied normal force (F_N) and inversely proportional to the room temperature hardness or yield stress (H) of the softer surface:

$$W_v = K \cdot \frac{F_N}{H} \cdot s \quad (\text{Eq. 2.4})$$

The coefficient of wear K is a proportionality constant number, and becomes equal to the wear volume per unit sliding distance if the applied normal force is identical to the hardness ($F_N = H$) or yield stress of the softer material. The coefficient of wear K can be determined for a wear system from laboratory tests or field data.

The hardness (or yield stress) is the singular material property included in Archard's wear equation. The indentation load for hardness evaluation is carefully chosen according to the anticipated hardness of the given material, so that the penetration of the indenter is limited to the near-surface region. Therefore, indentation hardness indicates the surface or near-surface region hardness. The bulk of the material may or may not have the same hardness as the surface. The wear behavior of a material relies upon the surface hardness of the solid [1].

Material loss in terms of volume is directly proportional to the normal force and sliding distance and inversely to hardness. There is a gradual increase in material removal (wear) per sliding distance and thus also with time. The wear rate can be high or low at the beginning or run-in stage, followed by a steady-state and culminating high in the final stage, leading to failure. The extent of the steady wear state determines the working life of tribo-components. If the severity of the environment increases, the duration of the steady stage diminishes. In extreme situations, this leads to merger of the initial steady-state to the final failure stage, thus severely affecting the wear life.

Conclusively, the wear rate k is normally defined as the wear volume W_v (mm^3) divided by normal load F_N (N) and sliding distance s (m), and is usually expressed in $\text{mm}^3 \text{N}^{-1} \text{m}^{-1}$ [37].

$$k = \frac{W_v}{F_N \cdot s} \quad (\text{Eq. 2.5})$$

2.1.2 Corrosion Behavior

According to the ASTM G15 standard, corrosion is defined as: “the chemical or electrochemical reaction between a material, usually a metal, and its environment that produces a deterioration of the material and its properties”. The word corrode is derived from the Latin “*corrodere*”, meaning “to gnaw to pieces” [12]. Electrochemical corrosion is based on oxidation reactions, in which metals transfer electrons to the environment and experience a valence change from zero to a positive value z [38]. Corrosion behavior can only be discussed in terms of a combination of material (in most cases metals) and environment. The environment might be a gas, liquid, solid or hybrid.

The most common forms of corrosion that might appear in the case of protective coatings are illustrated in Figure 2.7.

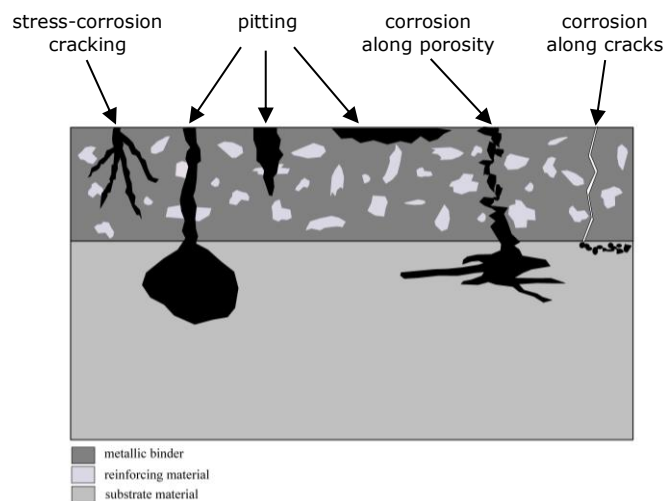


Figure 2.7 Common forms of corrosion in coatings

Corrosion is usually classified based on three factors:

Nature of the corrodent: can be classified as "wet" or "dry". A liquid or moisture is necessary for the former, while dry corrosion normally involves reactions with high-temperature gases.

Mechanism of corrosion: may involve either electrochemical or a direct chemical reaction (attack).

Appearance of the corroded material: is either uniform, when the material corrodes at the same rate over the entire surface, localized, in which case only small areas are attacked. Classification made by appearance is particularly suitable in failure analysis [12]. In the case of composite coated substrates, localized corrosion might appear as:

Coating corrosion:

- *pitting*, which typically appears on the coating surface confined to a point or small area. It can take several forms, e.g. cavernous, narrow and deep, or wide and shallow;
- *stress-corrosion cracking*, is a more complex phenomenon, influenced by numerous factors, including metallurgical, environmental and structural or stress variables. It is a destructive process that requires the presence of both tensile stress and a specific corrosive environment;
- *galvanic corrosion*, occurs between the reinforcing particles and the matrix material, reaction in which only one of the two is affected;
- *crevice corrosion*, occurs at the coating-substrate interface, most frequently because of inadequate preparation of the substrate, or due to defective adhesion.

Substrate corrosion:

- *because of pores in the coating*, the aggressive media penetrates the coating, corroding the substrate;
- *because of micro-cracks in the coating*, the aggressive media penetrates the coating down to the substrate, corroding it.

The resistance to corrosion depends on surrounding environment, the conditions of exposure and the nature of the given material. Each material has a unique and intrinsic corrosion behavior that can range from high resistance, to low corrosion resistance. This behavior is often the result of complex interactions between the material and the working conditions (environment) to which it is exposed, and depends strongly on the latter's chemical composition, temperature, velocity and many other characteristics.

The general relation between the rate of corrosion, the corrosivity of the environment, and the corrosion resistance of a material is [12]:

$$\text{rate of corrosive attack} \approx \frac{\text{corrosivity of environment}}{\text{corrosion resistance of material}}$$

Metallic matrix functional composite coatings are generally utilized to isolate the base material from the corrosive environment in order to protect it. Therefore, they are more noble than the substrate and offer protection by way of cathodic or barrier action. In order to possess adequate corrosion resistance, the structure has to be as dense as possible, without pores, cracks or any other defects. If the deposit is porous or it contains micro-cracks, the corrosive environment can reach down to the base material. In this case, the coating can detach and the substrate will come in direct contact with the corrosive environment [39].

2.2 Fundamentals of Brazing and Brazed Coatings

Brazing is defined by the American Welding Society as "a group of welding processes that produces coalescence of material by heating them to the brazing temperature in the presence of a filler metal having a liquidus above 450°C and below the solidus of the base metal. The filler metal is distributed between the closely fitted faying surfaces of the joint by capillary action" [40]. The main advantage of this joining technique is the ability to produce a cost effective metallurgical bond between the filler metal and base material without melting the latter. Braze joint quality is dependent on multiple factors. To accomplish a good joint utilizing any of the brazing methods, the components to be brazed must be properly prepared and protected from excessive oxidation.

There are several ways of heating and subsequently melting the BFM classified by the practical source of heat:

- Torch brazing
- Furnace brazing
- Induction brazing
- Dip brazing
- Resistance brazing
- Infrared brazing
- Laser brazing
- Exothermic brazing
- Weld brazing
- Microwave brazing

Each method possesses a characteristic heating rate, thermal gradient, and cooling rate, both external and internal, having noticeable effects on dimensional stability, distortion and metallurgical properties of the brazed structure [41].

For a better understanding of brazing, this chapter presents an overview on the aspects that are fundamental to the brazing process. Hereinafter, the present thesis will focus primarily on the high temperature vacuum furnace brazing process.

2.2.1 Capillary Attraction, Wetting, Spreading and Diffusion

Capillary action is the result of the relative attraction of the molecules of the molten filler metal to each other and to those of the solid base metal due to surface tension. It is also the physical force that governs the action of a liquid against solid surfaces in small, confined areas. Capillary attraction is the dominant physical phenomenon that guarantees quality brazements when the surfaces to be brazed are wet with the liquid filler metal. In practice, brazing filler metal (BFM) flow characteristics are strongly influenced by dynamic considerations involving fluidity, viscosity, vapor pressure, gravity, and chemical reactions occurring in the BFM and the interface with the base material [42].

Wetting occurs when liquid brazing filler metal spreads on the solid base metal, forming a thin continuous layer of adherent liquid, instead of balling up on its surface. It appears when the force of adhesion between the solid and liquid is greater than the cohesive force of the liquid. Wetting is dependent not only on the filler alloy but also on the nature of the material or materials to be brazed. There are considerable

indications that in order to wet properly, the molten BFM has to be able to dissolve, or alloy with, part of the material on which it flows. Wetting is only one of several important factors of a successful brazing process.

A very important aspect influencing wetting performance is the cleanliness of the surface to be brazed. Wetting and spreading are inhibited by the presence of grease, dirt, and other contaminants, which obstruct the contact between the brazing filler alloy and the base material. In this regard, one of the purposes of fluxes is to remove the oxide layer present at the joint interface and to expose the clean base material.

The most frequently used criterion to quantify wetting of solids by non-reactive liquids is the contact angle θ , as shown in Figure 2.8.

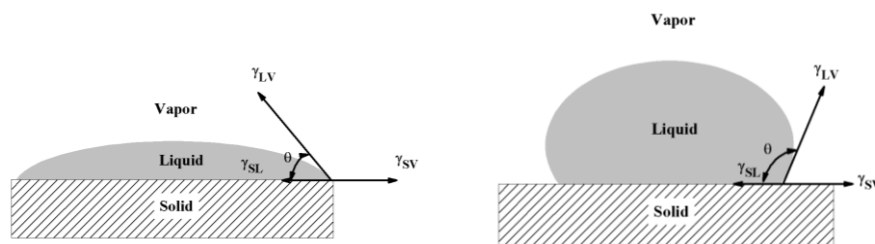


Figure 2.8 Contact angle (θ), for a liquid droplet on a solid surface: a) $\theta < 90^\circ$ (wetting); b) $\theta > 90^\circ$ (nonwetting)

The relationship between the contact angle and the surface free energies at the liquid-vapor, solid-vapor, and the solid-liquid interfaces is expressed as follows:

$$\cos \theta = \frac{(\gamma_{SV} - \gamma_{SL})}{\gamma_{LV}} \quad (\text{Eq. 2.6})$$

where θ is the contact angle, γ_{SV} is the solid-vapor surface energy, γ_{SL} is the solid-liquid surface energy, and γ_{LV} is the liquid-vapor surface energy.

Spreading describes the condition in which the liquid completely covers the solid surface. This occurs when θ approaches the value of 0° , and is illustrated in Figure 2.9.

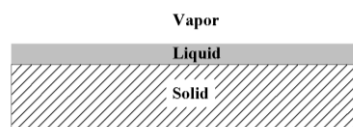


Figure 2.9 Contact angle $\theta = 0^\circ$ (spreading), for a liquid on a solid surface

Good wetting and spreading of the liquid filler metal on the base material are essential in brazing, because the mechanics of the process mandate that the BFM be brought smoothly, rapidly, and continuously to the joint opening. [41].

Diffusion is defined by the ASTM B 374 standard as "spreading of a constituent in a gas, liquid, or solid tending to make the composition of all parts uniform by thermal motion of atoms or molecules to new sites within a material". It is relatively fast in gases, slow in liquids, and very slow in solids, and represents a fundamental process in the science of materials. In a homogeneous material, atoms are routinely moving around, but the movement is random (i.e. there is always an

equal number of atoms moving in all directions). In an inhomogeneous material, all the atoms are moving near randomly, but there is a migration of atoms to areas where their concentrations are lower.

Atom diffusion can occur by the motion of host or substitutional atoms to vacancies, or interstitial impurities atoms to different interstitial positions. In order to move, an atom must overcome the bond energy due to nearby atoms. This is more easily achieved at high temperatures when the atoms are vibrating strongly.

Diffusion processes are significant for the kinetics of many microstructural changes that occur during preparation, processing, and heat treatment of materials, thus an important topic in the case of brazing. Representative examples of processes that involve diffusion are nucleation of new phases, diffusive phase transformations, precipitation and dissolution of a second phase, homogenization of alloys, recrystallization, high-temperature creep, and thermal oxidation [43].

Arguably the most important advancements have been made in the second half of the 19th century through the work of *Adolf Eugen Fick*, who mathematically described the diffusion processes with the aid of two laws.

Fick's first law explains the diffusion flux for steady-state diffusion (in one direction) as the number of atoms passing through a plane of unit area per unit time:

$$J = -D \cdot \frac{dc}{dx} \quad (\text{Eq. 2.7})$$

where J is the flux of particles, D is the diffusivity ($\text{cm}^2 \text{s}^{-1}$), and $\frac{dc}{dx}$ is the concentration gradient ($\text{atoms cm}^{-3} \text{cm}^{-1}$). The negative sign indicates that the direction of diffusion is down the concentration gradient, from higher to lower concentration.

In three dimensions the flux of atoms can be expressed using a vector notation as:

$$J = -D \cdot \nabla C \quad (\text{Eq. 2.8})$$

where ∇ is the Hamilton operator and expresses the vector operation on the right side of Eq. 2.8.

Fick's second law describes the nonsteady-state (dynamic) diffusion of atoms (in one direction) as:

$$\frac{\partial c}{\partial t} = D \cdot \frac{\partial^2 c}{\partial x^2} \quad (\text{Eq. 2.9})$$

In the case of metallic materials, diffusion is influenced by a series of technological and metallurgical factors.

The most notable technological factors are:

- *temperature*, influences diffusion kinetics through the diffusion coefficient;
- *heating rate*, at high values it leads to higher diffusion depth;
- *pressure*, diffusivity in solids depends on the hydrostatic pressure;

The most important metallurgical factors are:

- *concentration gradient*, modifies the diffusion coefficient or diffusivity, contributing to the overall net flux of diffusing species;
- *grain size* (smaller grains lead to higher diffusivity);
- *crystal structure* (carbon diffuses faster in Fe_γ than in Fe_α);
- *imperfections* (both vacancies and dislocations favor diffusion)
- *nature of the diffused element* (elements of smaller size diffuse easier).

Moreover, diffusivity differs depending on the material region where the diffusion process takes place. Accordingly, diffusion slows down from the surface to the grain boundaries and finally the bulk (volume) material [44].

2.2.2 Temperature and Time

The **temperature** of the brazing process has clearly a significant effect on the wetting and alloying action of the BFMs, increasing with temperature. Obviously, the temperature must be above 450°C, and the liquidus of the brazing filler metal and below the solidus of the base material. Within this interval, a brazing temperature that is most suitable global is usually chosen. Regularly, low brazing temperatures are favored, to reduce the heat energy required, mitigate the heat effect on the base material (e.g. grain growth, annealing, and deformation), minimize BFM/BM interactions, and increase the life of brazing equipment. Higher brazing temperatures promote base-metal interactions in order to modify the filler metal. Additionally, this technique is regularly used to increase the remelting temperature of the joint, avoid stress cracking and increase removal of surface contaminants and oxides effectiveness in vacuum brazing.

The **time** at brazing temperature also affects the wetting process. If the BFM has a propensity to creep, the distance usually increases with time. The alloying phenomenon between BFM and BM is, undeniably, a function of temperature, time, and nature of filler metal. For common industrial applications, where diffusion is not mandatory, temperature, time, and quantity of brazing alloy are generally maintained at a minimum, without compromising good quality.

Liquation represents the separation of brazing alloy constituents, and might occur during brazing, when the phase composition of the liquid and solid filler metal changes as the temperature increases from the solidus to the liquidus point. Clearly, this separation is unwanted and to be avoided. If the phase that has the lowest melting temperature is permitted to flow out, then the residual solid phases will have superior melting points than the initial BFM composition and may never melt, under the given brazing conditions, and it is left behind in the form of residues. Filler alloys with restricted melting intervals tend not to liquate, thus they flow quite freely in interstice with extremely narrow clearances as long as the solution and diffusion rates of the filler alloy with the base material are low enough. Separation or liquation of brazing alloy constituents with wide melting intervals can be minimized by rapid heating or by positioning the BFM in the joint area after the base material has reached the brazing temperature. Nevertheless, liquation cannot be completely eliminated and filler alloys with wide melting intervals, which tend to have more sluggish flow, will necessitate wider joint clearances that will generate larger fillets at the brazement extremities. Liquation can be mitigated by utilizing brazing alloys with narrow melting intervals and passing rapidly through the melting temperature during brazing. The optimal brazing temperature for the majority of BFMs is commonly around 10°C to 100°C above the liquidus temperature. This superheat ensures flow without liquation. Some brazing filler metals possess sufficient fluidity below the actual liquidus temperature, and produce adequate brazements, even though the liquidus point has not been reached, thus completely avoiding the phenomenon of liquation [42].

2.2.3 Surface Preparation

Surface preparation is a major factor of influence, independent of the brazing method. Clean, oxide-free surfaces are imperiously necessary to guarantee uniform quality and sound brazed joints. All oils, greases, dirt, and oxides must be thoroughly removed from the base and filler metals before brazing. Brazing must be performed as soon as possible after the material has been cleaned, in order to avoid possible

recontamination. The duration that the cleaning remains effective relies on the materials involved, atmospheric conditions, storage, handling, as well as other factors. Cleaning procedures are generally classified as being either chemical or mechanical. Chemical cleaning is the most effective method of removing all traces of organic contaminants. Oxides and hard scales that cannot be eliminated by chemical cleaners can be mechanically removed. Appropriate cleaning and drying of the components before brazing is essential to avoid surface contamination.

Additionally, to cleanliness and absence of oxides, **surface roughness** is another important aspect that defines the ease and uniformity of brazing filler alloy flow. Surface roughness refers to the micro-irregularities, or deviations in the direction of the normal vector of a real surface from the ideal one. An illustration of what highly magnified real surface roughness looks like is presented in Figure 2.10

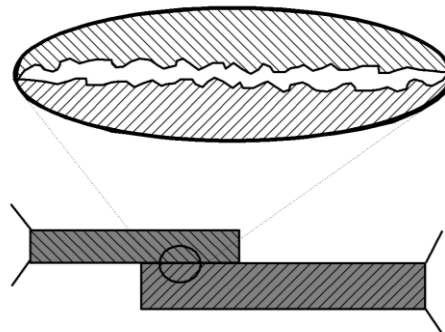


Figure 2.10 Roughness of a real (as-received) surface

It has been experimentally demonstrated that in practice, an as-received (as-drawn, as-rolled, as-machined, etc.) surface roughness is perfectly capable of supplying the necessary capillary action of BFMs, without the need for further preparation by roughening or polishing. Commonly, a liquid that wets a smooth surface will wet a rougher one even better. Furthermore, a rough surface will change filler-metal flow from laminar to turbulent, extending flow time and in some cases increasing the possibility of alloying and other interactions. Although, mechanical gripping aided by a rougher surface is to be considered in some circumstances (e.g. thermal sprayed coatings), in the case of brazing, the metallurgical bond due to diffusion and alloying provides far superior adhesion/cohesion (bond strength). Surfaces frequently are not actually planar, thus, occasionally, surface roughening will improve quality of the brazed seam [45].

2.2.4 Influence of the Brazing Atmosphere

All brazing environments present a characteristic amount of oxygen, even vacuum. In practice, no atmosphere is completely inert, they are either oxidizing or reducing. This is for the reason why it is not possible to eliminate and completely exclude oxygen from the brazing area, with the exception of strict laboratory settings. Therefore, when an atmosphere is defined as inert, it means that the residual level of oxygen is insufficient to negatively influence the brazing process under given conditions. Since the inertness of an atmosphere is assessed in relation to the explicit application, it is required to state a quantitative measure of the present oxygen. This

specific parameter is the oxygen partial pressure. Partial pressure quantifies the concentration of one individual gas in an atmosphere comprising of multiple gases. The partial pressure of a gas in a mixture of gases is defined as the hypothetical pressure it would exert if it alone occupied the entire volume. Representative inert atmospheres among the conventional gases consist of nitrogen, argon, and hydrogen. Hydrogen is counted in because it is not capable of reducing oxides formed on most metals at normal brazing temperatures.

Vacuum is regularly used as a protective atmosphere for brazing processes. It possesses numerous advantages compared to other environments, particularly the ability to measure and control the oxygen partial pressure more easily. In an arrangement considered leak-free, the oxygen partial pressure is one-fifth of the vacuum pressure, making it fairly easy to calculate, as compared with straight measurement of oxygen partial pressure. When required, even lower values of oxygen partial pressure can be achieved with the use of modern vacuum pumping systems. The disadvantages of utilizing a vacuum system to perform a brazing process are, mainly constrained access to the workpiece and the inadvisability of using materials with volatile constituents, which might be aggressive and corrode the vacuum chamber, damage its seals, and contaminate the pump oil. This problem does not concern only highly volatile elements. Various metals that have a negligible vapor pressure at ambient temperature will volatilize during high-temperature brazing ($>1000^{\circ}\text{C}$), particularly when the process involves vacuum.

Vacuum conditions are particularly suitable for brazing very large components, when solid or liquid fluxes cannot be removed effectively from the interfaces during brazing, and when gaseous atmospheres are not entirely effective because of their incapability to purge blocked gases evolved at close-fitting brazing interfaces. Vacuum is also suitable for brazing various similar and dissimilar base materials, including reactive and refractory metals, as well as ceramics.

Vacuum purges basically all gases from the brazing area, thus eliminating the requirement of purifying a supplied atmosphere. During the brazing process, the oxygen partial pressure inside the furnace chamber is kept at a level that prevents oxidation of all involved components. The actual vacuum levels utilized depend on the materials which are joined, the filler alloys that are utilized, the area of the brazement, and the degree to which gases are removed from the base materials surface during the brazing cycle. At sufficiently low vacuum levels, certain oxides of some base materials will dissociate at sufficiently high brazing temperatures. The mechanisms of oxide removal in vacuum are still not undoubtedly understood. Oxide films may be eliminated by evaporation, dissociation, diffusion, or a combination of diffusion and chemical reactions. Commonly, the surface characteristics and properties of the base materials themselves are improved. At elevated temperature, the low pressure existing around the base and filler materials can remove volatile impurities and gases from the surfaces. This phenomenon can cause problems if large quantities of elements from the filler alloy or base materials volatilize at the brazing temperature because of the low surrounding pressure. This predisposition can be amended by applying the correct vacuum brazing parameters (techniques). Many vacuum furnaces possess the capacity to be operated at a specific vacuum level or under a partial pressure of inert gas. Consequently, there are two main types of vacuum brazing, namely brazing in high vacuum and brazing in partial vacuum. High vacuum brazing is predominantly well fitted for processing of base materials that generate hard-to-dissociate oxide films [45].

2.2.5 Materials

Independent of the brazing technique, there are two indispensable components (materials) to the process, namely the base material(s) and the brazing filler metal or alloy.

2.2.5.1 Base Materials

The **base material** has a prime effect on joint strength. A high-strength base metal produces joints of greater strength than those made with softer base metals (other factors being equal). When hardenable metals are brazed, joint strength becomes less predictable. This is because there are more complex metallurgical reactions involved between hardenable base metals and the filler metals. These reactions can cause changes in the base-metal hardenability and can create residual stresses. Also, vitally important are the coefficients of thermal expansion (CTEs), where different materials make up the assembly and gaps can open or close as heating proceeds to the joining temperature. Also, during cooling, after the filler metal has solidified, differences between the CTEs generate residual stresses that may produce distortion. The relative ease of brazing some base metals and other materials is shown in Table 2.1.

Table 2.1 Relative ease of brazing various base materials [45]

Degree of difficulty	Materials
Impossible	None
Difficult	Ti, Zr, Be, and their alloys; ceramics, graphite; glass; TiC
Fair	Al, W, Mo, Ta, alloys with more than 5% metals forming refractory oxides, cast iron, WC
Easy	Cu, Ni, Co, and their alloys; steel; precious metals

There are several metallurgical phenomena that influence the behavior of brazed joints and, in some instances, necessitate special procedures. Included among these base-metal effects are alloying, carbide precipitation, stress cracking, hydrogen, sulfur, and phosphorus embrittlement, and oxide stability. In addition to the base-metal effects mentioned previously and the normal mechanical requirements of the base metal in the brazement, the effect of the brazing cycle on the base metal has also a strong influence. Base-metal alloys that are strengthened by cold working will be annealed and the joint strength reduced when the brazing-process temperature and time are in the annealing range of the base metal which is processed. Hot-cold-worked heat resistant base metals can also be brazed, however, only the annealed physical properties will be available in the brazement. The brazing cycle by its very nature will usually anneal the coldworked base metal, unless the brazing temperature is very low and the time at elevated temperature is very short. It is usually not practical to cold work the base metal after the brazing operation. When it is essential to design a brazement having strength above the annealed strength of the base metal after the brazing operation, specifying a heat treatable base metal is necessary. The base metals can be of the oil quench type, the air-quench type that can be brazed and hardened in the same or separate operations, or the precipitation-hardening type, in which the brazing cycle and solution treatment cycle may be combined. Parts can be hardened and then brazed with a low-temperature filler metal

employing short times at elevated temperature, in order to maintain the mechanical properties (prevent softening by annealing).

The strength of the base metal has a profound effect on the strength of the brazed joint; thus, this property must be clearly kept in mind when designing the joint for specific properties. Also, some base metals are easier to braze than others. This is particularly the case of certain base metals joined by specific brazing processes. For example, reactive metals (titanium, beryllium, etc.) brazed in vacuum or in an inert atmosphere in a furnace are easier to braze than with a torch process [45].

2.2.5.2 Filler Materials

The **filler alloy** is arguably the second most important component involved in the brazing process. The term *brazing filler metal* is essentially synonymous with the commonly employed term *brazing alloy*. Its selection is important but not for the reasons many engineers think. A specific filler metal cannot be chosen to produce a specific joint strength, which is unfortunate, but true. Actually, brazing can provide strong joints with almost any good commercial filler metal if brazing methods and joint design are selected and correctly applied.

Several characteristics that filler metals must possess or are desirable are:

- Proper fluidity at the brazing temperature to ensure flow by capillary action and to provide full alloy distribution;
- Stability to avoid premature release of low melting- point elements in the filler metal;
- Ability to wet the base-metal joint surfaces;
- Low-volatilization characteristics of the alloying elements of the filler metal at the brazing temperature;
- Ability to alloy or combine with the parent metal to form an alloy with a higher melting temperature;
- Controllability of the washing or erosion between the filler metal and the parent metal within the limits required for the brazing operation;
- Depending on the service requirements, the ability to produce or avoid base metal/filler metal interactions.

One of the most broadly misunderstood facts relating to filler metals is that brazed-joint strength is completely unrelated to the used melting method. This fact is hard to accept, because it seems to contradict a long-established metallurgical truth with regard to the manufacture of steels and other constructional metals. The effect of melting practice of filler metals, however, is not the same as that of melting practice of metals during primary manufacturing. If constructional metals are produced by vacuum melting, for example, there is a definite relationship between the vacuum-melting practice and the final strength of the ingot, bar, or rolled sheet. That is not true with a filler metal, because the joint strength depends on such factors as joint design, state of stress, brazing temperature, amount of filler metal applied, location and method of application, heating rate, holding time at the peak temperature, and many other considerations that make up what is termed *brazing technique*.

The process by which filler metals penetrate and alloy with base metals during brazing is referred to as diffusion. In applications requiring strong joints for high-temperature, high-stress service conditions (such as turbine rotor assemblies and jet engine components), it is generally good practice to specify a filler metal that diffuses readily and alloys with the base metal. When the assembly is constructed of

extremely thin base metals (as in honeycomb structures and some heat exchangers), good practice generally calls for a filler metal with a low-diffusion characteristic relative to the base metal being used. Diffusion is an essential and normal part of the metallurgical process that contributes to good brazed joints.

In choosing a filler metal, the first criterion is the working temperature. Very few filler metals possess distinct melting points. Filler metals in which the solidus and liquidus are close together, do not usually exhibit a strong tendency to separate, and they are relatively fluid. They flow readily and should be used with small joint clearances. Some typical brazing temperature ranges for various filler metals are shown in Figure 2.11.

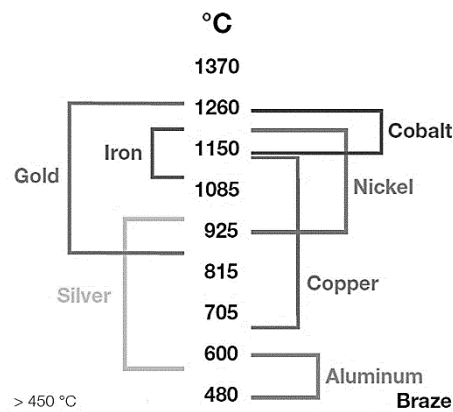


Figure 2.11 Typical brazing temperature ranges [47]

Other filler-metal selection criteria include corrosion resistance, such as oxidation and galvanic corrosion with other parts of the assembly and the service environment, color match to the base metal, electrical and thermal conductivity, joint-filling capacity; hardness and machinability, ductility and fracture toughness, and ability to form fillets.

Additionally, the engineer must consider the extent of alloying with the base metal. The improvement in mechanical properties of the joint and the increase in remelt temperature obtained by alloying could be beneficial. Structural changes in the interface layers of the base metals, aggressive, extensive alloying between the base metal and filler metals, formation of brittle intermetallic compounds, and erosion of components can be deleterious, and, at times, catastrophic. All such effects, beneficial or otherwise, vary greatly with the joint gap, temperature and time of brazing, and compositions of the base metals and the filler metal.

Although the mechanical properties of filler metals in massive form can provide a guide to their suitability for use in different capillary joining applications, in general, designers cannot work with the mechanical properties of assemblies brazed using different joint configurations or cycles of time and temperature.

The most common brazing filler metal forms are wire, powder, foil, flux paste, strip, shim, and non-fluxing paste. Preforms made from wire, strip, and foil can also be utilized [45].

Nickel based brazing alloys have been used for many decades for their brazing characteristics, high strength and corrosion resistance in numerous working environments, like materials processing, automotive, aerospace and nuclear applications. Nickel provides favorable high temperature chemical and physical

properties as well as machinability and it is highly compatible with other alloying elements.

In order to offer practical applicability as a brazing alloy and transform the pure Ni metal into a BFM, the initial high melting point (1455°C) has to be lowered. This decreasing is possible through the addition of specific quantities of melting point depression elements, most common of them being metalloids, such as boron, silicon and phosphorus or other transition metals, namely chromium.

For a better understanding, and easier visualization of phase boundaries and transition condition, binary mixtures of Ni and previously mentioned temperature suppressants are illustrated as follows [46].

Ni-B (Nickel-Boron)

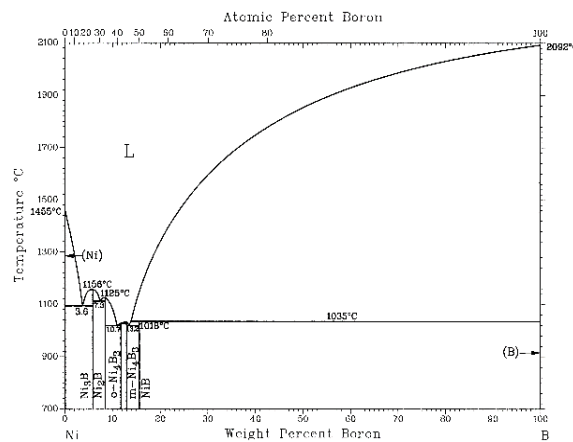


Figure 2.12 Ni-B binary phase diagram [46]

According to the Ni-B phase diagram illustrated in Figure 2.12, the melting point of nickel and boron at the pressure of 1 atm is 1455°C and 2092°C, respectively. The Ni-B binary system has a eutectic reaction, the eutectic composition having 10.7 wt.% B. Boron behaves as a temperature suppressant, aids wetting through self-fluxing of oxides and contributes to high temperature strength, increasing ductility and oxidation resistance. As an active deoxidizer, boron delivers additional joint strength and corrosion resistance. Can be readily diffused into the brazement and forms borides.

Ni-Si (Nickel-Silicon)

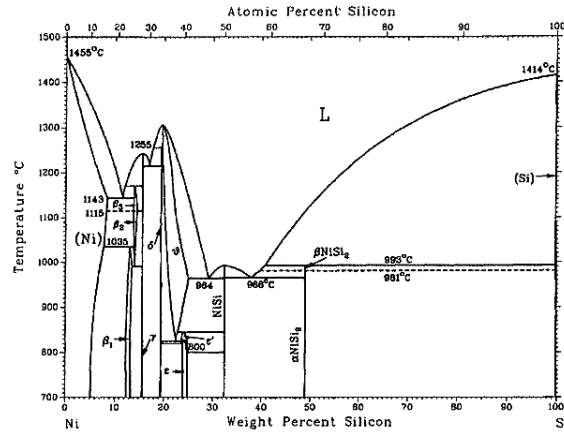


Figure 2.13 Ni-Si binary phase diagram [46]

According to the Ni-Si phase diagram given in Figure 2.13, the melting point of nickel and silicon at the pressure of 1 atm is 1455°C and 1414°C, respectively. The solubility of Si in Ni is rather high and the ordered Ni_3Si (L_{12}) phase is interesting for applications with heat resistant alloys. Silicon performs similarly to boron, although it cannot easily diffuse. Main responsibility is as a self-fluxing temperature suppressant. Secondary duty is as a grain refiner offering strength, oxidation and corrosion resistance at high temperatures.

Ni-P (Nickel-Phosphorus)

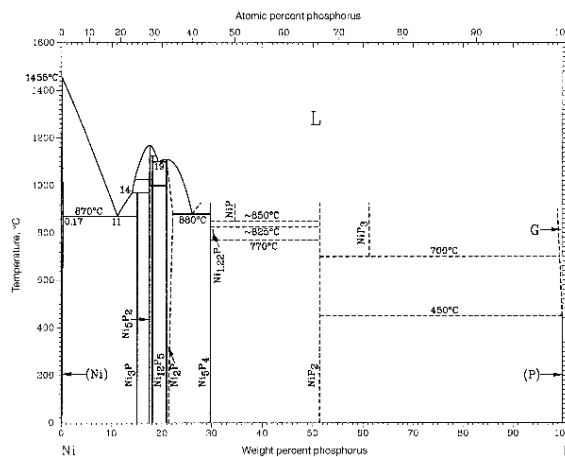


Figure 2.14 Ni-P binary phase diagram [46]

According to the Ni-P phase diagram displayed in Figure 2.14, the melting point of nickel and phosphorus at the pressure of 1 atm is 1455°C and 44.2°C, respectively. The Ni-P binary system has a eutectic reaction at 870°C, the eutectic composition being 11 wt.% P. Phosphorus is an effective element in lowering the melting temperature of Ni-based brazing filler alloys. Presence of P also improves flow behavior of molten BFM. It can be utilized individually, or together with Si in

environment where B is to be avoided or prohibited, for example boron susceptible base materials and nuclear applications, respectively.

Ni-Cr (Nickel-Chromium)

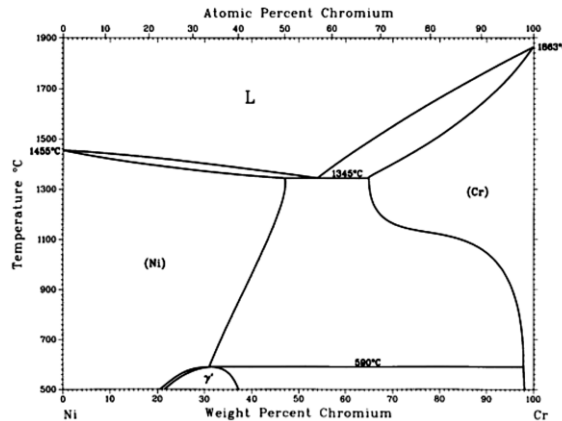


Figure 2.15 Ni-Cr binary phase diagram [46]

According to the Ni-Cr phase diagram showed in Figure 2.15, the melting point of nickel and chromium at the pressure of 1 atm is 1455°C and 1863°C, respectively. The Ni-Cr binary system has a eutectic reaction at 1345°C, the eutectic composition being 47 wt.% Cr. Chromium enhances joint strength, high temperature oxidation and corrosion resistance, being able to generate a dense self-healing Cr_2O_2 surface film. It can also form hard M_xC_y phases.

Various other elements are added to braze filler metals. The purpose and behavior of these alloying elements are listed below.

Cobalt has physical behavior comparable to nickel and can easily replace a major proportion of nickel in precise formulations. When added to nickel alloys, it improves solubility, service temperature and increased matrix creep strength.

Iron promotes flow of the molten alloy and lean towards making a tougher joint. Additionally, it is cost effective, and considered to be a barrier for the migration of base metal elements into the braze joint. On the other hand, it can decrease the corrosion and oxidation resistance.

Carbon is included in the commonly accepted impurities and minor constituents of brazing filler alloys. Consequently, its presence is kept to a minimum. Carbon functions to lower the solidus temperature.

Manganese acts as a melting temperature suppressant.

Tungsten has similar effects as Mo, increases matrix strength and corrosion resistance. Through matrix solid solutioning, it improves resistance to deformation under high temperature stressing. Unfortunately, it has a strong dendritical segregation.

Aluminum fulfills both the function of a grain refiner and an oxidation resistant additive by formation of Al_2O_3 phase. Supplementary, in combination with Ni it forms γ' (Ni_3Al) and β (NiAl) phases.

Copper favors wetting and molten metal flow properties, promoting at the same time corrosion resistance.

Molybdenum in combination with carbon can form complex carbides and strong covalent bonds with Ni. Additionally, it enhances joint strength and controls grain growth and it also increases the rigidity of the matrix.

Titanium and **Niobium** form carbides in the case of excess carbon and make available additional high temperature strength without any side effects. In solid solutions, they increase the corrosion resistance through matrix stabilization.

Germanium lowers the melting temperature and has the ability to toughen the braze. It is regularly observed as a finely dispersed nodular phase.

Lanthanum, Yttrium, Neodymium, Praseodymium and **Cerium** increase oxidation resistance, fluidity of the filler metal and final ductility of the joint and promote grain refinement [47].

2.2.5.3 Reinforcing Materials

In the case of vacuum brazed composite coatings, several types of reinforcing materials can be utilized. They are usually ceramic or intermetallic powders.

The materials generally referred as *cemented carbides* or *hard metal* are in fact an extensive diversity of metal matrix composites in which several kinds of hard ceramic particles are bound together by a ductile metallic binder. The discovery of cemented carbides is fairly recent. After being initially produced in the 1920s, they were employed in industrial applications in the 1930s as carbide-to-steel brazed cutting tools, offering a substantial increase in productivity and quality. Currently, cemented carbides are present in numerous applications that necessitate one or more of the remarkable physical and mechanical properties of these materials. Majority of the cermet materials possess extremely high hardness, high compressive strength, rigidity and impact resistance, excellent wear and corrosion resistance. Representative applications include brazed metal cutting tools, wood cutting tools, abrasive wheels, metal-forming tools such as punches and dies, slitters and rolls, seal rings and valve sets in combustion engines, wear and heat-resistant brazed parts in turbine engines. Several methods for making possible the utilization of cemented carbides in industrial applications have been developed. Brazing is an effective and consistent technique of joining ceramics to metallic materials. The particularities of the brazing process are mostly influenced by a large difference between ceramics and most structural alloy substrates with respect to the coefficient of thermal expansion (CTE) and the high amount of carbide phases in the structure of such materials. Special consideration should be addressed towards assuring sufficient wetting of the ceramics by the molten BFM and diminishing thermal residual stresses in brazements. Nevertheless, the strength of cemented carbide brazed joints is substantially higher, compared to that of ceramic ones, due to presence of metallic phases in the former's structure.

Cemented carbides differ extensively in compositions, but with regard to brazing, tungsten carbide (WC) with a cobalt (Co) binder, whose content may vary from 3 wt.% to 30 wt.%, depending upon the working conditions; have been reported to perform accordingly to the properties expected by the applications of the brazed components. The support materials are generally iron-based alloys such as carbon steels, alloyed, martensitic or austenitic steels. Applications with high-temperature environments employ nickel-based and cobalt-based alloys as support materials.

WC-cemented materials

The main physical and mechanical properties of tungsten carbide and metal binders used in the manufacturing of tungsten cemented carbides are displayed in Table 2.2.

Table 2.2 Physical and mechanical properties of carbides and metallic binders [41]

Carbides or binder	Hardness [HV50]	Melting point [°C]	Calculated Density [g cm ⁻³]	Modulus of elasticity [GPa]	Coefficient of thermal expansion [$\cdot 10^{-6} \text{°C}^{-1}$]
Carbides					
WC	(0001)2200 (1010)1300	≈2800*	15.70	696	(0001)5.2 (1010)7.3
Binders					
Co	<100	1495	8.9	207	16.0
Ni	<100	1455	8.9	207	15.0

*Temperature of dissociation.

Tungsten carbide is typically found in the W-C system under three main phases, namely WC (also called δ -WC), W_2C (with three polymorphs: β at high temperature, β' at intermediate temperature and β'' at low temperature) and the WC_{1-x} sub-carbide, denoted γ .

δ -WC has a simple hexagonal close-packed structure, and is stable at room temperature, with no significant deviation from stoichiometric composition up to 2384°C, it finally dissociates at 2800°C. The δ -phase is also the most technically important. The β and β'' -phases crystallize in the hexagonal close-packed tungsten sublattice, while the β' exhibits an orthorhombic structure. The polymorphs are stable at dissimilar temperatures and compositional ranges. The cubic sub-carbide γ - WC_{1-x} is considered to originate from a eutectoidal reaction between β and δ at the temperature of 2516°C and melts at approximately 2785°C. This phase is a cubic polymorph of the higher tungsten carbide (WC) [48].

Figure 2.16 shows the W-C phase diagram in order to better visualize the temperature and concentration stability range of the system.

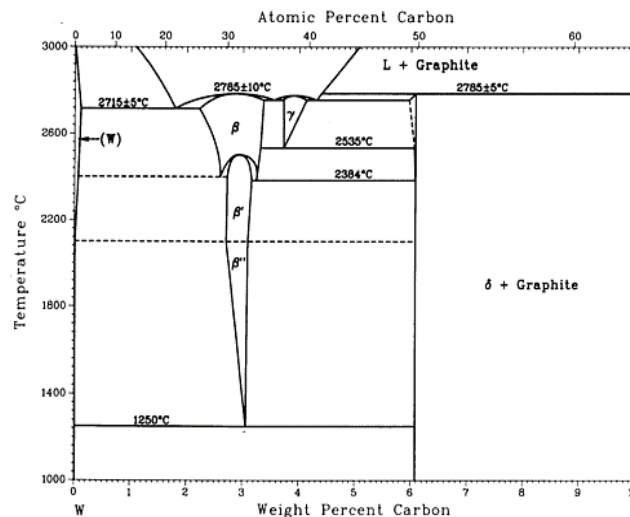


Figure 2.16 Phase diagram of the W-C system [46]

In the production of cemented carbides cobalt is the favored metal binder, due to its remarkable wetting and adhesion to bonded carbide powder. It is a ferromagnetic metal with the Curie point at 1115°C and density of 8.86 g cm⁻³.

The hexagonal close-packed (HCP) crystal lattice is stable up to 415°C, transforming into a face-centered cubic crystallographic structure at higher temperatures, and ultimately melting at 1495°C. Furthermore, Co is a weakly reducing metal, protected from corrosion by a passivating oxide layer.

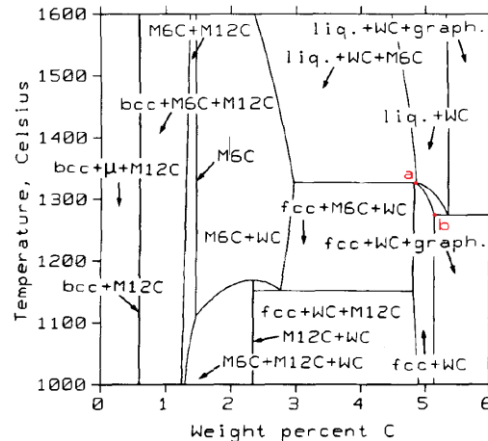


Figure 2.17 Vertical section of the W-C-Co ternary system [49]

The points symbolized by "a" and "b" describe the minimum and maximum carbon concentration of alloys that are in the two-phase state of FCC + WC just after the equilibrium solidification. It is obvious from the diagram presented in Figure 2.17 that alloys with a carbon percentage situated between the points designated by "a" and "b" will comprise, immediately after equilibrium solidification, of a mixture of face-centered cubic Co and hexagonal-close packed WC, only. Certainly, the interval of advantageous carbon percentage ought to be narrowed, when taking into account the precipitation of M₁₂C or graphite, that takes place at lower temperatures [49].

The desired microstructure of Co cemented WC, obtained after cooling from the sintering temperature, comprises of just two phases, namely: WC particles uniformly dispersed in a matrix of face-centered cubic (FCC) cobalt. This is obtained if the proportion between W and C atoms is close to the stoichiometric composition of WC. As Figure 2.17 illustrates, a shortage of C leads to the formation of M₆C (or M₁₂C), whereas an excess of C leads to the development of graphite. The existence of M₆C in Co cemented WC is unwanted as it decreases significantly the rupture strength [50].

The production of WC-Co cemented carbides comprises mixing fine powders of WC and Co precursors and sintering or hot pressing at ≈1400°C. This temperature is higher than the WC-Co eutectic temperature of 1320°C, but lower than the 1495°C melting point of Co, resulting in the formation of a liquid phase during the sintering. The tungsten carbide is partly dissolved in cobalt, with a liquid metal solution encompassing about 30 wt.% of the WC. This liquid wets the remaining WC particles, pending the equilibrium state reached at a WC content of ≈50 wt.%. Under cooling, new carbide particles precipitate, and subsequently, the liquid solution solidifies below 1320°C. Carbide particles continue to precipitate in the solid solution down to room temperature, upon which WC is practically insoluble in cobalt. Consequently, the

resultant cemented carbide (hard metal) is a composite material with the Co matrix recrystallized from the liquid WC-Co eutectic and with a reinforcing phase comprising of partially dissolved initial WC particles and precipitated WC particles that are ready to be dissolved again in the solid Co-based solution during the heating for brazing. The aforementioned structural transformations during the heating cycle point toward the following considerations:

- The brazing temperature ought to be below the WC-Co eutectic point;
- The brazing thermal cycle might affect the structure and properties of cemented carbides;
- The phase composition of the cemented carbide in Co-based solid solution has high WC content at "slow" furnace heating brazing processes;
- In the WC-Co system, the carbide surface is wetted not by pure molten Co but by liquid eutectic at a temperature much lower than the cobalt melting point;
- Especially in the case of furnace brazing, changes in composition and crystalline structure of the base metal may affect the wetting and flow of BFM.

Nickel is seldom used because of the poorer wettability of WC, which consequences leads to lower hardness and fracture toughness compared to cobalt-bonded carbides at equal binder content. In contrast, Ni-cemented tungsten carbide presents increased corrosion and oxidation resistance over WC-Co grades. Similar remarks of structural transformation during the thermal cycle are also reasonable for the WC-Ni system of cemented carbides. The ideal microstructure of WC-cemented powders should exhibit only two constituents, namely carbide grains and the metal binder matrix. The amount of free carbon must be strictly controlled. Excessive carbon content may result in the appearance of free graphite in the cemented carbide structure, but a small amount of graphite has no adverse effect. Nevertheless, shortage of carbon may conclude in the formation of double carbides (e.g., $\text{Co}_3\text{W}_3\text{C}$ or $\text{Co}_6\text{W}_6\text{C}$), known as η -phase, upon rapid cooling which can cause severe embrittlement. Advanced cemented carbides comprise submicron carbide particles to ameliorate toughness and edge strength. Grain refinement is accomplished by integration of up to 3 wt.% of TaC, NbC, VC, or Cr_3C_2 , amid these vanadium- and chromium carbides are the most efficient grain-growth inhibitors.

For applications that involve brazing, it is imperative to consider that the coefficient of thermal expansion (CTE) of carbides is about 2.5 times lower than that of iron-based alloys. The cemented carbides with low cobalt content exhibit minimal CTE. The resistance to failure of hard metal depends mostly on state of stresses: the ultimate tensile strength of cemented carbide is a fraction of approximately 0.5 to 0.7 of their flexure strength and a fraction of approximately 0.3 of compressive strength. Therefore, it is clear that compressive stresses in carbides are tolerable both during and after the brazing process.

Mechanical properties of cemented carbides

High compressive strength and Young's modulus are exceptional properties of cemented carbides. Nevertheless, their ductility is generally low at room temperature: the characteristic values of fracture toughness are in the range of 8 MPa $\text{m}^{1/2}$ to 2.5 MPa $\text{m}^{1/2}$. The fracture toughness of cemented carbides increases with cobalt content and with WC grain size, and decreases with the presence of cubic carbides. Because of the difference in strength and melting point between hard and soft phases, the yield strength and Young's modulus of both cemented carbides and brazements decrease drastically with rising temperature. The compressive yield strength of the cemented carbides at 800°C has a reduction of 50% compared to its room temperature value, and it declines to 30% at 1000°C.

In contrast, the fracture toughness of hard metal displays atypical high temperature behavior. The K_{Ic} parameter of fracture toughness is insensitive to temperature increase up to 600 °C; afterwards it increases rapidly from 22 MPa m^{1/2} to 30 MPa m^{1/2} between 800°C and 950°C.

The decrease in strength and the increase in ductility of the base materials must be taken into account when brazements involving cemented carbides are used at elevated temperatures. Frequently, these modifications are constructive because they bring the mechanical properties of hard metal closer to the properties of the base metals. Therefore, the stress concentration in the brazed joints of cemented carbides to metal is lower at high temperature compared to that at room temperature. Correspondingly, cemented carbides have the following attributes during elevated-temperature operation:

- Strength of cemented carbides at high temperatures remains higher than that of metals;
- Ductility at high temperatures is comparable to that of metals;
- Coefficient of thermal expansion is similar to the CTE of ceramics.

The **corrosion resistance of cemented carbides** depends mostly on the ability of Co or Ni binder to resist chemical or electrochemical attack of the corrosive environment. Consequently, WC-Co hard metal with a high cobalt content are more susceptible to corrosion. Nickel and chromium or both improve the corrosion and oxidation resistance of the metallic binder. Nevertheless, Cr promotes the formation of the carbon-deficient η -phase, therefore affecting the mechanical properties of cemented carbides. Unalloyed WC-Co hard metals are highly resistant to acidic corrosive environments with pH <6, but only moderately resistant at pH = 7 to 8. Correspondingly, WC-Co cemented carbides are not resistant in alkaline working environments. WC-Ni cemented carbides are resistant to acidic corrosive media with pH >2 and highly resistant at pH >7 alkaline environments.

The **thermal stability** of brazed WC-based hard metals depends on the brazing temperature and holding time. WC has a moderately low thermal stability above 1100°C. Free energy, ΔG_0 , equals $-62.28 \text{ kJ mol}^{-1}$ for the decomposition of WC to W₂C at 1100°C giving the reaction exposed in Eq. 2.7.



The significantly negative value of ΔG_0 directs towards an excessive predisposition for WC to decompose. The free carbon developing during decomposition of WC weakens the mechanical properties of the hard metal and has a negative effect on wetting by most brazing filler metals if they do not comprise any reactive elements such as titanium. Therefore, the brazing of cemented carbides at temperatures above 1100°C is not recommended [41].

2.2.5.4 Polymeric Binders

In the current state of the art regarding vacuum brazed composite coatings several binders were found to be utilized in the manufacturing of the flexible polymer bond tapes. Regardless of the filler alloy and reinforcing powders chemical composition, in order to perform the brazing process, the polymer bond tapes require to be subjected to temperatures in excess of 450°C, reaching in some circumstances about 2000°C. Unfortunately, the majority of presently used binding materials generate harmful products under thermal decomposition.

Polytetrafluoroethylene (PTFE)-based binders have been, starting with 1970, and continue to be extensively applied in the production of brazed coatings [51, 52]. Usually, a small amount of PTFE is mechanically worked together with the powder particles, until it fibrillates, entrapping the powder material. Commonly, the amount of polymer varies between 1 vol.% and 15 vol.%. The mixture is subsequently processed into a mat, tape or sheet of desired dimensions. Polytetrafluoroethylene has the advantage of offering superior flexibility and handleability, due to good strength and low modulus of elasticity, for a long period of time, without the need of special storage conditions [53, 54].

The disadvantages of utilizing PTFE are related to the formation of hazardous products during the thermal decomposition. Toxicity is due to irritation of upper respiratory tract and airways, and pulmonary edema caused by the evolution of vapors consisting of carbonyl fluoride, hydrogen fluoride, trace amounts of highly toxic perfluoroisobutylene, and very fine particulates, with diameter size in the range of 0.01 µm - 0.15 µm [55].

Polyethylene oxide (PEO) or polyethylene glycol (PEG)-based polymeric binders employed in the making of vacuum brazed claddings from green braze tape precursors [56] are flexible and water-soluble, but suffer from similar drawbacks when subjected to thermal processes. Formaldehyde (HCHO), a known human carcinogen and some organic peroxides are among the highly toxic products of PEO generated during the thermal decomposition [57].

Polyvinyl acetate (PVA) is an aliphatic synthetic rubbery polymer regarded as an alternative product for flexible tapes manufacturing [30]. Although, PVA is generally considered a nontoxic substance, it contains small amounts of its precursor, vinyl acetate, a known carcinogen. Moreover, inhalation of vinyl acetate irritates the eyes, nose, and throat, and it may also affect the immune system [58].

Nitrile-based compounds are widely used as glues and rubbers in a great variety of areas, from automotive to aeronautical industry, since they are very resistant to fuel and oils. Nevertheless, hardly any studies have reported the utilization of this type of organic binders with the aim to develop polymer bond tapes [59]. Experimental results have shown that this nitrile-based formulation can be successfully applied in the manufacturing of high temperature vacuum brazed coatings. However, it has been stated that thermal decomposition of organic nitrile takes place starting from 300°C, and generates harmful products, such as cyanide [60].

Besides the hazard on human health, several other negative effects may occur during the utilization of the above-mentioned materials. All binder constituents need to be carefully selected, in order to avoid disturbances during the brazing process and to prevent detrimental effects on the furnace components caused by evaporation or decomposition products [61]. Some of these products can be corrosive and deteriorate part of furnace components they come in contact with (chamber, seals,

sensors, pumps etc.). In addition, it is mandatory to filter the hazardous emissions in order to neutralize their toxicity. This process is often very difficult and implicates high costs.

One of the main purposes of this study is to evaluate the feasibility of using a **water-based fugitive organic binder** for the development of high temperature vacuum brazed functional coatings. In this regard, the commercially available Aleene's® Tack-It Over and Over water-based adhesive was used as binder for the manufacturing of the flexible tapes. Its proprietary, special formulation offers a clean alternative to the conventional binders. As specified by the producer, none of its ingredients are known to be hazardous substances (Appendix 1). Consequently, no filtering or additional precaution measures are required. Moreover, it provides superior flexibility and prolonged storage time without alteration of the specific properties.

2.3 Applications of Brazed Coatings

In spite of the fact that the brazing process is generally used as a joining technique, the possibility of using this method as a coating technology was also tested. This option brings fresh and innovative solutions for deposition of functional coatings, assuring also the indispensable characteristics required during service. Brazing manifests the ability to realize joints of high strength, by creating a metallurgical bond between the components. As a coating technique, this method provides high cohesion and adhesion of the cladding to the substrate material. The versatility of this method consists also in the possibility of combining and joining materials that belong to dissimilar groups. Different combination of materials offer usability in specific applications. Accordingly, these overlays are employed as wear and corrosion resistant coatings in a wide range of applications.

Starting with one of the first attestation presented in the patent of *J. Breton et al.* from 1975 [54], interesting areas of application have been suggested. Correspondingly, brazed coatings could be useful as a radiation shield for beta and alpha particles, neutrons and X or gamma radiation. Additionally, the team proposed them as structural elements and electronic resistors and components.

M. R. Dustoor et al. [53] stated that the unique flexibility and handleability of the cloths allows coating of complex geometries like plastics extrusion screws and barrels, valves, router bits, plowshares, diesel engine and oil drills components. In each of the mentioned applications, the claddings were engineered to resist severe environments.

Similarly, *C. Gill* from Conforma Clad [62] brought solutions for the aquafeed and pet food industry concerns regarding extruders wear performance. Even though the process was considered about two times more expensive than OEM parts, the coated components were proven to be from four to eight times more durable and efficient under the same working conditions. *D. W. Bucholz and C. B. Harley* [63], from the same company, presented infiltration brazed coatings that showed prolonged lifetime under erosion conditions, suitable for fly ash conveyance fans in power generation. In the same manner, *D. W. Bucholz and G. A. Saltzman* [64] evaluated the corrosion, abrasion and erosion resistance of the claddings prepared for applications like transport of abrasive materials, mixing, extrusion and injection molding, grinding, metal forming, power generation or general wear protection. They

observed that chromium and nickel addition reduced considerably the abrasion and erosion resistance, while the formability and machinability were increased.

In 2002, *W. C. Hasz et al.*, from the General Electric Company [56], patented the use of brazed claddings for increasing the wear resistance of turbine engine components at elevated operating temperatures (above 650°C). The selected turbine components (nozzle, shroud, shroud hanger, pressure balance seal or combustor components), are generally subjected to part-to-part wear and erosion due to contact with environmental particulates (dirt, sand) that enter the turbine engine during operation. For similar applications, *S. M. Uddin et al.* [65] developed excellent corrosion resistance and mechanical strength titanium-based BFMs combined with graphite additive powders. The formation of TiC phase leads to improved wear behavior in comparison to uncoated titanium alloys.

V. Mammadov et al. [66] focused the attention on improving the efficiency and reliability of centrifugal pumps. Their studies offered promising results with application of infiltration brazed tungsten carbide claddings (IBTCC) for Fluidized Catalytic Cracker Unit recycle pump components. Moreover, it was observed that after 13 months in service the IBTCC displayed no substantial signs of erosion.

Other specific applications, where severe erosion, corrosion and abrasion resistance is required, namely pulp and paper mill active parts were tested by *C. Juliot et al.* [67]. The approx. 800 µm thick coatings were applied to impellers, suction heads and pump casings, and experienced only minimal wear after 13 months of operation, reducing operating and maintenance costs.

Generally, WC-based cermets are widely utilized in fields which require high wear and corrosion stability and resistance. Thus, components such as cutting tools, drill tips, tools and dies are regarded as suitable engineering applications for brazed overlays [68]. Furthermore, brazed WC composite coatings have a great potential for component repairing and dimensional restoration [69].

G. B. Stachowiak investigated the tribochemical characteristics of WC-based claddings in order to determine the wear/corrosion mechanisms in order to associate the coatings to appropriate utilizations. An improved corrosion resistance correlated with superior wear performance is important in applications like industrial slurry pumps, seawater and mine water environments [70].

Besides the already mentioned applications, the high temperature vacuum brazing process is a versatile technique which can be employed in several other areas of exploitation. By combining different materials, further applications can be discovered.

3 Methodology and Equipment

3.1 Equipment and Materials

Main **equipment** used to complete the experimental program is composed of:

- Mixing Device (generic kitchen mixer)
- Rolling Mill (DRM F150 RE, Durston)
- Vacuum Furnace (HITERM 80-200, HITEC-MATERIALS)
- Cut-off Machine (Discotom-2, Struers)
- Hot Mounting Press (ProntoPress-20, Struers)
- Grinding and Polishing Equipment (RotoPol-V, Struers)
- Scanning Electron Microscope (ESEM XL 30, Philips)
- Energy-dispersive X-ray Spectrometer (EDAX)
- Confocal Laser Scanning Microscope (VK-X, Keyence)
- X-ray Diffractometer (X'Pert, Philips)
- Thermogravimetric Analysis Instrument (STA 449 F1 Jupiter, Netzsch)
- Universal Hardness Tester (KB250, KB Prüftechnik)
- Micro Vickers Hardness Tester (ZHV μ , Zwick/Roell)
- Pin-on-Disc Tribometer (TRB, CSM Instruments)
- Universal Testing Machine (5584, INSTRON)
- Potentiostat/Galvanostat (VoltaLab PGP201, Radiometer Analytical)
- Thermostated Electrochemical Cell (CEC/TH, Radiometer Analytical)

The key **materials** used for the experimental program are:

- 16MnCr5 substrate material (Commercially available)
- WC-Co cermet powder (Hoganas AB)
- Ni-based self-fluxing alloy powders (Hoganas AB)
- Water based fugitive binder (Tack-It Over&Over, Aleene's Premium Glue)
- Ethanol, 96% vol., (VWR Chemicals)
- Hydrochloric acid, HCl 38% purity (Sigma-Aldrich)
- Sodium chloride, NaCl, $\geq 99,5\%$ purity (Carl Roth)

The experimental results were processed using the following **software**:

- STA 449 F1 Software Netzsch Data Collector
- Proteus Thermal Analysis, Netzsch Data Processing
- X'Pert Data Collector, XRD Philips
- X'Pert HighScore 3.0, PANalytical
- ImageJ, open access
- VK-X Analyzer, Keyence
- VoltaMaster 4, Radiometer Analytical
- Microsoft Office® 2016
- OriginPro 2016

3.2 Brazing Equipment

3.2.1 Mixing, Rolling and Tape Preparation

A generic kitchen mixer was used to mix the main components of the green tapes, namely the reinforcing phase, metallic filler, and the organic binder in certain compositions. Subsequently, the mixture was turned into flexible tapes with the aid of a rolling mill (DRM F150 RE, Durston), maintaining a constant desired thickness. The obtained tapes were cut to the desired shape and size, and positioned onto the substrate material.

3.2.2 High Temperature Vacuum Brazing

The high temperature brazing process was performed in a HITERM 80-200 cold wall (water cooled) vertical vacuum furnace at a stable vacuum state of $3.5 \cdot 10^{-4}$ mbar. This high temperature vacuum furnace is equipped with a usable chamber of $\approx 140 \text{ cm}^3$, and can reach a maximum service temperature of 2000°C . High vacuum is obtained with the aid of an oil sealed rotary vane pump, assisted by a turbomolecular pump. Accordingly, this type of furnace is well suited for brazing processes of experimental samples. The working parameters can be finely adjusted to perform reliable and high accuracy heat treatments, which in the present case led to the production of coatings with low porosity and a good metallurgical bond with the substrate material.

3.3 Microstructural Characterization

In order to find the ideal working parameters for the brazing development, it is necessary to correlate the optimization process with a severe characterization of the resulted samples. Therefore, the materials as well as coatings developed in this experimental program have been analyzed using Scanning Electron Microscopy (SEM) combined with Energy Dispersive X-ray Spectrometry (EDX) for morphological and structural characterization correlated with X-ray Diffraction (XRD) investigations for chemical and phase composition identification. Moreover, the binding of the coating to the substrate, porosity, crack inside the coating and dilution phenomena were also investigated. Thermogravimetric Analysis (TGA) was employed to evaluate the thermal behavior of the BFM and polymeric binder.

3.3.1 Metallographic Preparation

For the microstructural characterization of the coating, samples require a well-defined metallographic preparation before subjecting them to further investigations. Consequently, the samples were cross-sectioned, embedded (mounted) in a polymer resin, ground and polished to the desired grade.

3.3.2 Scanning Electron Microscopy (SEM)

SEM is regarded as an important method to investigate the microstructure and chemistry of a wide range of materials. It can provide significant information on topography of the studied surface, crystalline structure, chemical composition, or other properties of the specimen. This technique uses electrons in order to obtain an image of the analyzed sample surface. Electrons produced by a thermal emission source, such as a tungsten heated filament, are accelerated and passed through a combination of lenses and apertures to produce a focused beam of electrons, which hits the surface of the sample and interacts with the atoms. The process is conducted under a high vacuum level. The electron beam interaction with the sample produces secondary, backscattered and Auger electrons, as well as characteristic X-rays, and light, which are collected by various detectors [71, 72].

In this experimental program, a Philips XL 30 ESEM device has been used for morphological and structural characterization, offering as main characteristics an acceleration voltage up to 30 kV, resolution up to 2 nm and magnification ranges between 25 X – 250 000 X [73].

The imaging techniques are based on:

Secondary Electrons (SE), which are low energy electrons (< 50 eV) formed when the electrons are ejected from the k-orbitals of the sample atoms by applying the imaging beam. As electrons are negatively charged, positive sources attract them. Consequently, the SE are attracted into a Faraday cage and subsequently are accelerated towards a scintillator. The electrical signal is directed to a photomultiplier and the amplified signal is projected on a display as a video image. The topography of the surface influences the number of electrons that reaches the detector. The variation in the electron intensity creates the image contrast, which reveals the surface morphology.

Backscattered electrons (BSE), which are higher energy electrons (> 50 eV) elastically backscattered by the atoms of the investigated sample. The accelerated beam impacts the surface of the sample, creating elastic and inelastic collisions. Elastic scattering creates changes of the incoming beam trajectory when it interacts with the sample, although kinetic energy remains constant. When the beam hits an atom with a greater atomic number, the likeliness of collision is higher due to the greater cross-section area. The number of electrons returning to the BSE detector is higher and therefore, a brighter area corresponds with elements of higher atomic number Z [74].

3.3.3 Energy Dispersive X-ray Spectroscopy (EDX)

The described SEM is additionally equipped with an EDX spectrometer. This technique is intensively used for elemental analysis of a specimen. To stimulate the emission of characteristic X-rays, a high-energy beam of accelerated electrons is focused onto the investigated sample. The atoms within a sample contain unexcited electrons and the incident beam may excite an electron in the inner shell, ejecting it from its shell and creating an electron vacancy. Another electron from an outer higher energy shell fills the hole and the energy difference between the shells is released in form of X-rays. As the energy of the X-ray is characteristic of energy difference between two shells of an atomic structure, the elemental composition of a specimen can be in this way measured. EDX offers the possibility to detect almost the complete X-ray spectrum of a specimen, with the exception of the first four chemical elements.

Due to their easy manipulation, both SEM and EDX can be used in a wide range of applications, in chemistry, materials science, or materials development. SEM investigations can be easily interpreted and furthermore, materials of different sizes, forms, and shapes can be analyzed. As-polished surfaces or cross-sections, rough, or etched surfaces, and powders can be subjected to SEM or EDX investigations [72, 75].

3.3.4 Confocal Laser Scanning Microscopy (CLSM)

In this experimental program, a Keyence VK-X 3D Confocal Laser Scanning Microscope has been utilized to performed several types of microscopical investigations. This device offers as main characteristics a 16-bit photomultiplier, and 408 nm wavelength violet laser with a 0.5 nm Z-resolution

CLSM is a method of optical microscopy, where a focused beam of a laser is scanned over a sample and the reflected intensity is presented as a function of position to display a digital image of the sample. Scanning of focused laser beams permits the acquisition of digital images of substantially higher resolution, because the resolution is given by the position of the beam and not by the pixel size of the detector. CLSM allows an extensive variety of qualitative and quantitative investigations on complex samples. These investigations comprise of topography mapping, extended depth of focus, 3D visualization etc. CLSMs are built on conventional optical microscopes, although in this case a laser beam is focused onto the sample. The intensity of the laser beam is adjusted by neutral density filters and guided to an arrangement of scanning mirrors that can move them very precisely and quickly. The light is then guided to the objective lens which focuses it onto the sample. Subsequently, the light travels backwards through the same path that the laser does. The purpose of the scanning mirrors on this light is to generate a spot that is not scanning, but rather holds still. This light goes afterwards through a semi-transparent mirror, reflecting it away from the laser and on the way to the detection system. The first object in the detection system is the pinhole aperture, which is in the intermediate image plane of the microscope. This allows only a small central portion of the light through to the light detectors. If reflected light is being examined, it will be passed through a polarizer that will allow only laser light with a different polarization angle from the initial laser light to pass. Any light that emerges from the CLSM's optical system may have a very low intensity, and so the photomultiplier tube (PMT) is used to detect and amplify this light signal. The output from the PMT is an electrical signal with amplitude that is proportional to the initial light signal. This analog electrical signal is converted to a series of digital numbers by an analog to digital converter in the computer. As the laser beam moves along the specimen, the detection system constantly samples and converts the PMT output and displays them on the computer monitor in correct order [76].

CLSMs can perform non-contact, high-accuracy surface measurements on any material or surface shape. When using a roughness meter or contact profiler to measure a surface, there is a risk of damaging the surface of the object, particularly if the material is soft. Additionally, it is impossible to accurately measure any changes in the surface that are smaller than the tip of the stylus. Since laser microscopes perform non-contact scanning of a surface, there is no damage done to even soft objects. Also, with a laser beam diameter that is significantly smaller than a stylus tip, these systems can collect much more accurate data of the surface. Besides the scanning process, laser microscopes also make it much easier to actually measure.

Instead of having to place the stylus in the proper location to collect data, laser microscopes can quickly scan an entire area and measurements can be done at any location on the screen. High-definition 16-bit color images of any object can be obtained without sample preparation. Laser microscopes can provide color images at digital magnifications of up to 28 000 X without requiring sample preparation or a vacuum. These systems are much faster and easier to operate, yet still allow users to obtain high-resolution images. The CLSMs employ high-resolution photomultipliers as light receiving element, that are able to capture incredibly accurate surface data even on steep angles or complex shapes, collecting data over wide areas or on materials with large changes in contrast [77].

3.3.5 X-ray Diffraction (XRD)

X-ray diffraction is a rapid indispensable technique mainly used for non-destructive characterization of thin films, phase identification and quantification of pure materials, simple mixtures, as well as polycrystalline materials based on their crystalline structure. Moreover, it is a common technique to study the crystal structures and atomic spacing of the investigated material [78]. The XRD principle is based on a constructive interference between a monochromatic beam of X-rays and a crystalline specimen. During the analyses, the sample is irradiated with X-rays generated from a cathode tube, which are further diffracted at angles determined by the atomic planes of the specimen. The intensity and spacing of the diffracted beams are unique, function of the analyzed material.

In the present study, XRD investigations were performed with the aid of a X`Pert MPD System from Phillips, Netherland. This device is equipped with a high resolution vertical goniometer and a Cu anode, which is one of the most common target materials for single-crystal diffraction, reaching max. 3 kW and 60 kV [79].

X-rays are formed as the electrons with sufficient kinetic energies interact with the sample. The emitted spectrum consists in a continuous part, called Bremsstrahlung, and characteristic spectral lines corresponding to the chemical elements from the target material [80]. Electrons generated from the cathode filament are accelerated towards the anode, which is typically fabricated from copper, chromium, aluminum or molybdenum. The electrons are slowed down by their interaction with the target plate, producing X-ray emissions.

X-rays have the ability to penetrate the opaque materials, which makes them suitable for a wide range of applications. Two of the most common X-ray diffraction techniques are:

Single crystal X-ray diffraction, which is employed for structures identification of crystalline materials like inorganic compounds or complex molecules. Single crystal X-ray crystallography represents a main method for determining the unit cell dimensions, bond-lengths, bond-angles of the investigated material.

Powder X-ray diffraction, which is mainly used to characterize crystallographic structure, grain size, or preferred orientation in polycrystalline or powder samples. Unknown compounds can be identified by comparing the diffraction data with a standard database.

Diffraction pattern was collected by varying the incidence angle of the X-ray beam by θ and the scattering angle by 2θ , while measuring the scattered intensity $I(2\theta)$ as a function of the latter. This analysis can be successfully applied for investigation of coatings and films, especially if the layers are polycrystalline and have been deposited on flat substrates.

3.3.6 Thermogravimetric Analysis (TGA)

Thermal analysis (TGA) is frequently used to measure physical or chemical changes in a material as a function of temperature. Common thermal analysis techniques include thermogravimetric analysis (TGA), differential thermal analysis (DTA), differential scanning calorimetry, thermo-mechanical analysis, and dynamic mechanical analysis.

TGA is based on an accurate measurement of a sample weight, as a function of temperature and time. This method requires a precision balance, the sample is placed in a thermoresistant crucible and heated up in a controlled manner, with constant heating rate, in a programmable furnace. The atmosphere around the sample can be generally divided into two categories, namely interactive like oxygen or nitrogen and non-interactive such as helium or argon.

DTA measures a difference in temperature between a sample and a reference material by means of a differential thermocouple, being plotted against time or temperature. While TGA measures changes caused by mass loss, DTA can register changes in material where no mass loss occurs, like crystal structure changes, melting, or glass transition temperature. The sample is placed in the crucible and as reference, (usually an empty crucible) is simultaneously submitted to the same programmed time/temperature routine [81].

In the present study, TGA measurements (TGA and DTA) were carried out using an STA 449 F1 Jupiter[®] instrument from Netzsch (Germany), to determine the thermal behavior of the samples as well as the melting temperature of the feedstock powder. This device is equipped with a top-loading system and the silicon carbide furnace (SiC) and operates from room temperature up to 1600°C. The system permits measurements of samples up to 5 grams, having a digital resolution in the nanometric range (0.025 µg). The built-in gas supply unit, with three mass flow controllers for purge and protective gases, offers an optimum control of the working atmosphere. Heating and cooling rates can be chosen in the range of 0.001 K min⁻¹ to 50 K min⁻¹.

3.4 Mechanical Testing

3.4.1 Micro Vickers Hardness Tester

Hardness of the composite coatings was determined with a Zwick/Roell YHVµS microhardness tester using a Vickers microindenter (ISO 6507).

Microindentation hardness testing, more commonly called microhardness testing, is widely used either to measure the hardness of a material or study fine scale changes in hardness, either intentional or accidental. A precision diamond indenter is impressed into the specimen at specific loads situated between 0.01 kg and 2 kg.

Heat treaters have utilized the technique for many years to evaluate the success of surface hardening treatments or to detect and assess decarburization. Metallographers and failure analysts use the method for a host of purposes including evaluation of homogeneity, characterization of weldments, as an aid to phase identification, or simply to determine the hardness of specimens too small for traditional bulk indentation tests. In the Vickers test, a pyramidal diamond indenter

penetrates the surface of the specimen, the load is applied smoothly, without impact. The indenter is held into the test piece for 10 or 15 seconds. The use of diamond allows the Vickers test to be used to evaluate any material (except diamond) and, furthermore, has a very important advantage of placing the hardness of all materials on one continuous scale [82]. The samples are further evaluated (sometimes automatically) using conventional optical microscopy. The measured indentation and the test load are used to calculate the hardness value. Moreover, the indentation technique may be used to estimate the interfacial adhesion of thin films and coatings to a substrate material.

3.4.2 Universal Testing Machine

The evaluation of the mechanical behavior of the brazed samples under conditions of tension was performed to provide basic material characteristics which are critical for component engineering, design and service performance.

Determination of tensile adhesive strength was carried out on an INSTRON 5584 universal testing machine, having in mind the indications of EN 582 standard. This method provides also various information regarding the elastic limit of the materials, elongation, modulus of elasticity, strain or yield point. Tensile tests are conducted on specially prepared test specimens. The sample arrangement has cylindrical geometry, with a diameter of 20 mm, a total length of 62 mm, and a coating thickness of 2 mm. The test is performed by fixturing the specimen into the instrument and applying a force by separating the testing machine crossheads. The speed can be varied in order to control the rate of strain in the test specimen. The measurement of the sample dimensions after the test can provide important information regarding ductility, tensile strength, modulus of elasticity.

3.4.3 Wear Testing and Wear Measurement

For the current work, sliding friction and wear investigations were performed with a CSM Instruments tribometer under a ball-on-disk arrangement, following the instructions of DIN 50324.

Tribological characterization can offer important information regarding friction, wear, and lubrication of materials under defined conditions. There are several standardized test methods designed to simulate a particular type of wear or field of application. The pin-on-disk (POD) test is regarded as a relatively simple investigation which provide a fast answer to the abrasion wear resistance of materials. Typically, in a pin-on-disc wear testing arrangement, a pin is loaded against a plane rotating disc specimen in such a manner that a circular wear track is described by the instrument. This type of equipment can be utilized to evaluate wear and friction properties of materials under dry or lubricated sliding conditions. Either the disc or the pin can serve as test sample, while the other one as static partner (counterface or counterbody). Pins of various geometries and chemical compositions can be utilized. A convenient approach is to utilize balls of commercially available materials such as bearing steel, tungsten carbide, silicon carbide, ruby or alumina as static partner, therefore the name of ball-on-disc is frequently preferred.

The mechanism consists in a stationary partner in permanent contact with the surface of the specimen which is fixed into a rotating mandrel. The pin can have any shape, but spherical forms are usually used to simplify the contact geometry.

3.5 Corrosion Investigation

Potential sweep method (linear voltammetry) is one of the most widely used methods to investigate the electrochemical corrosion behavior of a studied system in an electrolyte solution. Linear voltammetry represents the variation of the working electrode potential in time with a linear scan rate (v) between 2 different values, the initial (E_i) and final (E_f), while the current density value (i) is measured. This technique employs a potentiostatic configuration for the electrochemical cell, which is composed of three electrodes: working electrode or the sample of interest (WE), reference electrode (RE) and counter electrode (CE), placed in the electrolyte solution. The electrodes are connected to an electronic instrument called potentiostat.

Usually, the CE is made off inert materials like platinum, gold, or graphite and practically, it closes the electrical circuit, being not involved in the electrochemical reactions. The RE is a stable electrode with a well-known potential, being used to measure and control the system potential. Currently, a saturated calomel electrode (SCE) has been employed as reference. A Luggin capillary was used for the RE to minimize the electrolyte resistance and samples with 1 cm^2 were prepared as working electrodes for the electrochemical investigations. The working electrodes consist in the samples with 1 cm^2 geometric surface, mounted in a specimen holder. The current flows between the CE and WE, with the response of the later one being detected by the RE.

Potentiodynamic experiments provide a great variety of information regarding pitting, crevice corrosion and passivation behavior for specific sample/solution systems. Moreover, electrochemical corrosion investigations can be used to determine corrosion rates (Tafel slope), active/passive characteristics, passivation rates or anodic and cathodic protection. Tafel slope method offers the possibility to determine the corrosion rate of a tested material using the measured current density values.

The potentiodynamic plot describes de current density dependence on the potential values, being usually represented in a logarithmic form.

The corrosion rate can be calculated using Eq. 3.1:

$$i = i_o \left\{ \exp \left[\frac{2,303}{b_a} (E - E_{eq}) \right] - \exp \left[-\frac{2,303}{b_c} (E - E_{eq}) \right] \right\} \quad \text{Eq. 3.1}$$

where $\frac{2,303}{b_a}$ and $\frac{2,303}{b_c}$ represents the anodic and cathodic slope, b_a and b_c are the anodic and cathodic Tafel plots constants, E_{eq} - equilibrium potential and i_o - exchange current density.

4 Experimental Program

During the current study, for the development of high temperature vacuum brazed functional composite coatings from polymer bond flexible tapes, the following main steps have been taken into consideration:

- **Materials selection;**
- **Manufacturing of polymer bond tapes;**
- **High temperature vacuum brazing;**
- **Characterization of obtained coatings;**
- **Evaluation of results and drawing conclusions.**

Main steps of the experimental program are schematically presented in Figure 4.1.

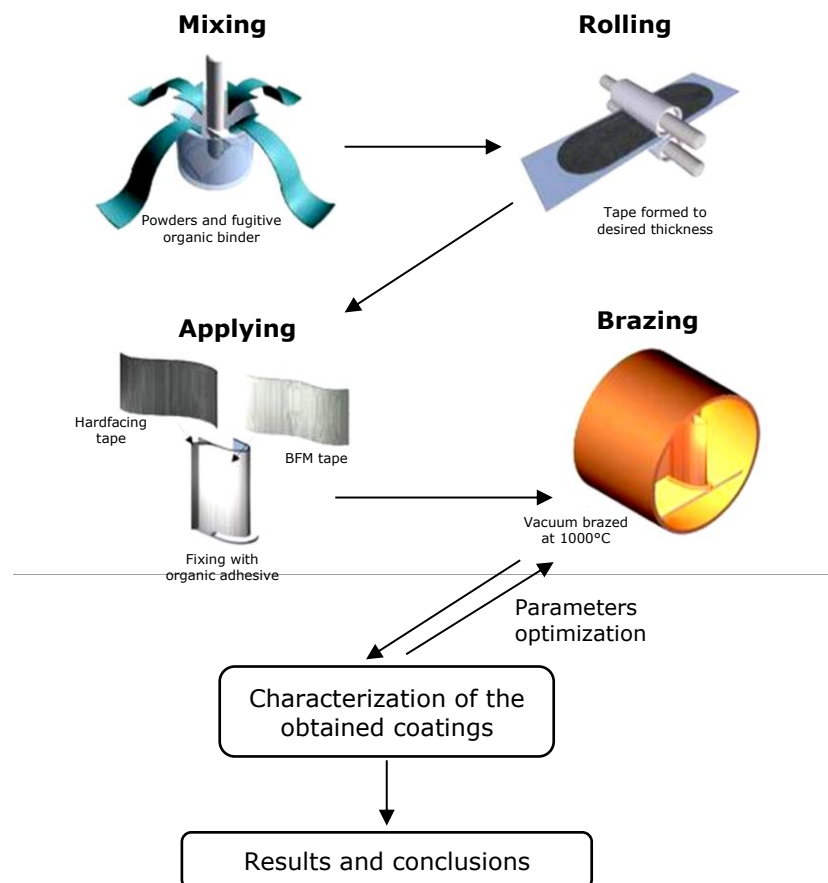


Figure 4.1 Schematic representation of the experimental program

4.1 Materials

Even though the brazing process is usually employed as a joining technique, this study aims to evaluate the possibility of using this method as a coating technology, bringing fresh and innovative solutions for deposition of functional coatings to different surfaces. Brazing exhibits the capability to generate joints with high strength, through the formation of a metallurgical bond between the components. Applied as a coating technique this method concludes in increased cohesion, and adhesion of the coating to the substrate. These coatings are usually employed as protection against wear in a wide variety of applications, most of which requiring at the same time high corrosion resistance.

Utilizing carefully selected brazing filler metal and reinforcing powders with specific chemical compositions, bonded together by certain organic binders, brazing can produce coatings for many different substrate materials, tailored to precise applications. This chapter will introduce the constituents, namely the substrate material, brazing filler alloy, reinforcing material, and organic binder utilized in this study and the reasons for their selection.

4.1.1 Substrate Material

It is undeniable that the base (substrate) material has a major effect on the final properties of the entire component (coating-substrate). Therefore, the substrate must be selected in accordance with the processing, structure, material properties, and service characteristics. As mentioned in Chapter 2, basically every base material is brazable if the appropriate filler metal, brazing technique and optimum process parameters are used.

In the case of this study, 1.7131 (16MnCr5) case hardening steel was utilized as substrate material due to availability and its importance as a structural material. It possesses core strength of 800 N mm^{-2} to 1000 N mm^{-2} , excellent machinability, good brazeability, with a coefficient of linear thermal expansion of $13.9 \cdot 10^{-6} \text{ }^\circ\text{C}^{-1}$ for the interval 20°C to 500°C . This material was also selected due to its substantial role in the production of extrusion screws and barrels, one of the main applications of high temperature infiltration brazed coatings [53, 62]. The chemical composition of the 16MnCr5 steel is presented in Table 4.1, additional information regarding the material is given in the data sheet from Appendix 2.

Table 4.1 Chemical composition of 1.7131 (16MnCr5) steel

	C	Si	Mn	F	S	Cr
1.7131 16MnCr5	0.14-0.19	≤ 0.40	1.00-1.30	≤ 0.025	≤ 0.035	0.80-1.10

Prior to the coating process, the substrate material was machined, in order to obtain several distinct geometries, each of them specific to subsequent investigation requirements. The geometries and correlated dimensions will be specified in the corresponding section. Nevertheless, in all cases the only necessary preparation involved grinding to remove potential oxides or scale from the surface, without the requirement of reaching a specific roughness. Afterwards, the specimens are rinsed with a degreasing solution (ethanol) and dried in a stream of warm air. The cleaned components must be handled with increased attention. These preliminary steps are performed right before the thermal treatment in order to avoid possible recontamination.

4.1.2 Filler Alloy

When deciding on a BFM there are numerous factors to consider. The selected BFM is required to generate a brazement with compulsory strength, ductility, toughness, temperature resistance, erosion resistance, corrosion resistance and stability. It is advantageous if the thermal expansion coefficient of the brazing filler metal is as close as possible to the one of the base metal, in order to avoid residual stresses in the brazement. The BFMs brazing temperature must be inferior to the melting temperature of the base metal but higher than the service temperature during exploitation. The chemical compatibility between the involved materials, namely BFM and BM must be considered, in order to avoid corrosion. BFMs must be able to wet the base metal and fill all gaps to produce strong brazements and avoid generating brittle phases. The price differs greatly between filler metals and it is important to consider if the benefits are worth the use of more expensive materials.

The filler alloy is arguably the second most important component involved in the deposition of high temperature functional brazed coatings. Accordingly, the selected brazing alloy must possess several important characteristics, like: ability to wet the substrate and reinforcing material, and form a strong metallurgical bond, as well as, the capability to withstand the service requirements (wear and corrosion resistance) etc. Moreover, in order to manufacture the flexible overlays, the BFMs must be able to undertake processing through mixing and rolling. Therefore, the metallic binder selected for this thesis will be a powder, part of the Ni-based self-fluxing alloys group. Nickel-base filler materials are regularly utilized in applications where their outstanding corrosion and heat resistance is needed. They are description as high-temperature brazing filler materials. The most frequently brazed base metals are stainless steels as well as nickel- and cobalt-base super alloys. Carbon- and low-alloy steels can also be brazed if explicit properties in the finished brazements are required. Generally, vacuum brazing is the favored heating method for use with these materials [83]. Consequently, after intensive research, a list comprising a total of five potential filler metals was compiled from commercially available products. The draft also included two powders normally intended for thermal spraying techniques, due to similarities in chemical composition, melting range and manufacturer (Höganäs [84]) recommended application areas of the coatings. These are usually gas atomized particles with a well-defined chemical composition, in concordance with the desired properties of the final joint. Chemical composition and melting range of the considered powders are given in Table 4.2.

Table 4.2 Chemical composition and melting range of proposed powders

Powder		Ni wt. %	Cr wt. %	B wt. %	Si wt. %	P wt. %	Fe wt. %	C wt. %	Melting range [°C]	Brazing temp. [°C]
1	1345	Bal.	8.89	1.92	3.75	-	2.81	0.34	980- 1034 [#]	n/a
2	1660	Bal.	14.42	9.23	4.36	-	3.83	0.72	983 [#]	n/a
3	Ni6	Bal.	-	-	-	10.0- 12.0	-	max. 0.06	899 [#]	925- 1095*
4	Ni7	Bal.	13.5- 15.0	-	-	9.7- 10.5	-	max. 0.06	905 [#]	980- 1095*
5	Ni613	Bal.	29	-	4	6	-	n/a	949- 986 [#]	min. 1090*

* Offered by the manufacturer

Determined by DTA

Because the melting range of the BFM plays a major role in the brazing process all five considered powders were firstly subjected to thermal analysis under the same testing conditions, in order to determine their melting temperature. This was necessary because not all powders have a precise melting point or interval offered by the manufacturer, due to variations in the chemical composition of different batches. The DTA measurements are performed with the aid of a thermogravimetric analyzer (Netzsch STA 449 F1) in an Al_2O_3 crucible on approximately 300 mg of powder, under 25 ml min^{-1} flowing N_2 atmosphere, with $15^\circ\text{C min}^{-1}$ heating rate from 30°C up to a final temperature of 1200°C . Region of interest from the powders DTA curves is displayed in Figure 4.2.

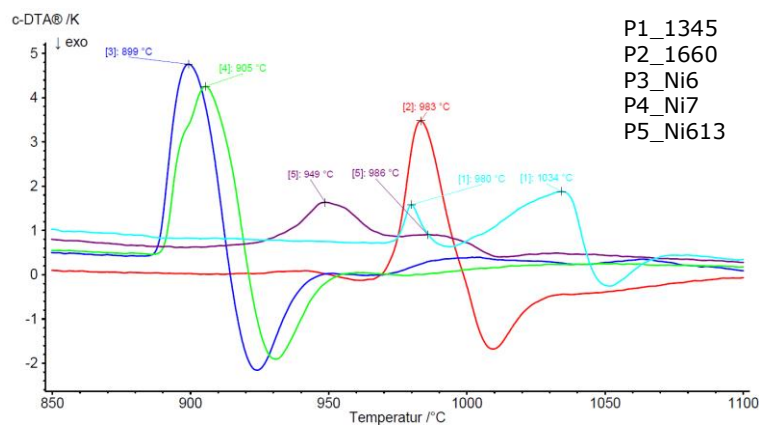


Figure 4.2 DTA curves of the proposed powders

From the DTA thermograms shown in Figure 4.2 it can be observed that two (P1_1345 and P2_1660) out of the five at first taken into account feedstocks have melting temperature above 950°C . This will lead to a brazing temperature above 1100°C , value at which cemented WC starts to undergo thermal decomposition [41]. Moreover, presence of B can cause intergranular erosion of the base material, because of the prolonged thermal cycle, and will limit the application areas of the composite coatings. Furthermore, Fe could reduce the corrosion resistance in aggressive media, further affected in the case of P1_1345 by the Cr content under the minimal amount of 12 wt.%.

Because of the relatively low amount of P (6 wt.%), powder P5_Ni613 also has a melting range situated above 950°C , with a manufacturer recommended brazing temperature of minimum 1090°C . For the present work, the BFM must be molten to an even higher temperature in order to infiltrate and form a metallurgical bond with the substrate. Additionally, BFMs containing alloying elements with high oxygen affinity, namely Si and Cr, necessitate vacuum values much higher during the heating up stages [85]. As the furnace employed in the current study is unable to achieve vacuum levels below 10^{-4} mbar, feedstocks containing such elements should be in this case avoided.

As seen from the DTA curves illustrated in Figure 4.2 and the values from Table 4.2 specimen P4_Ni7 has a slightly higher melting temperature (905°C) compared to P3_Ni6 (899°C), caused by the lower P content. Moreover, the P4_Ni7 BFM manifests an inferior fluidity, producing brazed coatings with higher porosity under the same thermal cycle parameters.

The previous statement was made in response to the microscopic investigations of preliminary high temperature vacuum brazed claddings presented in Figure 4.3.

As a response, the feedstock selected for further investigations and

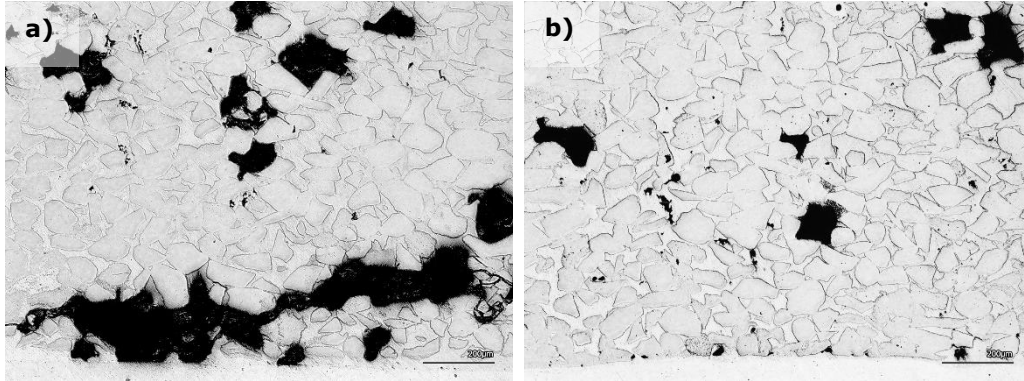


Figure 4.3 CLS micrographs of hardfacing brazed with: a) P4_Ni7, and b) P3_Ni6

manufacturing of flexible tapes intended for the coating deposition is P3_Ni6. This filler metal is a gas atomized powder with a well-defined chemical composition (see Table 4.2). It is suitable for different applications, brazing conditions and braze properties. Applications are found in a wide range of industrial areas such as automotive, nuclear power and aerospace. The most established processing technique is vacuum furnace brazing, it can also be brazed in reducing atmospheres, or under inert gas.

The Ni6 BFM powder presents a dense and homogeneous microstructure, with occasional satellite type formations on the surface of some particles.

Morphology and cross-section microstructure of the selected powder can be observed in the SE micrograph a), and BSE micrograph b) of Figure 4.4.

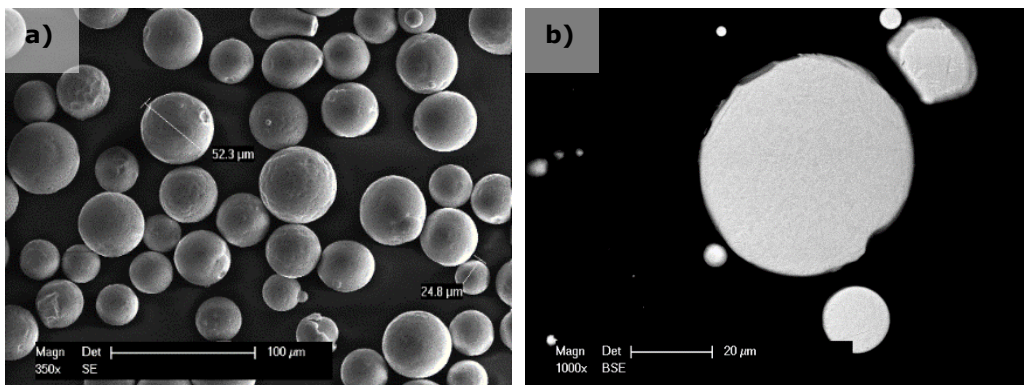


Figure 4.4 SE micrograph a), and BSE micrograph b) of the Ni6 BFM

The EDX spectral analysis performed on the cross-section surface of the selected feedstock powder demonstrates an oxide- and inclusions free microstructure. As denoted by the EDX spectrum displayed in Figure 4.6, the qualitative elemental composition comprises only of Ni and P.

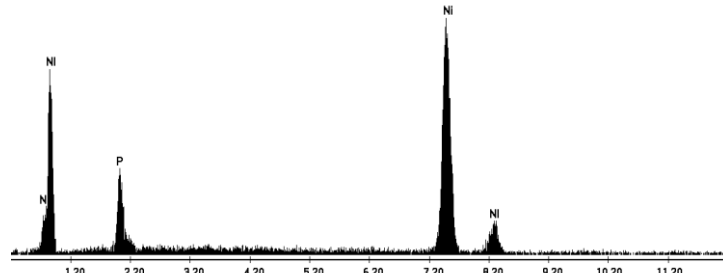


Figure 4.6 EDX spectrum of the Ni6 filler metal

Many of the notable properties of the Ni6 arise from its generic constitution. Clearly it is based on nickel, element that has a melting point of 1455°C. Nevertheless, the melting ranges listed in Table 4.2 show that the resultant material displays a remarkable decrease in melting point, achieved in the brazing filler metal, this reduction being in the order of over 400°C. This effect is obtained by incorporating a powerful melting point depressant, namely phosphorous. However, except for a minute proportion (1 wt.%) P is not present elementally in any significant quantity, but in the form of their lower intermetallic compound with nickel. For the brazing filler metal powder utilized in this study, the phase composition, determined by XRD analysis (see Figure 4.5) consists of 76.8 wt.% Ni₃P, 16.2 wt.% Ni, 3 wt.% Ni₂P, and 4 wt.% NiP. Moreover, the diffractogram showed that this pulverulent material in a highly crystalline one.

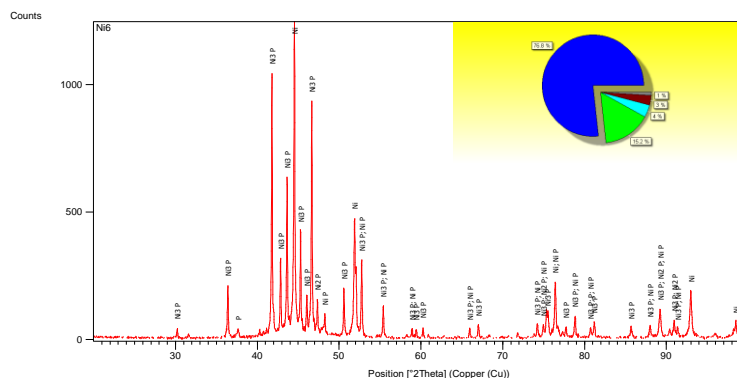


Figure 4.5 XRD pattern of the Ni6 powder

In several aspects, these intermetallic compounds serve to mask the presence of melting point depressants until close to the actual solidus. For example, their elevated temperature properties, although differing from plain nickel, do not rapidly plunge with temperature as the melting intervals might suggest. Nickel-base filler metals retain useful properties close to their solidus values and, in a few carefully monitored applications, above the brazing temperature that was employed. Technically, the nickel-base filler metals depend for their utility on eutectics formed between nickel and the first occurring intermetallic compounds of phosphorous. Because these metalloids are present as compounds, their properties are modified.

4.1.3 Reinforcing Material

In many cases, functional composite coatings must be able to withstand elevated temperature and severe temperature gradients, thermal shock, fatigue, abrasion, attrition, and chemical induced wear and corrosion. Therefore, the reinforcing materials must have high hardness to combat wear, hot strength to overcome the heat involved, and sufficient toughness to withstand dynamic stress or vibrations, occurring under the service conditions.

Tungsten carbide (WC) is notorious for its exceptional hardness and wear/erosion resistance. Hard alloy is basically an aggregate, of hard and brittle tungsten carbide fine particles bonded with a softer metallic matrix by means of liquid-phase sintering. Matrices of ductile metals or alloys, such as cobalt, and/or nickel greatly increase its toughness so that brittle fracture can be prevented. Cemented tungsten carbides are some of the materials with the broadest and most successful use in the production of hard functional coatings. Various processes, counting thermal spraying, laser cladding, fusion welding, have been successfully applied to deposit WC-based hardfacings for numerous applications. The characteristics and properties of cermet materials are resultant from those of the constituents, namely the hard and brittle carbide and the softer, more ductile metallic binder. The applications of coatings that comprise cemented carbides arise due to their particular blend of mechanical, physical, and chemical properties [68].

The reinforcing material selected for this study is a commercially available WC-Co powder obtained from recycling of hard metal tools. This is a crushed cemented carbide, with an angular shape and a granulometric fraction situated between 45 and 500 μm , sold by Höganäs AB under the trade name PA2. The chemical composition given by the producer consists of 5.7 wt.% C, 7.5 wt.% Co and W as balance [86]. Cemented tungsten carbide is an ideal reinforcing material for the manufacturing of functional composite coatings due to its hardness (superior wear resistance), compressive strength, good elevated temperature and corrosion resistance. WC-Co cemented carbides have a low linear expansion coefficient situated between $5 \cdot 10^{-6} \text{ }^\circ\text{C}^{-1}$ and $8 \cdot 10^{-6} \text{ }^\circ\text{C}^{-1}$ for the interval 20°C to 800°C , depending on the ratio of Co. Moreover, in the case of infiltration braze cladding the cermet material retains its general characteristics, because the final brazing temperature will not exceed 1100°C , value at which WC is susceptible to thermal decomposition [41].

Morphology and cross-section microstructure of the WC-Co powder can be observed in the SE micrograph a), respectively BSE micrograph b) of Figure 4.7.

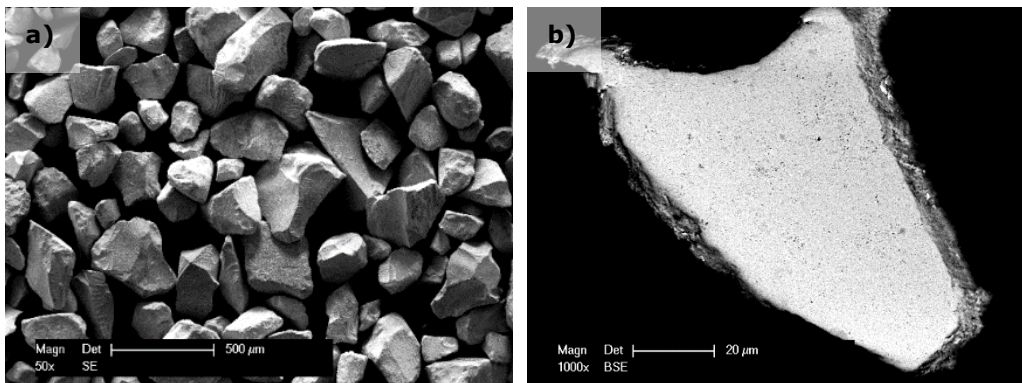


Figure 4.7 SE micrograph a), and BSE micrograph b) of the WC-Co powder

The EDX spectral analysis performed on the cross-section surface of the reinforcing WC-Co powder demonstrates an oxide- and inclusions free microstructure. As denoted by the EDX spectrum displayed in Figure 4.8, the qualitative elemental composition comprises only of W, Co and C.

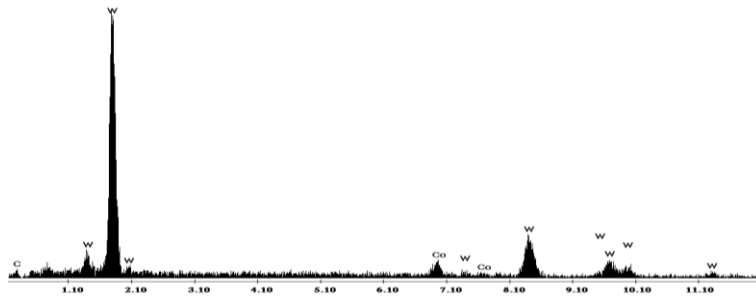


Figure 4.8 EDX spectrum of the WC-Co powder

In order to detect potential phase transformations, due to the thermal treatment, the initial cermet powder was subjected to X-ray diffraction measurements. The diffractogram presented in Figure 4.9 reveals that previous to brazing the material consists purely of 93 wt.% hexagonal close packed WC and 7 wt.% face centered cubic Co.

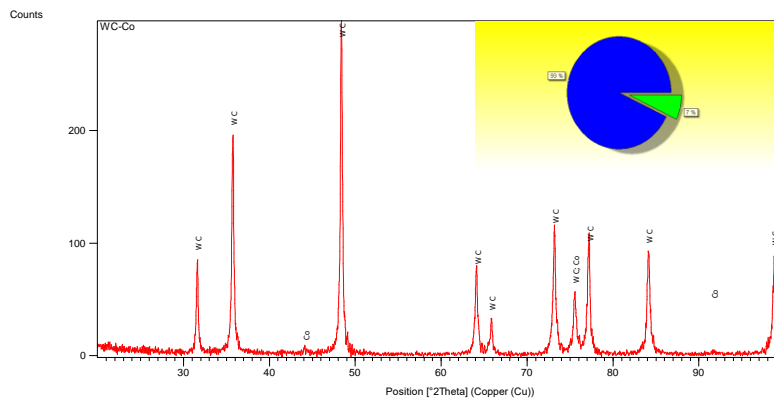


Figure 4.9 XRD pattern for the WC-Co powder

As described in Chapter 2, the desired microstructure of Co cemented WC, obtained after cooling from the sintering temperature, comprises of just two phases, namely: uniformly dispersed HCP WC particles in a matrix of FCC cobalt. This is obtained if the proportion between W and C atoms is close to the stoichiometric composition of WC, more exactly at a carbon content in the range between ≈ 5.65 wt.% and ≈ 5.80 wt.% (see Figure 4.10).

The properties of cemented tungsten carbide (WC-Co) are primarily dependent on their final composition and structure. Minor deviations from the stoichiometric carbon content causes either the formation of graphite or a ternary compound. Both of these phases are usually undesirable, and result in degradation of mechanical properties and performance.

According to the region of interest (ROI) from the vertical section of the WC-Co phase diagram illustrated in Figure 4.10, a shortage of C leads to the appearance of

M_6C . A further decline in carbon content will lead to the formation of $M_{12}C$ carbides. The existence of M_6C in Co cemented WC is unwanted as it decreases significantly the rupture strength. An excess of C leads to the development of graphite inclusions, which significantly reduce the hardmetal service life.

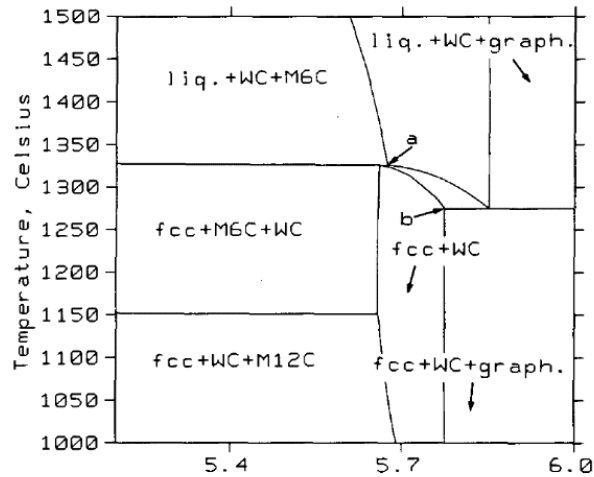


Figure 4.10 ROI of the WC-Co phase diagram vertical section [49]

Therefore, the carbon content must be maintained within narrow limits to obtain the desired composite with optimum properties. It is now well established that two types of η -phase can be obtained – $M_{12}C$ (Co_6W_6C) of substantially constant composition and an M_6C in which the composition can vary within the range of $Co_{3.2}W_{2.8}C$ and Co_2W_4C . The M_6C type of η -phase is in equilibrium with the liquid phase and can nucleate and grow during the sintering process. This not only embrittles the structure by replacing the binder with a brittle phase, but also reduces the effective contribution of WC to the strength of the composite. The $M_{12}C$ type is formed in the solid state (during cooling) with small grains distributed throughout the matrix and is therefore effectively less embrittling [87, 88].

Tungsten carbide has a moderately low thermal stability above $1100^\circ C$, and thus an excessive predisposition for WC to decompose into the W_2C subcarbide and free C. This develops during decomposition of WC weakens the mechanical properties of the hard metal and has a negative effect on wetting by most brazing filler metals if they do not comprise any reactive elements such as Ti [41].

With a 5.7 wt.% C (value given by the manufacturer), the XRD pattern illustrated in Figure 4.9 confirms that the currently employed WC-Co reinforcing powder contains an optimal phase composition. Therefore, as long as the brazing process temperature will not exceed $1100^\circ C$ all desired properties of the reinforcing phase will be kept.

4.1.4 Organic Binder

The commercially available (Aleene's® Tack-It Over and Over) water-based adhesive was used as binder for the manufacturing of the flexible tapes. Its proprietary, special formulation offers a clean alternative to the conventionally used binders. According to the producer, none of its ingredients are known to be hazardous substances (Appendix 1). Consequently, no filtering or additional precautionary measures are required. Moreover, it provides superior flexibility and prolonged storage time without alteration of the specific properties.

Thermal analysis is a feasible way to observe and collect valuable data concerning the thermal behavior of the water based organic binder. The measurements were performed with the aid of a thermogravimetric analyzer (Netzsch STA 449 F1) in an Al₂O₃ crucible on approximately 5 mg of substance, under 25 ml min⁻¹ flowing N₂ atmosphere, with 15°C min⁻¹ heating rate from 30°C up to a final temperature of 1200°C. When the maximum temperature was reached, the system was maintained isothermally for 20 min.

Thermogravimetric analysis (TGA) provided important information about the change in the mass and subsequent decomposition of the organic component (fugitive glue) from the flexible composite cloth upon heating.

From the TG curve shown in Figure 4.11, it was determined that the organic binder loses significant mass in two steps. The minor weight loss, between 100°C and 300°C represents the evaporation of liquids (water), solvents and other volatile compounds, about 3% of the total mass. The second and most relevant decline has a maximum at approximately 480°C, corresponding to the breakdown of around 92% of the entire matter, and relative total decomposition. The maximum decomposition rate of the binder is achieved at around 400°C. The final mass corresponds to the non-flammable compounds existing in the material composition and represents roughly 2% of the initial mass.

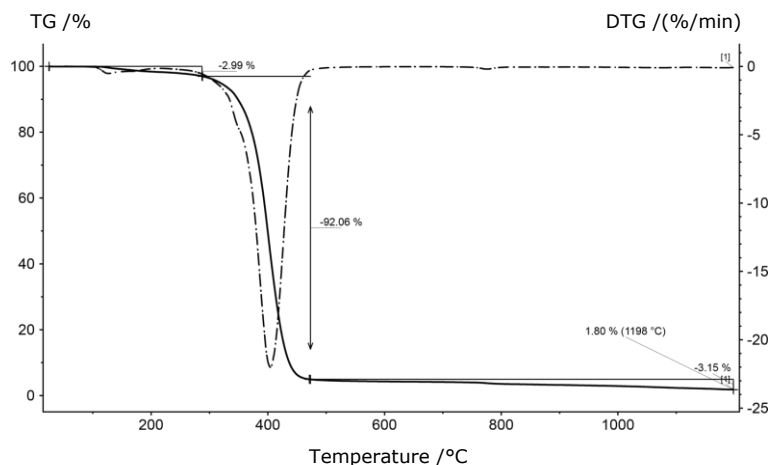


Figure 4.11 TG analysis of the fugitive organic binder

The information retrieved from the TGA curve is vital in the process of establishing optimal parameters of the brazing thermal treatment. Therefore, the temperatures at which the major mass changes occur have to be introduced as holding plateaus in the first heating up section of the thermal cycle.

4.2 Manufacturing of Flexible Tapes

Manufacturing of polymer bond hardfacing tapes involves mixing precise amounts of selected powders and organic binders until the latter one fibrillates, and doing so, anchors the powder particles, allowing further processing steps. The mixture is subsequently rolled to a predetermined thickness, forming a flexible cloth. For this step, a Durston DMR F130 RE manual rolling mill was utilized. Usual cloth thicknesses range from 0.5 mm to 3.5 mm, dimensions outside this interval are also obtainable. Figure 4.12 a) displays a SE micrograph of the brazing filler metal green tape, in which one can easily observe the fugitive glue fibrils that hold together the alloy particles. Complementary, Figure 4.12 b) offers a magnified view of the WC-based hardfacing green overlay. This cloth contains additionally a small amount (around 2 wt.%) of BFM particles in order to promote capillary action during the brazing process.

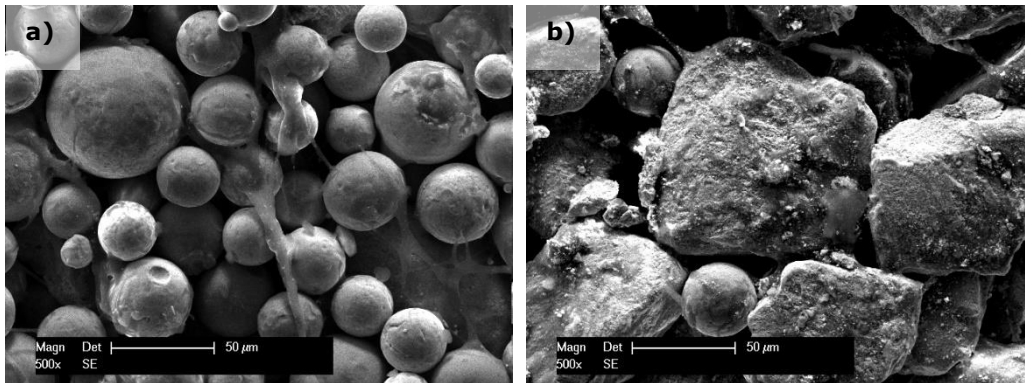


Figure 4.12 SE micrograph of: a) BFM tape, and b) hardfacing tape

The braze coating technique can be performed utilizing a single or multiple arrangement of polymer bond tapes.

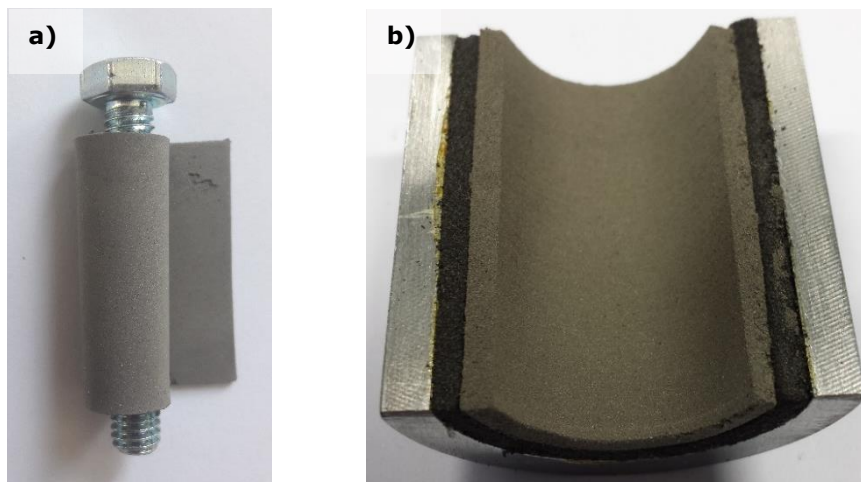


Figure 4.13 Macroscopic images of: a) BFM tape, and b) multiple tape arrangement

As illustrated by the macroscopic images of Figure 4.13, the polymer bonded composite cloths possess high flexibility, for example a 0.5 mm thick tape can be wrap tightly around a M6 bolt.

The advantage of using the single cloth method is its simplicity, containing both the hardfacing material and braze filler metal in one single handleable product. This procedure is handicapped by the three-dimensional shrinkage of the layer during the brazing process. The drawback can be in some cases avoided, applying specially formulated glues to lock the cloth on the substrate surface up to the brazing temperature. Often, the presence of such a compound in the interface region can have a negative effect on diffusion and consequently adhesion strength. Usage of multiple, overlaid tapes, consisting individually of reinforcing particles and respectively matrix material avoids the handicap of single cloth technique. Furthermore, it allows the deposition of multilayer (gradient) and/or much thicker coatings. After the forming process, the cloths can be cut or stamped to shape and immediately overlaid on the areas of components needing protection, or be stored for later use. A small amount of the organic binder is applied onto the clean, oxide-free substrate, holding the tape in place in almost any position, whether it is a horizontal, vertical, inverted or internal surface. For the double or multiple cloth technique, after the WC-based sheet is in place, the overlay composed of braze filler metal particles is glued onto the former.

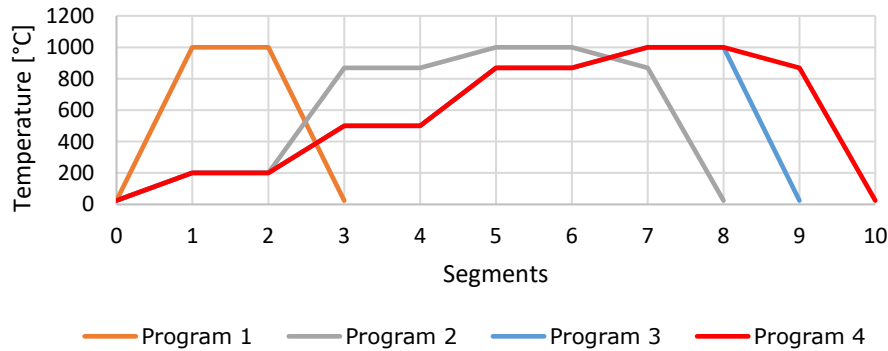
The component thus prepared is subsequently positioned inside the vacuum furnace chamber, in order to be heated above the melting temperature of the BFM. The molten alloy will infiltrate, wet and envelope the hard particles, and diffuse into the substrate generating a metallurgical bond and finally solidifying into a hardfacing.

4.3 Brazing Process Optimization

The high temperature vacuum brazing process was carried out in a HITERM 80-200 cold wall vertical vacuum furnace. The stable pressure of around $3.0 \cdot 10^{-4}$ mbar was achieved with the aid of an oil-sealed rotary vane pump assisted by a turbo molecular pump. In order to determine the optimum parameters for the thermal cycle, a process parameter optimization was performed. Different values for the heating ramps, soaking time, cooling rate and intervals were applied. The four dissimilar heat treatment programs are illustrated in Table 4.3.

A standard, extremely basic set of parameters was utilized as guideline. For this first set of parameters (**Program 1**), heating was performed with the rate of $15^\circ\text{C min}^{-1}$ up to 1000°C followed by a 30 min brazing hold. Finally, a rate of $30^\circ\text{C min}^{-1}$ was applied for cooling the sample down to room temperature.

Table 4.3 Experimental brazing process parameters



	1	2	3	4	5	6	7	8	9	10
Program 1										
Segment	1	2	3							
Type	Ramp	Hold	Ramp							
Duration [min]		30								
Temp. [°C]	1000		25							
Rate [°C min ⁻¹]	15		30							
Program 2										
Segment	1	2	3	4	5	6	7	8		
Type	Ramp	Hold	Ramp	Hold	Ramp	Hold	Ramp	Ramp		
Duration [min]		15		15		30				
Temp. [°C]	200		870		1000		870	25		
Rate [°C min ⁻¹]	15		15		30		10	30		
Program 3										
Segment	1	2	3	4	5	6	7	8	9	
Type	Ramp	Hold	Ramp	Hold	Ramp	Hold	Ramp	Hold	Ramp	
Duration [min]		15		30		15		30		
Temp. [°C]	200		500		870		1000		25	
Rate [°C min ⁻¹]	15		15		15		30		30	
Program 4										
Segment	1	2	3	4	5	6	7	8	9	10
Type	Ramp	Hold	Ramp	Hold	Ramp	Hold	Ramp	Hold	Ramp	Ramp
Duration [min]		15		30		15		30		
Temp. [°C]	200		500		870		1000		870	25
Rate [°C min ⁻¹]	15		15		15		30		10	30

Program 2, employed a three-interval heating, the first heating ramp used a rate of $15^{\circ}\text{C min}^{-1}$ up to 200°C , temperature at which the TGA curve (Figure 4.11) presents the minor weight loss, followed by a 15 min holding time. This step allows solvents, water and other volatile compounds from the organic binder and brazing cloth to evaporate, it also restores the atmosphere quality. Faster heating rates are inadvisable due to potential part distortion and probability of excessive outgassing.

The second ramp increased the temperature up to approx. 10°C below the NiP brazing alloy solidus temperature of 880°C determined by the DTA. Since the experimental samples are relatively small in size, the 15 min stabilization hold at 870°C was sufficient for the temperature to equalize throughout the furnace chamber, the composite to be brazed and metallic substrate and to arrive to the set ΔT and pressure level before proceeding to brazing temperature.

The final $30^{\circ}\text{C min}^{-1}$ ramp up rate to the brazing temperature of 1000°C was as fast as possible, without part distortion or compromise of metallurgical properties, to counteract liquation (separation of metals in the brazing alloy), erosion and excessive alloying of brazing filler with the base metal.

Although the liquidus temperature of the NiP alloy was ascertained by the DTA at 899°C , the manufacturer recommends for the vacuum brazing process between 25°C and 200°C to be added to the normal melting temperature. This concluded in a theoretically applicable brazing temperature interval of 925°C to 1100°C .

The samples were subsequently cooled down by slowly reducing the temperature with a rate of $10^{\circ}\text{C min}^{-1}$ arriving at 870°C , which is 10°C below the solidus temperature in order to allow the molten alloy to solidify in place. This initial low cooling rate also prevents generation of residual stresses caused by the high temperature gradient, due to the differences in thermal conductivity of ceramic and metallic components and phase transformations that occur during solidification.

The final cooling ramp was performed at a rate of $30^{\circ}\text{C min}^{-1}$ until the vacuum furnace chamber reached a stable temperature of 25°C .

Program 3 employed a four-stage heating procedure. The first heating ramp had a rate of $15^{\circ}\text{C min}^{-1}$ up to 200°C , for 15 min of holding time, identical to *Program 2*. The second ramp increased the temperature up to 500°C with $15^{\circ}\text{C min}^{-1}$, corresponding to the second weight loss observed on the TGA curve. This value was maintained for 30 min in order to provide the organic binder sufficient time to decompose, become gaseous and be pumped out by the vacuum system. The longer holding time is necessary due to the relatively high amount of organics that needs to be removed in order to allow the pressure and quality of the atmosphere to return to prior state.

Soaking temperature was set at 10°C below the NiP self-fluxing alloy solidus temperature of 880°C , previously determined by the DTA. Considering that the size of the experimental samples is relatively small, a 15 min stabilization hold at 870°C was once again sufficient. Meanwhile, the pressure level stabilized before proceeding to brazing temperature.

The $30^{\circ}\text{C min}^{-1}$ ramp up rate to the brazing temperature was as fast as possible, without part distortion or compromise of metallurgical properties, to counteract liquation and excessive alloying of brazing filler with the base metal. The liquidus temperature of the NiP alloy that was ascertained by means of DTA having a value of 900°C , together with the producers' suggestions, helped to establish the optimum brazing temperature for the current process. In the case of vacuum brazing, the manufacturer of the filler metal powder recommends one to add 25°C up to 200°C to the normal melting temperature. This concluded in a theoretically applicable brazing temperature interval between 925°C and 1100°C . In practice, it is advantageous to

apply the lowest possible process temperature within the suggested limits that results in adequate joints, to avoid excessive flow of the molten alloy and consequently hot erosion of the substrate. The selected brazing temperature of 1000°C and the 30 min brazing hold provided the optimum conditions for the alloy to melt completely and achieve the mandatory fluidity to entirely envelope the hard WC particles.

The final cooling ramp was performed with a rate of 30°C min⁻¹ until the vacuum furnace chamber reached a stable temperature of 25°C.

The optimized parameters of **Program 4**, followed the exact heating steps and soaking periods of *Program 3*, but the cooling was performed in two stages. Consequently, the samples were cooled down to 870°C by slowly reducing the temperature with a rate of 10°C min⁻¹. This temperature was set 10°C below the solidus temperature of the NiP BFM, in order to allow the molten alloy to solidify in place. This initial low cooling rate also prevents generation of residual stresses caused by the high temperature gradient, due to the difference in thermal conductivity of ceramic and metallic constituents and phase transformations that occur during rapid solidification.

The final cooling ramp was performed with a higher rate. In the case of this study, a cooling speed of 30°C min⁻¹ was applied until the vacuum furnace chamber reached a stable temperature of 25°C. These settings ensured the required metallurgical properties and production needs, while avoiding part distortion and at the same time reducing the process duration.

The characteristics of the obtained specimens were investigated by means of Scanning Electron Microscopy (Philips XL 30 ESEM) and 3D Confocal Laser Scanning Microscopy (Keyence VK-X) combined with an Image Analysis and Processing Software (ImageJ)

Based on the results of the TGA, DTA, selected bibliographic references, suggestions from the NiP powder manufacturer and experience gained from practice of numerous experiments, the initially basic brazing cycle was meticulously optimized.

During the heating up process, the organic binder decomposes at approximately 500°C creating numerous small interconnected pores favorable for the capillary action. As the temperature increases, at 880°C the self-fluxing alloy reaches its solidus temperature. It is mandatory to keep the samples at approximately 10°C below this temperature for a pre-determined soaking time (depending on different factors, like the size, shape and chemical composition of the components to be brazed) in order to have a uniform heat distribution. The final brazing step performed at 1000°C for 30 min assured the high fluidity of the Ni-based alloy necessary for wetting, infiltrating and filling the micro voids. This temperature is also required for the diffusion process along the interface region between the coating and base metal in order to obtain high quality coatings and a strong metallurgical bond.

Microscopic investigations of the samples in cross-section were performed in order to examine the morphology, microstructure and metallurgical bond of the cladding to the substrate material. Microstructure of the composite coatings obtained through the brazing process is shown in the BSE micrographs of Figure 4.14 and the corresponding processed optical micrographs presented in Figure 4.15.

Whereas the cross-sections of the coatings obtained with the parameters of *Program 1* and *Program 2* (Figure 4.14 a) and Figure 4.14 b), respectively) exhibit a high degree of internal porosity and the ones of *Program 3* (Figure 4.14 c) show micro-cracks induced by residual stress, the micrographs of the optimized coatings of *Program 4* (Figure 4.14 d) revealed a very dense structure. Results of the electron microscope investigations proved that the best coating quality was produced by applying the optimized parameters of *Program 4*, which eliminated the initial problem of high porosity, crack evolution and fracture occurrence.

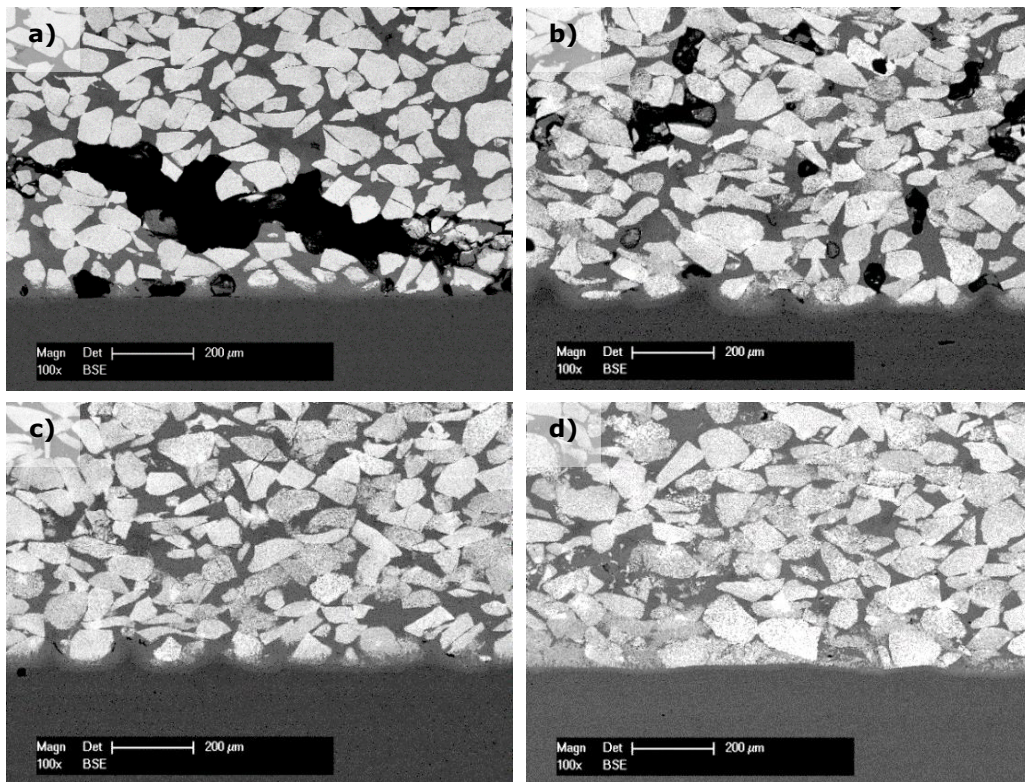


Figure 4.14 BSE micrographs of the WC based claddings deposited with: a) *Program 1*; b) *Program 2*; c) *Program 3*; d) *Program 4*

In order to determine an admissible mean value of internal porosity, optical micrographs have been taken from ten different sectors of the cross-sectioned samples and processed with the aid of the porosity analysis software. It can be clearly observed that the porosity degree decreased from an initial value of around 19% shown in Figure 4.15 a), to nearly 14% for the samples obtained with *Program 2*, exemplified in Figure 4.15 b).

Even though the actual porosity degree of the hardfacings produced with *Program 3* (Figure 4.15 c), is comparable to that of *Program 4*, one cannot overlook the presence of trans- and intercrystalline micro-cracks. In this study, micro-cracks were processed in the same manner as pores, concluding in a relative value of around 2%. A significantly lower value, of approximately 1% resulted in the case of the coatings deposited with the parameters of *Program 4* (Figure 4.15 d), confirming once again the beneficial aspect of the optimization process.

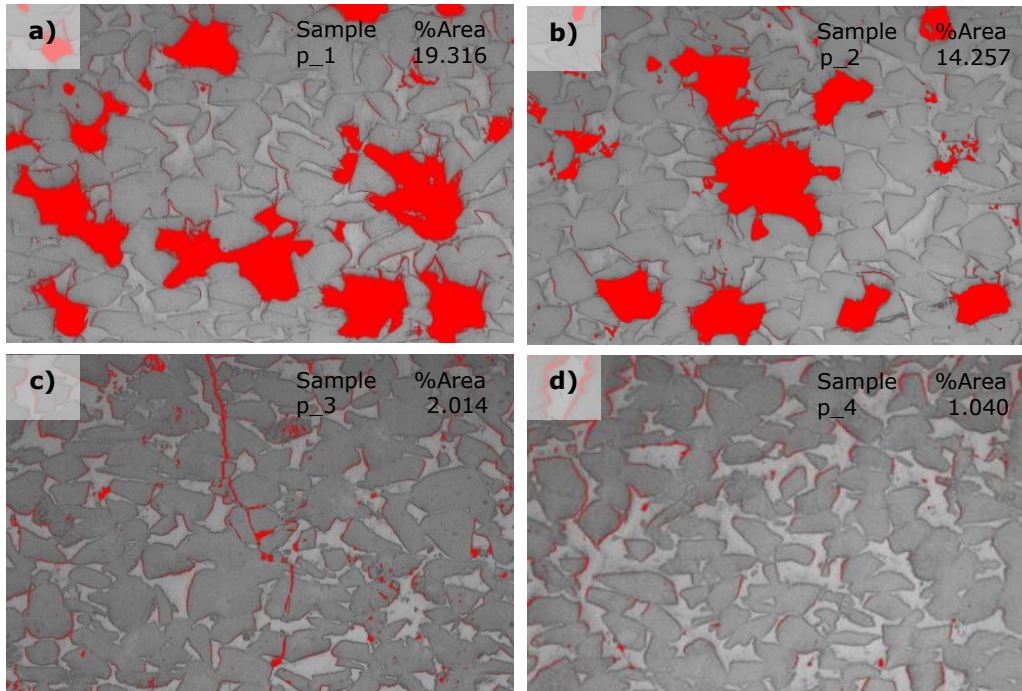


Figure 4.15 Processed micrographs of the coatings deposited with: a) *Program 1*; b) *Program 2*; c) *Program 3*; d) *Program 4*

Porosity degree has a drastic influence on the mechanical properties (e.g. hardness, cohesive and adhesive strength) as well as the tribological and corrosion behavior. Vacuum brazed overlays are barrier coatings, protecting the substrates by isolating them from the aggressive medium, rather than using sacrificial action. That is why the deposit must be as much as possible free of pores and other defects.

The optimized heat treatment leads to deposition of high quality hardfacing coatings with low porosity, a good distribution of both large and small hard phases, excellent metallurgical bond and minimal dilution. Simultaneously, the optimization process has eliminated the initial problem of cracks and fracture building and reduced by almost 20 times the size and occurrence frequency of interconnected and individual pores. This work highlights the crucial importance of optimizing the brazing process parameters for each chemical composition, thickness and combination of flexible composite cloth and substrate material.

4.3.1 Influence of Vacuum Quality

It is well known that the vacuum quality has a great impact on the brazing process and final characteristics of the brazed coatings. The required vacuum level depends largely on the composition of the filler alloy. Chemical elements with high oxygen affinity, like Cr, Mn, B, Si (in increasing order of oxygen affinity, according to the Ellingham diagram), found in the substrate material or reinforcing powder can also have an influence on the necessary oxygen partial pressure [85].

Vacuum brazing is performed in the absence of reducing agents, therefore the basic oxide removal mechanism is by dissociation, according to Eq. 4.1.



Consulting the diagram illustrated in Figure 4.16, one can evaluate the equilibrium oxygen partial pressure for the oxides of interest, as well as its dependency to the system temperature.

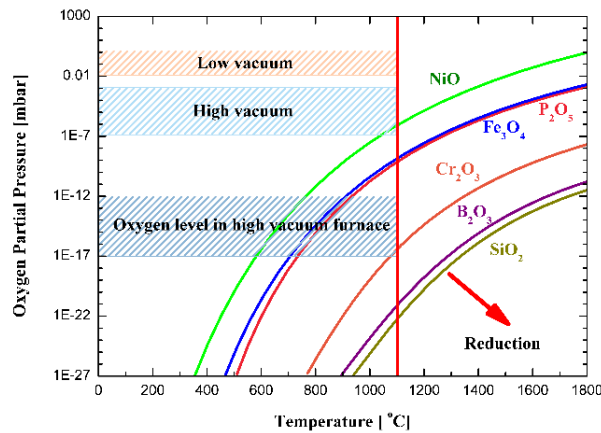


Figure 4.16 Equilibrium oxygen partial pressure for elements of interest relative to the vacuum level [85]

In accordance, at oxygen partial pressure values situated under the curve of each oxide from the diagram, the chemical compound will decompose. Contrary, at values located above every curve, the element will oxidize. Diagram analysis indicates that even the decomposition of less thermodynamically stable oxides, as the ones of Ni, Fe, P demand considerable decrease of oxygen partial pressure. Thereby, even at 1100°C in order to reduce Ni and Fe oxides, which are predominant in the studied brazing system, the oxygen partial pressure must be lower than $1.0 \cdot 10^{-9}$ mbar and $1.0 \cdot 10^{-6}$ mbar, respectively. Nevertheless, it has to be mentioned and taken into consideration that the majority of residual gas present inside the furnace chamber during thermal cycle is represented by the inert purging gas (Ar) and not oxygen. Hence, the vacuum level indicated by the sensors do not characterize the real oxygen potential of the brazing atmosphere, which is actually situated much lower, as seen in Figure 4.16. However, the oxygen partial pressure is still too high to permit reduction of the more stable Cr, B and Si oxides. Therefore, if these compounds are formed during the heating stage, their dissociation throughout the thermal cycle will not be possible. Consequently, the most important stage regarding oxide formation in the case of brazing alloys with high content of Cr, B and Si is the heating step

4.4 Characteristics and Properties of the Brazed Coatings

Due to the vast diversity of possible chemical compositions of substrate material, filler alloy and reinforcing phase, little is known about the characteristics and properties of specific substrate/brazed coating systems.

In this study, WC-Co-NiP functional composite coatings deposited by high temperature vacuum brazing have been subjected to several types of investigations.

4.4.1 Microstructure

All the final properties of vacuum brazed coatings depend strongly on the microstructure. Mechanical properties, tribological behavior, corrosion resistance and many other aspects are all influenced by the size and distribution of the carbides, amount of pores, metallurgical interactions, as well as formation of specific phases. Accordingly, microscopic investigations are conducted utilizing a Philips XL 30 ESEM scanning electron microscope and a Keyence WK-X 3D confocal laser scanning microscope. The porosity degree is evaluated with the aid of the ImageJ open access image analysis and processing software. Elemental analysis of the coatings is carried out by energy-dispersive X-ray spectroscopy with a EDAX XL-30 microanalyzer. Phase identification is performed implementing a Philips X' Pert X-ray diffractometer.

During the high temperature vacuum brazing process, the organic binder decomposes at approximately 500°C, leaving behind numerous interconnected pores, favorable for the capillary action. Simultaneously with the rise in temperature, at 899°C, the Ni-based self-fluxing alloy reaches its liquidus temperature. A 30 min hold at the brazing temperature of 1000°C provides sufficient time for the brazing filler alloy to melt, gain the fluidity to infiltrate, fill the hollow spaces between the WC-Co particles and properly wet them and the substrate. Additionally, this hold ensures the propitious environment for the diffusion process between the braze alloy, cermet particles and base material in order to obtain high quality hardfacings with a strong metallurgical bond.

In connection with the previous statements, the morphology and microstructure of the coating and coating-substrate interface is illustrated in the BSE cross-section micrographs of Figure 4.17.

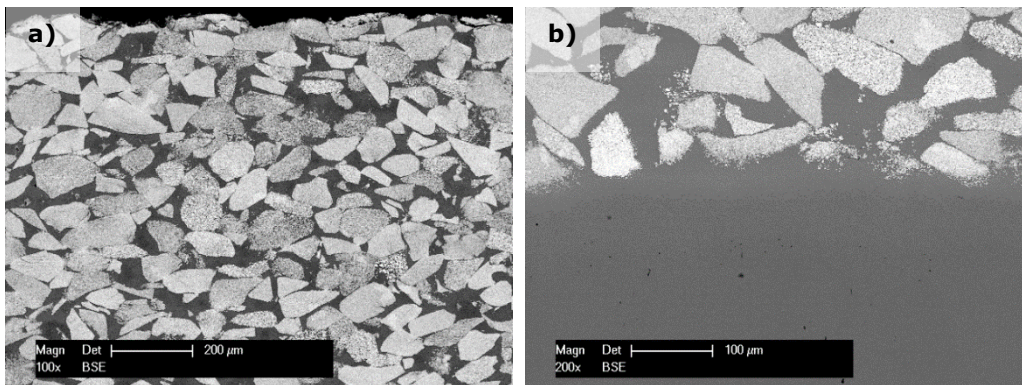


Figure 4.17 BSE micrographs of: a) coating, and b) coating-substrate interface

The high temperature vacuum brazed coatings display a dense structure, with uniform distribution of the cermet particles. One can clearly observe that the molten self-fluxing alloy infiltrated between the WC-Co particles, cementing them together, and at the same time bonding the entire system with the metallic substrate.

The maximum temperature to which the materials are exposed during the brazing process (1000°C) is insufficient to melt tungsten carbide. Although, diffusion from the metallic matrix towards the cemented WC and substrate, as well as dissolution of Co into the matrix has been reported during brazing of WC-based coatings [69]. A similar behavior was also observed in the current study.

A qualitative evaluation of the elemental distribution (without a precise determination of the concentration) was obtained by line-scanning the metallographically prepared sample (see Figure 4.18). The line-scan graph represents the number of X-ray quanta being counted (roughly the amount of element present) in relation to the spatial location along the scan line. Thus, plotting the diffusion profile of the elements comprising the coating-substrate system.

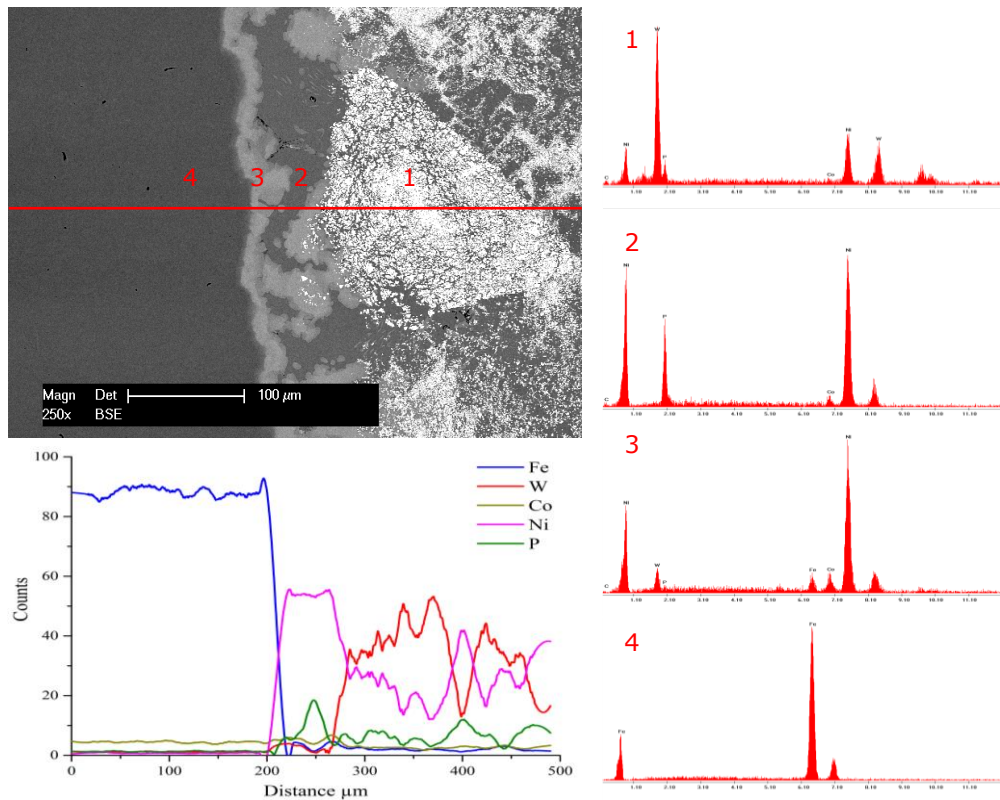


Figure 4.18 BSE cross-section micrograph and EDX spectra corresponding to the line-scan and the four distinct regions across the interface

Furthermore, EDX spectra collected from four distinct regions are also presented in Figure 4.18. In spot 1 (bright grey), the corresponding EDX spectrum indicates the presence of Ni, which confirms the statement regarding the diffusion of elements from the BFM into the cermet particles. Spot 2 is typical for dark grey areas of the coatings' BSE micrographs, and the matching EDX spectrum displays signals of

Ni and P for the eutectic matrix, and diffused Co. The third spot (light grey) was made at the interface region, where the main inter-diffusion reaction between the metallic matrix and the substrate takes place, and solid solution loops are formed. A clean, inclusion and pore free interface can be observed, while the EDX spectrum manifests peaks for Ni, Fe, but also W and Co, due to the dissolution of the hard metal particles. Deeper in the base material, at a distance of about 50 μm (area 4, dark grey), the spot EDX analysis indicates only elements matching the chemical composition of the 1.7131 steel. The EDX scan corresponding to the line drawn on the SEM micrograph further consolidates the data obtained from the microscopic investigations and the affirmations regarding diffusion and alloying, especially at the interface region.

Additionally, in order to better understand the microstructure of the WC-Co-NiP coated 16MnCr4 metallic substrate, as well as the alloying degree, EDX mapping was used to collect information regarding the elemental composition and distribution in the sample. The EDX mapping was performed in the same region as the previously described EDX line-scan investigation.

The representative spectral maps illustrated in Figure 4.19 offers a two-dimensional qualitative analysis, identifying the elements and showing their distribution and relative proportion (intensity) of previously defined elements over the scanned area.

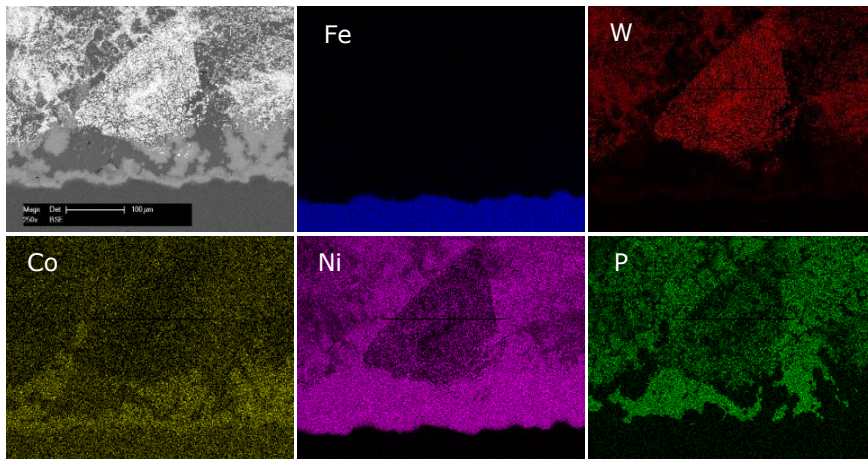


Figure 4.19 SEM micrograph with EDX maps of the WC-Co-NiP coated 16MnCr4 substrate

Accordingly, it is easy to observe that the presence of Fe is limited to the substrate, and in smaller amounts in the interface region. As expected, tungsten is found in the areas corresponding to the WC particles. Nonetheless, it appears to have diffused towards the interface, as shown also by the EDX spectrum 3 from Figure 4.18. But it did so in lesser quantity compared with Co. The latter seems to be the only element that moved into the substrate in a concentration high enough to be detected by both EDX line-scan and the EDX mapping analysis. Concurrently, Ni diffused into the WC-Co particles, replacing part of the cobalt. At the same time, it appears to formed some Ni/Co-rich regions, matching the apparent "missing mass" (part of the dark regions) from the phosphorus EDX map. Phosphorus, as anticipated is concentrated in the areas of high Ni concentrations, and less noticeable in the W- and Co-rich regions. Moreover, seems to have also diffused into the substrate, although in a substantially smaller amount compared to Co.

4.4.2 Phase Composition

The qualitative and quantitative phase composition of the WC-Co-NiP brazed coatings was assessed at room temperature, with a Philips X'Pert diffractometer at 45kV, 40mA (Cu K α radiation). To record the diffraction pattern, the input parameters are: start and end limits $20^\circ < 2\theta < 100^\circ$, step size for $2\theta = 0.015^\circ$, with a step time of 1.5 s. Diffraction data of the crystalline structures is analyzed with the X'Pert High Score and compared with reference patterns from the ICDD and PAN-ICSD databases.

In order to better understand the effect of the thermal cycle on the phase composition and transformations occurring during the brazing process, a small amount of Ni6 powder was molten into a bulk alloy specimen. This sample was heat treated with the exact same parameters utilized for the manufacturing of the brazed coatings (process temperature of max. 1000°C for a 30 min hold).

The XRD pattern of the bulk Ni6 alloy is shown in Figure 4.20, and presents a phase composition consisting of 60 wt.% Ni₃P and 40 wt.% Ni. This is to be expected due to the phenomenon of BFM elements segregation (liquation).

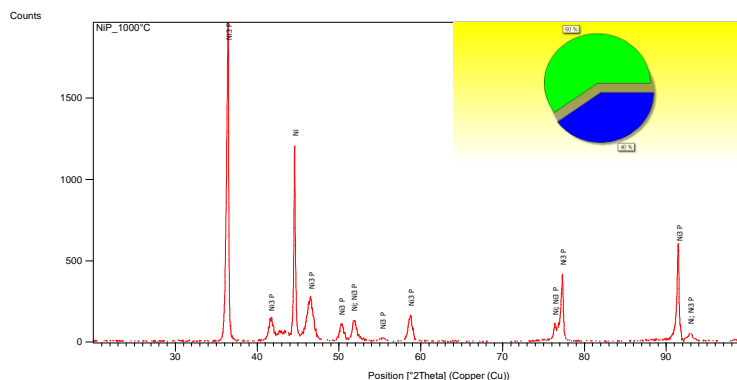


Figure 4.20 XRD pattern of bulk (thermal treated) NiP alloy

Liquation consists in the separation of brazing alloy constituents, and occurs during brazing when the phase composition of the liquid and solid filler metal changes as the temperature increases [42]. This process explains the phase transformation, and the significantly higher amount of free Ni in the heat-treated sample compared to the Ni6 feedstock powder, diffractogram of which is given in Figure 4.5. The resulted phase composition is also consistent with the Ni-P phase diagram, for this particular elemental composition of the brazing alloy.

If it will also be found in the composition of the brazed coating, the high amount of body centered tetragonal Ni₃P phase is expected to offer beneficial mechanical, tribological and corrosion characteristics. Superior hardness, wear and galling resistance of the Ni-P system are especially visible in heat treated state of so-called high phosphorus (10 wt.% - 13 wt.% P) coatings. Adversely, prolonged heat treatment at high temperature (over 1 h at temperatures exceeding 500°C) was observed to have in some cases a negative impact on the corrosion performance. This was due to the transformation from the fully amorphous to a polycrystalline structure [89, 90, 91, 92].

It is expected for the free Ni generated by liquation to diffuse in the coating mass, forming new metallic or intermetallic phases. Moreover, small quantities could

WC (normally resulting in the formation of the more brittle W_2C or W_3C phase) was observed. Presence of other phases (in undetectable quantities) is highly plausible, because of the high number of elements involved.

Even though brazing filler metals containing only Ni and P tend to form softer intermetallic phases, compared to the ones that encompass also Cr and/or B and Si, the superior toughness of the former represents in the case of this study a more desired mechanical property for the metallic matrix.

A comparative representation of the XRD patterns collected from a) as-received NiP (Ni6) brazing filler metal powder, b) NiP alloy obtained from heat treating the Ni6 BFM powder with the optimized brazing thermal cycle, c) as-received WC-Co (PA2) reinforcing powder, d) WC-Co powder heat treated with the optimized brazing thermal cycle, and e) the high temperature vacuum brazed WC-Co-NiP functional coating is given in Figure 4.23.

From the superimposed XRD patterns it is clear that the as-received gas atomized NiP BFM powder experiences during the brazing process noteworthy phase transformations. From the initial composition consisting of 76.8 wt.% Ni_3P , 16.2 wt.% Ni, 4 wt.% NiP, 3 wt.% Ni_2P and 1 wt.% P (see Figure 4.5), after the heat treatment performed with the parameters of the optimized brazing process (Program 4), the phases detected and quantified in the bulk alloy (nugget) comprised of 60 wt.% Ni_3P and 40 wt.% Ni (see Figure 4.20). This accentuated transformation is mainly attributed to dilution. Contrary, the X-ray diffraction performed on the brazed WC-Co-NiP functional coatings do not indicate any presence of free (elemental) Ni. Instead, this element has formed an intermetallic phase with W, more exactly 7 wt.% crystalline $Ni_{17}W_3$. Meanwhile, the free Co (metallic binder of the cermet powder) has diffused, forming 4 wt.% of the tougher tungsten rich η_2 - complex carbide Co_2W_4C [87, 94].

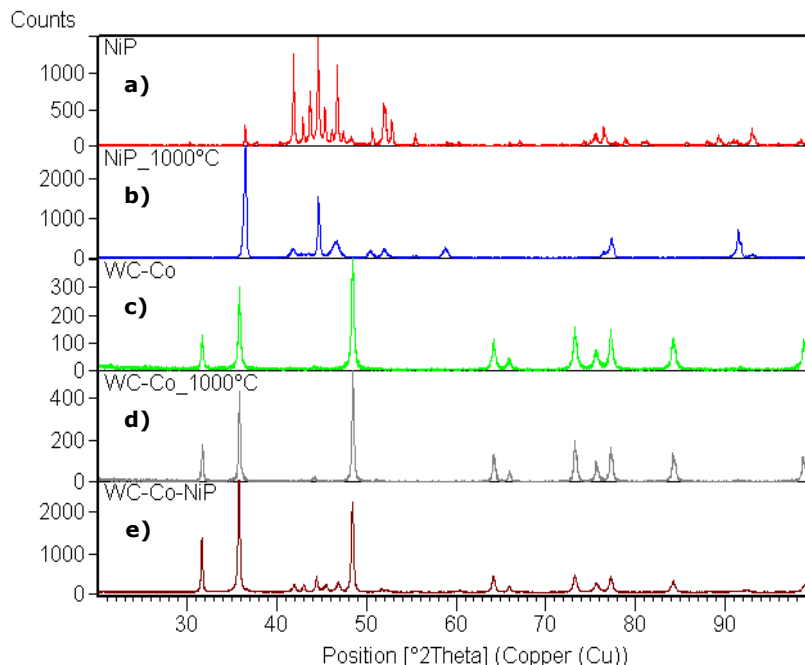


Figure 4.23 XRD patterns of: a) as-received NiP BFM, b) heat treated NiP BFM, c) as-received WC-Co powder d) heat treated WC-Co powder, and e) WC-Co-NiP brazed coating

4.4.3 Mechanical Properties

4.4.3.1 Hardness

Coating surface macrohardness was determined with the aid of a KB 250 BVRZ universal tester, while the microhardness was assessed with Zwick/Roell ZHV μ -S tester equipped with a Vickers microindenter.

Materials hardness is largely characterized by the intermolecular bonds, chemical composition and microstructure. Hardness is the only material property contained within the wear equation established by Archard [36]. Hardness investigations can be performed in depth (cross-section), often applied for coatings, or onto the surface of a sample. In the case of surface hardness evaluation, the indentation load is chosen according to the anticipated hardness of the material, so that the penetration of the indenter will be restricted to the near-surface region. Therefore, indentation indicates the hardness of the surface or near-surface region. The rest of the material may or may not possess equal hardness as that of the surface. Wear behavior of a vast number of material depends on the surface hardness of the solid [1]. Thus, hardness measurements will provide a better understanding of the investigated materials, especially in relation to the tribological characteristic.

Surface hardness values are given in Table 4.4, with the matching indentations illustrated in the CLS micrograph of Figure 4.24 a).

Table 4.4 Surface hardness test values

	1	2	3	4	5
HV10	776	864	1048	1592	768
\bar{x}	1010HV10				

The vacuum brazed WC-Co-NiP composites, deposited during this study exhibit a variable microhardness in the coating cross-section. The values range from a minimum of 647HV1 (metallic matrix) up to a maximum of 1132HV1 (cermet particles), with a mean of 896HV1. Lower hardness values are attributed to pores located in the tested areas, as it can be observed in Figure 4.24 b). The substrate material (1.7313) is known to have 470HV if case hardened and 170HV when soft annealed (see Appendix 2).

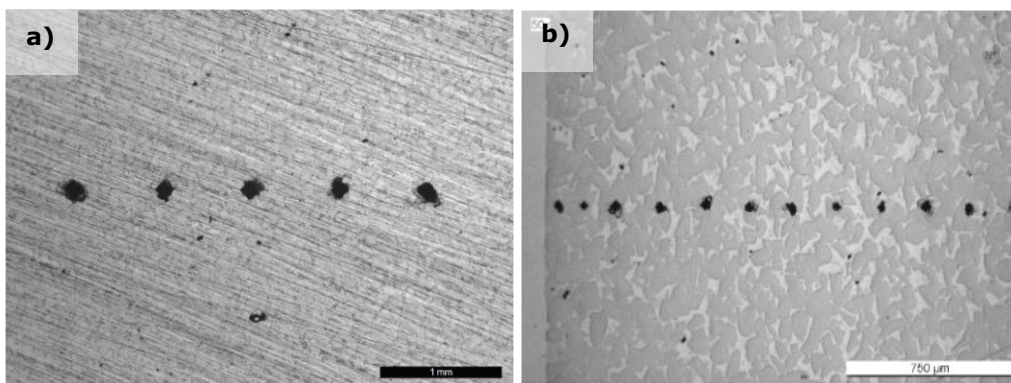


Figure 4.24 CLS micrographs of Vickers indentation: a) surface hardness HV10, and b) coating cross-section HV1

In addition to the microhardness measurements performed into the coating cross-section, which provided the numerical values expressed in Table 4.5, indentations have also been made at interface region with the substrate material.

Table 4.5 Cross-section microhardness test values

	1	2	3	4	5	6	7	8	9	10	11	12
d [mm]	0.2	0.4	0.6	0.8	1.0	1.2	1.4	1.6	1.8	2.0	2.2	2.4
HV1	965	1022	647	1076	968	656	751	939	726	927	1132	947
\bar{x}	896HV1											

Interfacial fracture toughness. Different loads, ranging from 0.1 kgf up to 120 kgf were exercised for a duration of 15 s at the coating-substrate interface, with the intention to determine the adhesive strength. The interface indentation test permits a critical indentation load to be concluded, which in turns characterize the adhesion strength in relationship to an apparent interfacial toughness [95].

For this method, Vickers indentations are utilized to produce and propagate cracks at the coating-substrate interface. By means of a logarithmic scale, the relation between the crack length l_c , including the half diagonal of the indent at the interface, and the applied load P is embodied by a straight line for a specific substrate and a coating thickness e . In some situations (e.g. annealed treated materials), these straight lines are revealed to meet in a sufficiently delimited area to permit the assumption that they converge at a single point. In practical thearms, for a specified coating-substrate system, exists a load independent of the coating thickness, under which the interface will crack. When the applied load is not enough to generate a crack at the interface, the value of l_c is only half from the diagonal of the indent at the interface. This situation relates to an apparent hardness which is the product of both substrate and coating influence. It has been reported by J. Lesage et al. [96] that the diagonal at the interface is the mean of the diagonals which are measured independently for the substrate and for the coating under identical load. Correspondingly, it is then possible to estimate the mean diagonal from hardness tests performed with disparate loads.

The apparent interfacial toughness K_{IC} , function of critical load P_c , and crack length l_c , apparent elastic modulus E_i and apparent hardness H_i of the interface is expressed by the relation developed by D. Chicot and J. Lesage as [97, 98]:

$$K_{IC} = 0.015 \frac{P_c}{l_c^{3/2}} \cdot \left(\frac{E}{H}\right)_i^{1/2} \quad \text{Eq. 4.2}$$

where, the square root of the ration of elastic modulus E divided by the Vickers hardness H at the interface is expressed by:

$$\left(\frac{E}{H}\right)_i^{1/2} = \frac{\left(\frac{E}{H}\right)_s^{1/2}}{1 + \left(\frac{H_s}{H_c}\right)^{1/2}} + \frac{\left(\frac{E}{H}\right)_c^{1/2}}{1 + \left(\frac{H_c}{H_s}\right)^{1/2}} \quad \text{Eq. 4.3}$$

where the subscripts i , s and c represent the interface, substrate and coating, respectively.

Figure 4.25 illustrates a typical mark (in order to ensure accuracy and reproducibility a number of 5 indentations have been performed on each of 3 separate samples), generated by the piramidal diamond penetrator during the interfacial indentation test. What appears to be a crack on the right hand side of the indentation (see Figure 4.25 a) is in fact an optical effect caused by plastic deformation of the substrate material. This observation is supported by the CLS micrograph of Figure 4.25 b).

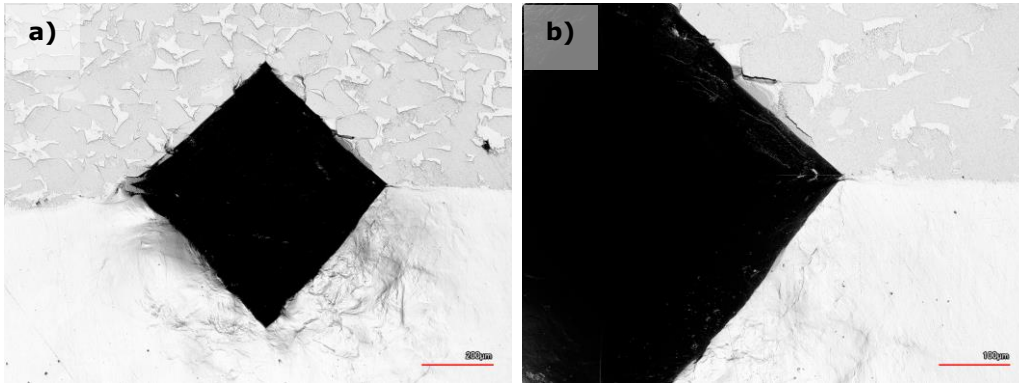


Figure 4.25 CLS micrograph of HV120 indentation at the coating-substrate interface:
a) overview, and b) detail

Because even at 120 kgf (the maximum applicable load with the KB 250 BVRZ hardness tester) a mechanically stable crack could not be generated (see Figure 4.25), and thus no critical load P_c and/or crack length l_c could be determined, the only feasible method to evaluate the adhesion remains the tensile adhesive strength test.

4.4.3.2 Tensile Adhesive Strength

Adhesion of vacuum brazed coatings to the substrate materials has been a primary focus to researchers ever since vacuum brazed composite coatings were introduced to proposed for various applications. This is because the process cannot be effectively employed for industrial exploitation if the coating does not bond well to a substrate.

The adhesion strength of a hardfacing depends on the bonding between the coating and substrate as well as on the coating microstructure. In the case of vacuum brazed coating it is governed by the metallurgical processes (mainly diffusion), especially at the interface region. The bonding between reinforcing particles, brazing filler metal and substrate is critical to ensure the quality of the entire system. Cracking and debonding of the overlay from the substrate material are the two main forms of coating failure. Therefore, the structure integrity assessment of the coatings is mandatory, in order to guarantee the safety and reliability of the coated components. Consequently, investigation on the bonding mechanisms of coating-substrate, which is an important element of vacuum brazed coatings, has lately attracted some researchers' attention [99, 100, 101]. The procedure utilized to evaluate tensile adhesive strength for the current study is the tension test based on EN 582. This test method determines the degree of adhesion (bonding strength) of a coating to a substrate or the cohesion strength of the coating under a tension normal to the surface (see Figure 4.27). The test consists of placing a cut to shape flexible composite cloth between substrate fixture, vacuum brazing them together, and subjecting this assembly of coating and fixtures to a tensile load normal to the plane of the coating. The technique was adaptation of EN 582, which is normally used for testing coatings applied by thermal spray, overcoming its limitations generated by the use of adhesive bonding agents with a maximum tensile strength of ≈ 100 MPa. This test method is still limited to testing the cohesive strength of the coating, if this one is greater than the adhesive bond of the coating to the substrate. The limitation is imposed because the adhesion of the BFM to the WC (ceramic) reinforcing particles is inferior to the metallurgical bond with the metallic substrate. As a result, in most situations (when the brazing parameters are optimized) it cannot reflect the true interface adhesive characteristic because the tensile strength is superior at the interface, compared to the one of the coatings' bulk. However, this evaluation method offers precious information regarding the tensile adhesive strength, a vital aspect for the production of high temperature vacuum brazed WC-Co-NiP functional composite coatings.

Determination of tensile adhesive strength was carried out on an INSTRON 5584 universal testing machine, having in mind the indications of EN 582 and EN 10002. The sample arrangement displayed macroscopically in Figure 4.26, and detailed in Figure 4.27 a) has a diameter of 20 mm, a total length of 62 mm and a coating thickness of 2 mm.

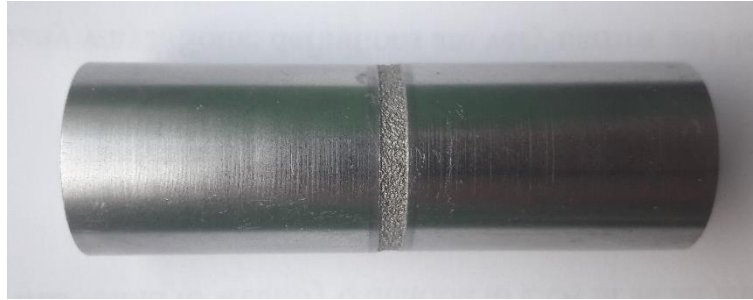


Figure 4.26 Macroscopic image of tensile test sample

The sample is clamped torque-free with the tensioning device into the tensile testing machine, and is tensioned uniform as well as impact-free until fracture (see Figure 4.27 b). As specified in EN 582, increase of the tensile force per second did not exceed (1000 ± 1) N.

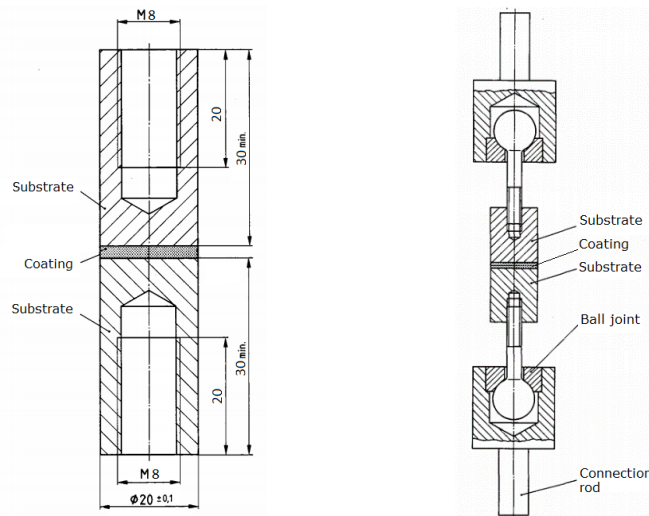


Figure 4.27 Tensile test sample: a) geometry, and b) clamping

Tensile cohesive strength of the coating itself reached a mean value of 150 MPa (determined after three tests), with a mean value for the maximum load of 50 kN, which is well correlated with values reported by other researches [101, 99, 102].

The relatively high elongation (strain) visible on the stress-strain curve of Figure 4.28 is a result of the plastic deformation of the metallic screws used to tension the samples.

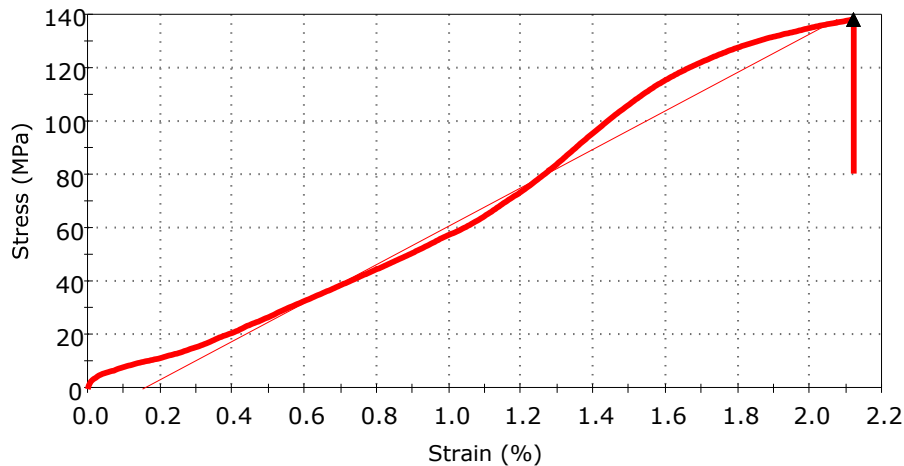


Figure 4.28 Stress-strain curve of the coated specimens

Unfortunately, tensile adhesive strength of the coating-substrate system was unable to be directly determined through this method. Although, according to similar studies, and having in mind that the coating technique is in fact a vacuum brazing process employing the Ni6 BFM and a low alloy steel substrate it is expected for the adhesive strength to reach values around double that of the cohesive one.

The correlation of macroscopic and microscopic fractograms provide valuable data regarding the fracture morphology, vital for a correct interpretation.

Areas susceptible to stress concentration can appear while loaded under working conditions due to considerable differences in microstructure, physical and mechanical properties between the WC-Co cermet, Ni-based metallic matrix and substrate material. Because of the high quantity of ceramic type reinforcement, tensile fracture of the functional coatings is predominantly a brittle one.

As the macroscopic image presented in Figure 4.29 shows, fracture occurred only through the coating, without any noticeable traces of delamination.

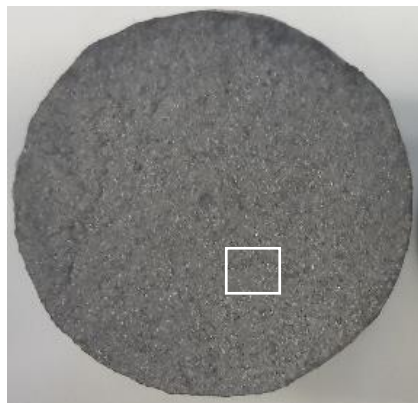


Figure 4.29 Macroscopic image of fractured surface

This fact denotes higher adhesive strength, compared to the cohesive one, hence a superior metallurgical bond between coating and substrate.

Because the surface of the tested sample exhibits a singular fracture mode, detailed examination was performed only in the marked area of Figure 4.29.

Cracks were found to usually propagate through the carbide particles (trans-granular fracture), leaving behind a small amount of plastic deformation in the ductile matrix, as exemplified in Figure 4.30.

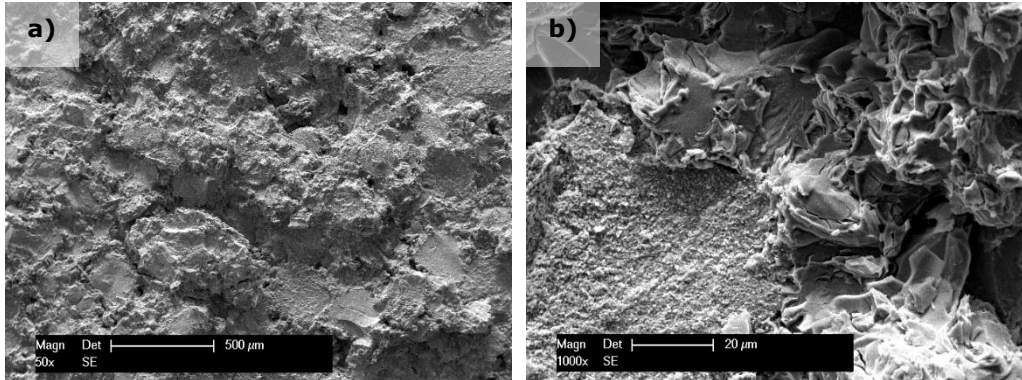


Figure 4.30 SEM micrographs of the tensile fracture surface: a) SE 50X, and b) SE 1000X

4.4.4 Tribological Behavior

Cemented carbides possess excellent resistance to sliding wear and to abrasion wear, even at high temperatures. They are commonly used in the construction of machining tools, sliding bearings, seals, components or parts subject to abrasive wear, chains, rolls for rolling, punches for molding plates, matrices for extrusion. Two limitations characterize these materials: the low formability and the high cost. It is then necessary to fully exploit the potentiality of powder metallurgy for producing near net shape components. Because of this, cemented carbides are often deposited as surface layers by the HVOF technique.

Cemented carbides display a very high sliding wear resistance when dry sliding against steel. In general, wear rate decreases as hardness is increased, i.e., as the amount of metallic binder and the average carbide grain size are decreased. It has been observed that wear was characterized by the progressive removal of the metallic binder.

Cemented carbides are able to retain a relatively high hardness also at high temperature. Therefore, they are also used in dry sliding, where high temperatures are reached in the contact regions, such as in cutting tools. Under these conditions these materials exhibit excellent wear resistance when mating cast iron or non-ferrous alloys, but they do not afford a good performance in sliding against steel. In fact, at high contact temperatures (above 800°C) tungsten carbide grains decompose and then carbon diffuses easily into the austenitic steel phase of the counterface (the chip in case of cutting tools). This leads to a considerable reduction in mechanical strength with a corresponding increase in adhesive wear. However, it has been verified that the addition of titanium and tantalum carbides significantly increases the wear resistance, because these carbides are more stable at high temperature.

Mild wear (and, correspondingly, a low friction coefficient) is attained when the applied pressure is lower than a critical value. In this condition, an asperity-scale brittle contact only may take place, and wear is mild because of the formation of protective scales of compacted and possibly oxidized small wear fragments. But if the applied pressure is larger than a critical value, brittle contact occurs with the formation of quite large fragments, typical of a severe wear regime. Severe wear in ceramics may also be induced by thermal shock phenomena.

In steels (but this applies also for other metals), specific wear rate decreases markedly with increasing hardness. In fact, as hardness increases, the ability of the underlying metal to support the oxide layer also increases.

Ceramic materials (often employed as coatings), display low values of specific wear rate. Ceramics are generally hard, and they are able to maintain their hardness at high temperatures. They undergo mild wear as long as contact pressure is lower than a critical value, and they are not submitted to thermal shocks.

In addition to the cementing metal (Co), the XRD measurements showed that the metallic matrix of the hardfacings comprise a large amount of Ni₃P phase. This nickel phosphide is often encountered in electroless Ni-P coatings, which are known to exhibit excellent microhardness, wear and corrosion resistance. Because of the phosphorus content, the Ni₃P phase possesses a natural lubricity, offering low coefficients of friction in both lubricated and unlubricated conditions [103].

In order to compare the tribological behavior of the WC-Co-NiP coating to that of the 16MnCr5 steel substrate, investigations were performed on a CSM Instruments tribometer with a ball-on-disk arrangement. The total sliding distance was 1890 m (100000 laps) with a linear speed of 15 cm s⁻¹ on a radius of 3 mm, and a normal load of 10 N applied through a 6 mm 100Cr6 ball (static partner). All tests were carried out under dry sliding conditions, at ambient temperature and pressure.

The coefficient of friction (μ) was monitored and registered during the entire testing period and can be observed in Figure 4.31.

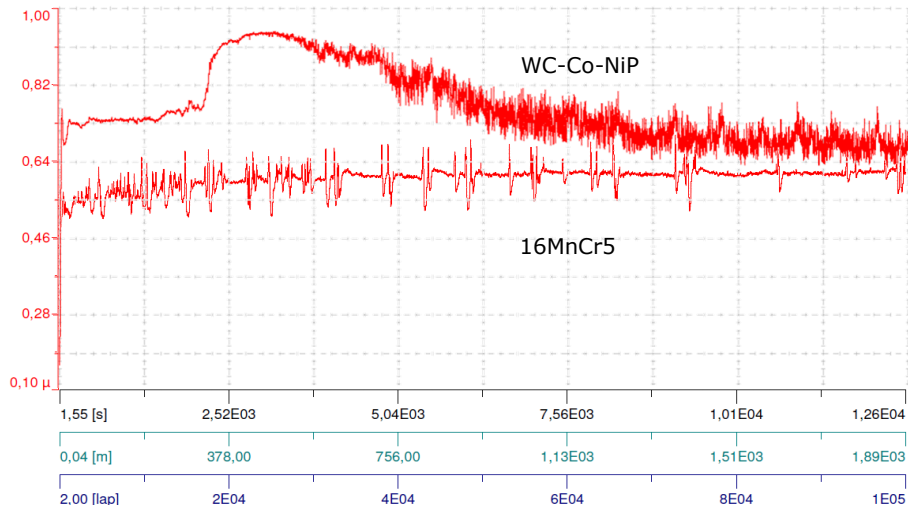


Figure 4.31 COF evolution for 16MnCr5 and WC-Co-NiP vs. 100Cr6

The COF value for both types of samples observed shortly after starting the investigation is also the lowest, more specifically 0.17 for the base metal and 0.16 for the coating. However, it quickly increases, up to approximately 0.55 in the case of

the substrate material and around 0.75 for the coated sample. Simultaneous with the completion of the first couple of laps, a decrease is observed, but this event lasts only an extremely short period. During the next ≈ 1000 laps, the coefficient of friction remains relatively stable for both samples. After an additional ≈ 500 laps, the WC-Co-NiP coating shows an increase in friction, up to the maximal coefficient of around 0.9, due to formation of wear particles locked between the sliding surfaces. Meanwhile, the COF for the 16MnCr5 sample reaches the mean value of 0.6 and enters steady state which lasts until the end of the test. After the short rise in friction value, the hardfacing undergoes a considerable decrease in COF, which subsequently stabilizes at around 0.70. This reduction in frictional force is attributed to the gradual removal of asperities from the hard surface by the softer static partner. Wear particles cannot anchor anymore due to the polished surface.

Conclusively, the coatings experienced a maximal friction coefficient of 0.95, with a mean of 0.77. Substantially lower values were determined in the case of the base metal, with a maximum of 0.70, and an average of 0.60. Minimal coefficient of friction was similar for both investigated materials. The numerical results are given in Table 4.6.

Table 4.6 Coefficients of friction and wear rates for the POD tests vs. 100Cr6 static partner

Sample	COF minimal	COF maximal	COF mean	Wear rate [$\text{mm}^3 \text{N}^{-1} \text{m}^{-1}$]
16MnCr5	0.17	0.70	0.60	$9.07 \cdot 10^{-2}$
WC-Co-NiP	0.16	0.95	0.77	$5.36 \cdot 10^{-4}$

The wear rates assessed after measuring the depth and width of the tracks left behind by the WC-Co static partner are in good agreement with the results of the hardness values. One can clearly notice the difference in sliding wear behavior between 16MnCr5 substrate and WC-Co-NiP functional coating in the micrographs of Figure 4.32.

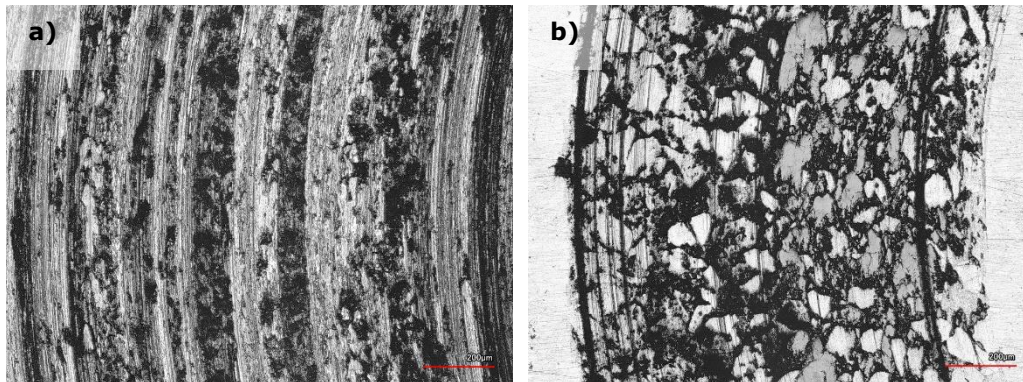


Figure 4.32 CLSM of the sliding wear tracks on: a) 16MnCr5, and b) WC-Co-NiP vs. 100Cr6

The considerably wider and deeper worn track found on the surface of the 16MnCr5 base metal concluded in numerical values for the wear rate of $\approx 9.10 \cdot 10^{-2} \text{ mm}^3 \text{N}^{-1} \text{m}^{-1}$, compared to only $\approx 5.40 \cdot 10^{-4} \text{ mm}^3 \text{N}^{-1} \text{m}^{-1}$ in the case of the composite hardfacing. Furthermore, the formation of an unstable oxide film and galling causing additional friction and adhesion between the static partner and the sliding steel specimen can be observed in Figure 4.32 a) and Figure 4.33 a).

The digital micrographs (see Figure 4.33 b) of the coated surface display areas where the pull-out caused by friction-welding (adhesion) between the coating material and the relatively soft static partner occurred. The presence of adhesion is also denoted by the frequent fluctuations of COF during the second steady state region (see Figure 4.31).

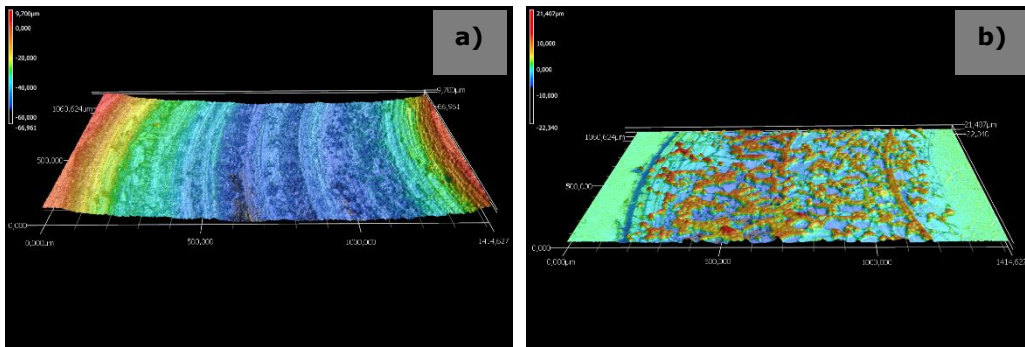


Figure 4.33 Wear track profile of: a) 16MnCr5, and b) WC-Co-NiP vs. 100Cr6

In the case of sliding arrangements involving 100Cr6 against coatings, soft asperities from the two counter surfaces (metallic matrix for WC-Co-NiP coating) adhered strongly to one another, resulting in junctions and material transfer. Subsequently, the auto-lubricating tribo-layer is unstable and repetitively destroyed, reason for the high coefficient of friction for the WC-Co-NiP to 100Cr6 combination.

Even though the wear track for the coated sample is relatively wide, it lacks depth, and thus only superficial. This feature is attributed to the fact that material removal (loss) takes place mostly at the softer 100Cr6 ball.

The SEM micrograph and EDX spectrum of WC-Co-NiP coating against 100Cr6 static partner confirm the previous affirmations, displaying in Figure 4.35 the presence of iron oxide scales onto the surface of the wear track.

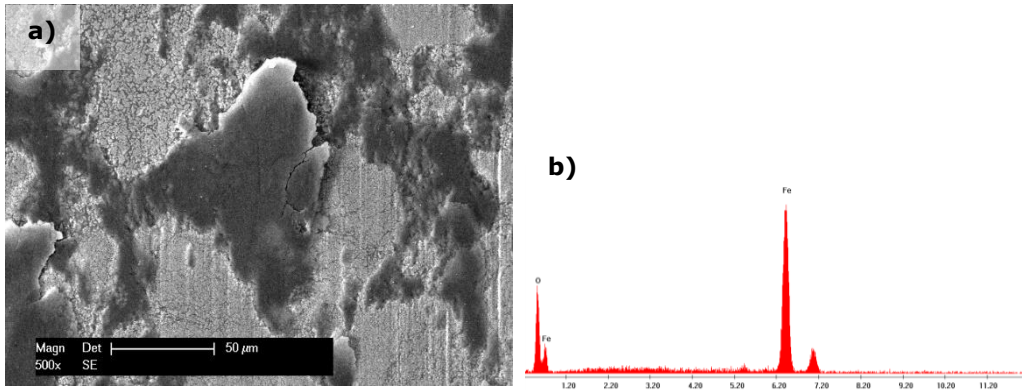


Figure 4.35 SE micrograph a), and corresponding EDX spectrum b) from the wear track

Moreover, the 100Cr6 static partner wear rate concluded in numerical values of around $5.30 \cdot 10^{-6} \text{ mm}^3 \text{ N}^{-1} \text{ m}^{-1}$ against 16MnCr5, and a significantly higher value, of approximately $2.40 \cdot 10^{-5} \text{ mm}^3 \text{ N}^{-1} \text{ m}^{-1}$ against WC-Co-NiP. The substantial difference is clearly noticeable in the digital micrographs corresponding to the worn caps from the 100Cr6 static partner illustrated in Figure 4.34.

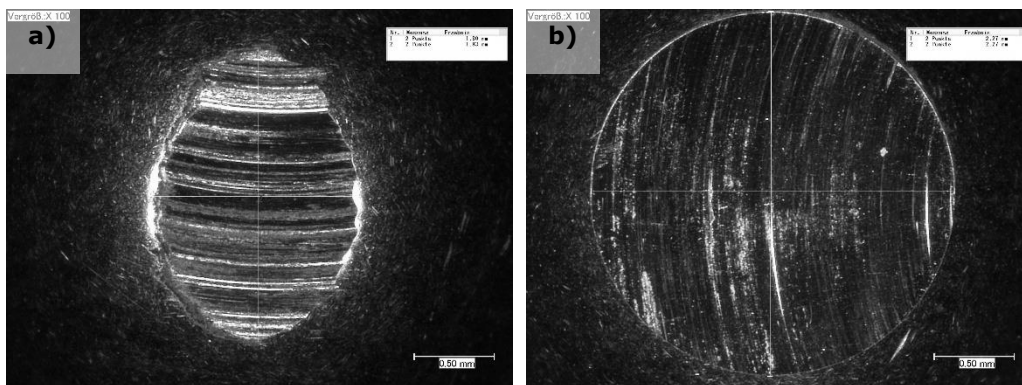


Figure 4.34 Micrograph of the 100Cr6 static partner against: a) 16MnCr, and b) WC-Co-NiP

In case of dry sliding against the hard WC-Co-NiP counterface, the specific wear coefficient, of the softer 100Cr6 steel is quite high. In the case of couplings between similarly hard materials, it is expected to be lower. Accordingly, by a proper selection of a tribological pair it is possible to achieve very low wear rates.

Because friction is not merely a material property, but a system response, tribological POD investigations have also been performed against a WC-Co ball, maintaining the rest of the testing parameters identical as in the previous case.

Accordingly, the coefficient of friction was once more monitored and registered during the entire testing period and can be observed in Figure 4.36.

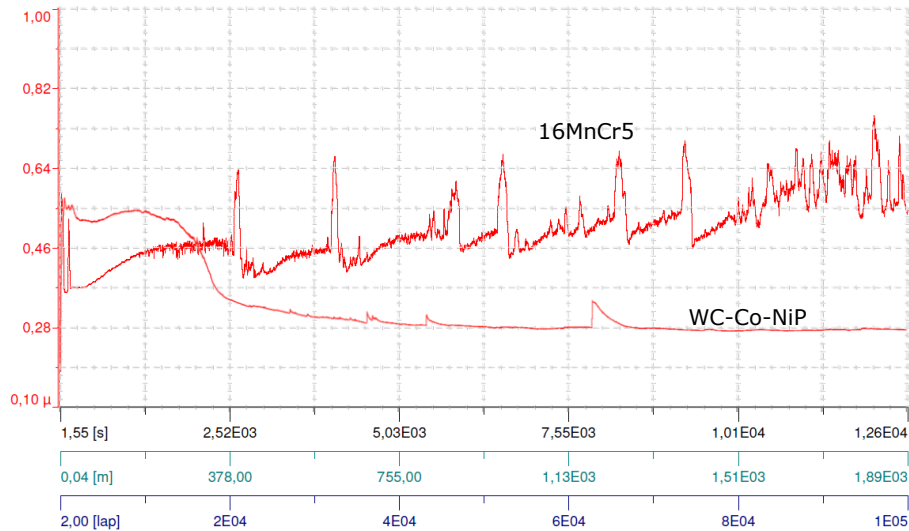


Figure 4.36 COF evolution for 16MnCr5 and WC-Co-NiP vs. WC-Co

Once again, the friction development follows a chronological evolution, with a strong influence on the frictional behavior. Basically, both tested systems start with a run-in stage, followed by a steady-state stage, which the WC-Co-NiP coating maintains until the end of the test, and ends in breakdown in the case of the unprotected 16MnCr5 base metal.

The lowest value for both types of samples coincided with the start of the investigation (0.18 for the steel and 0.21 in case of the coating). However, it quickly changes, when the systems enter kinetic friction, increasing up to approximately 0.55 for both materials. Concomitant with the completion of the first couple of laps, a decrease is observed. This phenomenon lasting only a very short period is due to reduction in surface roughness, being more visible for the substrate material because of the lower bulk hardness. Subsequently, after ≈ 1500 laps, the coefficient of friction rises again for the base metal during the next ≈ 50000 laps. Contrary, after ≈ 1000 laps, the WC-Co-NiP coating shows a lessening in friction, which reaches steady state after ≈ 40000 laps, and remains generally stable, with a coefficient of around 0.28 until the end of the test. Friction reaches quickly a steady-state value, because the coating surface is easily polished by the hard, static partner (WC-Co ball) and probably develops a tribo-layer. When the COF for the uncoated 16MnCr5 sample reaches approximately 0.46 (after ≈ 1000 laps), it also enters steady state. This lasts up until the surface degrades and the friction becomes highly unstable, behavior which is accordant with sever wear. Meantime, the hardfacing shows only a few deviations, attributed to sporadic pull-out of metallic matrix caused by adhesion (friction-welding) [104]. Transferred material from the softer 100Cr6 ball to the hard coating surface hindered the self-lubricating nature of the WC-Co-NiP overlay normally provided by the Ni₃P compound.

Decisively, a maximal friction coefficient of 0.76 was measured during the ball-on-disk testing of the steel substrate, with a mean of 0.50. Significantly lower

values were determined in the case of the functional coatings, registering a maximum of 0.57 with an average of 0.33 (see Table 4.7).

Table 4.7 Coefficients of friction and wear rates for the POD tests vs. WC-Co static partner

Sample	COF minimal	COF maximal	COF mean	Wear rate [$\text{mm}^3 \text{N}^{-1} \text{m}^{-1}$]
16MnCr5	0.18	0.76	0.50	$1.03 \cdot 10^{-3}$
WC-Co-NiP	0.21	0.57	0.33	$1.55 \cdot 10^{-4}$

The wear rates assessed after measuring the depth and width of the tracks left behind by the WC-Co static partner are in good agreement with the results of the previous investigations (microhardness, coefficient of friction). One can clearly notice the difference in sliding wear behavior between 16MnCr5 substrate and WC-Co-NiP functional coating in the micrographs of Figure 4.37.

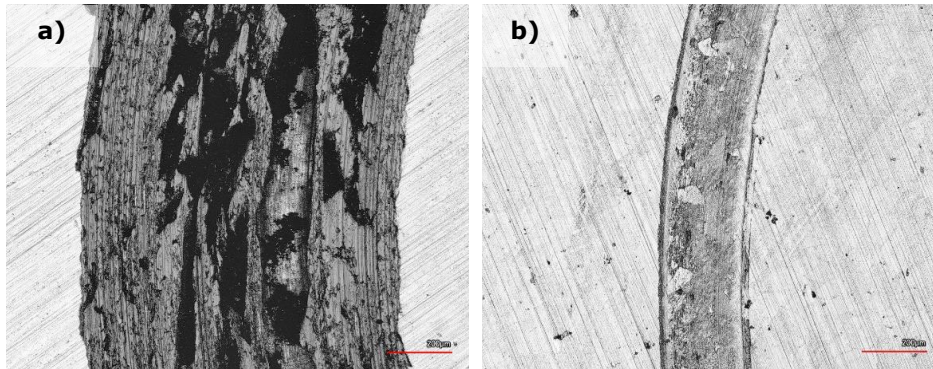


Figure 4.37 CLSM of the sliding wear tracks on: a) 16MnCr5, and b) WC-Co-NiP vs. WC-Co

The considerably wider and deeper worn section found on the metallic surface concluded in numerical values for the wear rate of $1.03 \cdot 10^{-3} \text{ mm}^3 \text{N}^{-1} \text{m}^{-1}$, compared to only $1.55 \cdot 10^{-4} \text{ mm}^3 \text{N}^{-1} \text{m}^{-1}$ in the case of the composite hardfacing. Furthermore, the formation of an unstable oxide film and galling causing additional friction and adhesion between the static partner and the sliding (rotating) 16MnCr5 case hardening steel specimen can be observed in Figure 4.37 a).

The digital micrograph (see Figure 4.38 b) of the wear track from the coated surface displays sporadic areas where the pull-out occurred.

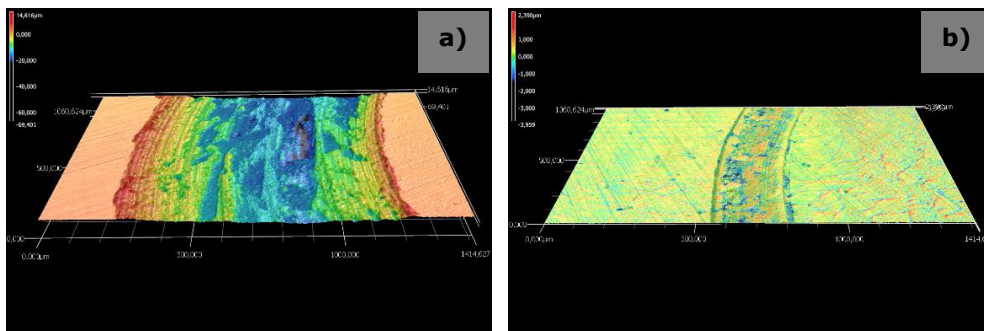


Figure 4.38 Wear track profile of: a) 16MnCr5, and b) WC-Co-NiP vs. WC-Co
Meanwhile, the SEM micrograph and EDX spectrum corresponding to the wear track of 16MnCr5 base material against the WC-Co static partner confirms the

formation of an unstable iron oxide layer. Additionally, transferred material comprising of WC particles from the WC-Co ball was found embedded in the wear track of the steel sample, as illustrated by Figure 4.39.

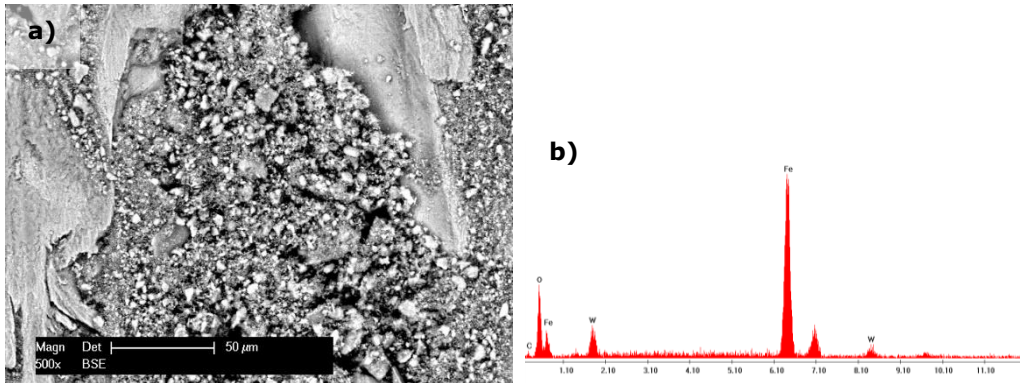


Figure 4.39 BSE micrograph a), and corresponding EDX spectrum b) from the wear track

As already mention, wear caused by severe adhesion between the sliding surfaces in the form of galling was observed on uncoated samples in both testing conditions, specifically versus 100Cr6 as well as WC-Co static partners.

In the ASTM G40 standard, galling is defined as: “a form of surface damage arising between sliding solids, distinguished by macroscopic, usually localized, roughening and creation of protrusions above the original surface; it often includes plastic flow or material transfer or both” [105]. It occurs under transverse motion, and especially if the tribo-system is not or poorly lubricated.

According to *J. R. Davis* propensity of a material to gall is affected by its ductility, thus, harder materials are more impervious to galling. Correspondingly, plastic deformation behavior plays a key role in severe adhesive wear. Materials with face-centered cubic lattice are exceedingly prone to galling due to effortless cross slip of dislocations. Alloys or elements that crystallize in systems with lower stacking-fault energy (i.e. body-centered cubic BCC structure) are less susceptible to galling. To an even greater degree, hexagonal close packed materials are extremely resistant to galling [106].

The damage on the uncoated samples shows characteristic galling patterns, with an uneven surface, caused by severe plastic deformation. Moreover, large volumes of material are adhesively transferred, indicating the perpetual destruction of the surface oxide tribo-layer. This is more easily noticeable for the 16MnCr5 versus WC-Co, where, in the vicinity of the worn caps transfer material is a fortiori present.

On the contrary, due to the high amount of WC with a HCP lattice and Ni_3P , crystallized in the body-centered tetragonal (BCT) system, the coated samples show little to no signs of severe adhesive degradation.

Contrasting other types of wear, galling happens rapidly, and is typically not a progressive process. Accordingly, it is safe to make the assumption that the WC-Co-NiP coatings will not suffer wear by galling even under prolonged exposure to the testing conditions employed in the current tribological investigations.

Furthermore, the WC-Co static partner wear rate concluded in numerical values of $6.07 \cdot 10^{-7} \text{ mm}^3 \text{ N}^{-1} \text{ m}^{-1}$ against 16MnCr5, and a considerably lower value, of only $3.16 \cdot 10^{-8} \text{ mm}^3 \text{ N}^{-1} \text{ m}^{-1}$ against WC-Co-NiP. This significant difference is clearly noticeable in the digital micrographs corresponding to the worn caps from the WC-Co static partner displayed in Figure 4.40.

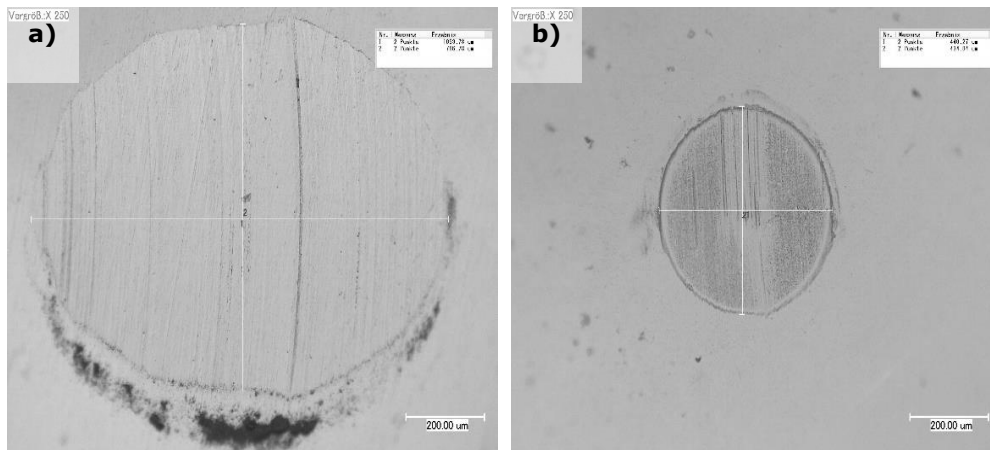


Figure 4.40 Micrograph of the WC-Co static partner against: a) 16MnCr, and b) WC-Co-NiP

The main mechanisms that govern the surface degradation in the currently investigated sliding systems are adhesion and tribo-oxidation. If the tribological system comprises third-bodies, namely hard particles (much harder than the two surfaces in contact), abrasive wear might also occur. This was found to be the case of the coupling between 16MnCr5 and WC-Co, which lead to the formation of abradable WC particles. Thus, the wear mechanism changed from an adhesive and tribo-oxidative one to a process that encompasses also abrasion.

During sliding between the two bodies in contact, the wear volume, increases with the sliding distance. Consequently, several stages of wear can be observed.

Running-in (run-in or break-in). During this stage (quite short in dry sliding), the wear rate, is usually very high. In fact, the mating surfaces are wearing out to remove the asperity peaks and to compensate for possible misalignments. Moreover, they get cleaned, totally or partially, from the contaminants.

Stage 1. After run-in, a steady state stage is entered. Wear rate is usually lower than during run-in. Very often, this is the main stage of the tribological process and it lasts up to the end of the component life. It is typically controlled by adhesion, tribo-oxidation or a combination of the two.

Stage 2. In some cases, a wear transition may occur after a certain sliding distance. Wear rate may increase or it may decrease. Such transitions are caused by a change in the wear mechanisms, often accompanied by a change in the friction coefficient [35].

In case of dry sliding against the 16MnCr5 steel counterface, the specific wear coefficient, of the WC-Co static partner is quite low. In the case of couplings with the similarly hard WC-Co-NiP material, it is even lower. Therefore, it can be concluded that through the optimal selection of a tribological pair it is possible to achieve very low wear rates for both tribo-partners.

The numerical values for the specific wear rate coefficients have been computed with the aid of the equation developed by *J. F. Archard* in 1953 [36]:

$$k = \frac{W_v}{F_N \cdot s} \quad \text{Eq. 4.4}$$

Where the wear rate k is defined as the wear volume W_v (mm^3) divided by normal load F_N (N) and sliding distance s (m), and is expressed in $\text{mm}^3 \text{N}^{-1} \text{m}^{-1}$.

The rotating specimens worn volume W_v can be calculated with the relation:

$$W_v = 2\pi r \cdot A \quad \text{Eq. 4.5}$$

where A is the area (μm^2) of the worn track cross-section expressed as:

$$A = \frac{h}{6 \cdot s} (3 \cdot h^2 + 4 \cdot s^2) \quad \text{Eq. 4.6}$$

where h is the height and s is the width (section) of the circular segment.

Area of the worn track cross-sections as well as the worn cap diameters of the static partners have been determined with the VK-X software by analyzing the profilometric measurements realized with the confocal laser scanning microscope.

For a more accessible visualization and comparison of the POD specific wear rate coefficients for both types of rotating samples and static partners the numerical values are presented as cluster bar charts.

Figure 4.41 displays the specific wear rate coefficients for the uncoated 16MnCr5 case hardening steel and WC-Co-NiP functional coating, tested under the load of 100Cr6 and WC-Co counterbodies, respectively.

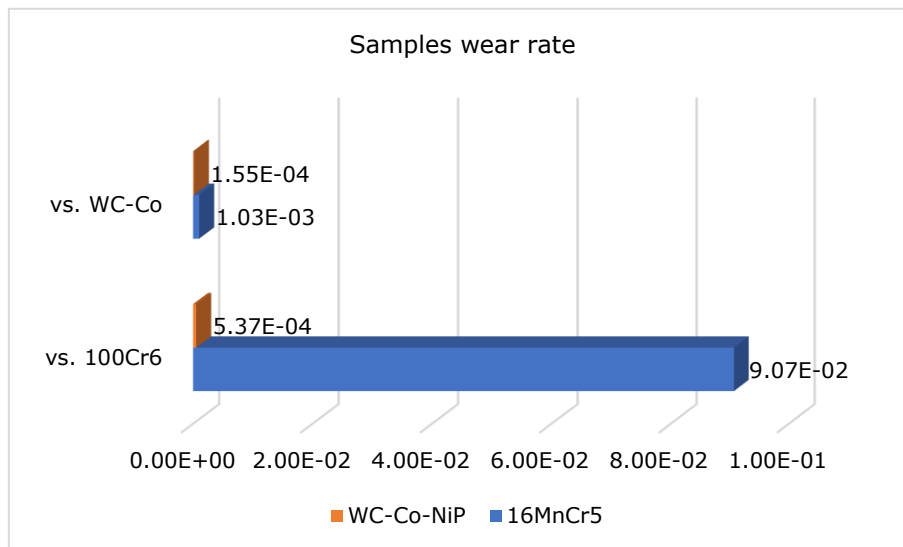


Figure 4.41 Specific wear rate coefficients for the rotating samples

Figure 4.42 illustrates the specific wear rate coefficients for the 100Cr6 steel and WC-Co cermet static partners tribologically coupled against the uncoated 16MnCr5 case hardening steel and WC-Co-NiP brazed hardfacings, respectively.

The tribological behavior of the present high temperature vacuum brazed WC-Co-NiP functional coatings was found to be in good compliance with those of WC-based claddings tested under similar conditions by other researchers [70].

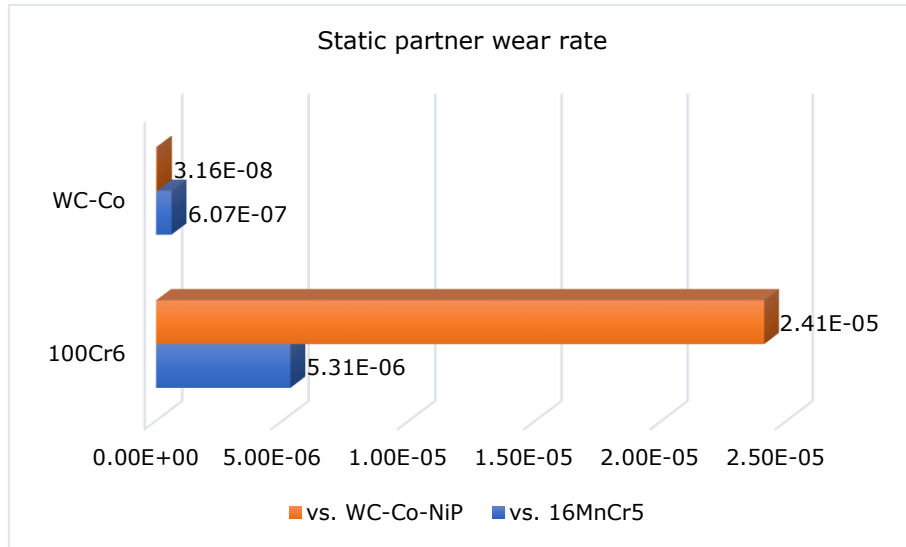


Figure 4.42 Specific wear rate coefficients for the static partners

4.4.5 Corrosion resistance

According to the International Union of Pure and Applied Chemistry “*Corrosion is an irreversible interfacial reaction of a material (metal, ceramic, polymer) with its environment which results in consumption of the material or in dissolution into the material of a component of the environment. Exclusively physical or mechanical processes are not included in the term corrosion*” [107].

In order for electrochemical corrosion to take place, four indispensable components are required, namely: an anode, a cathode, a corrosive environment supplied by an electrolyte and an electrical path between the anode and the cathode. Two chemical or electrochemical (if an electric current is involved) reactions, oxidation and reduction, arise between the anode and the cathode, governing the process of corrosion attack. Oxidation occurs at the anode and involves the loss of electrons from the atoms electron shells, meanwhile reduction takes place at the cathode, where atoms gain electrons.

Cobalt cemented tungsten carbides (WC-Co) possess a heterogenous structure, where corrosion occurs predominantly in the metallic binder (Co), which has lower corrosion resistance than the ceramic phase (WC). For example, the cobalt binder has relatively low corrosion resistance in sulfuric, hydrochloric, nitric and other strong acids. The corrosion behavior of cemented carbides is highly dependent on the nature and proportions of metallic binder constituents. For instance, the presence of nickel significantly improves the corrosion resistance. Addition of chromium will improve the resistance to oxidation, but can affect particular mechanical properties through the formation of chromium-rich carbides [108].

Consequently, the electrochemical corrosion behavior was evaluated through potentiodynamic polarization, employing a VoltaLab PGP201 potentiostat/galvanostat in a three-electrode cell. Working electrodes were prepared from the WC-Co-NiP functional coatings developed throughout the present study, and two types of thermal sprayed coatings with similar chemical composition, namely WC-Co-Mo and WC-Co respectively. The chemical composition of the thermal sprayed coatings is only similar and not identical because at the present time there are no available depositions with the chemical composition of the vacuum brazed coatings, namely WC-Co-NiP. A platinum disk was used as counter electrode and a saturated calomel electrode as reference. Prior to the investigations, all WEs have been ground with metallographic paper in order to remove potential contaminants and oxides and to ensure as close as possible the same surface roughness (R_a 0.03). Subsequently, the specimens are rinsed with ethanol and dried under a stream of warm air.

Polarization studies were performed at room temperature in the potential interval between -1000 mV and +1000 mV versus SCE, with a scan rate of 10 mV min^{-1} . The 1 cm^2 geometrical surface area of the samples allowed current readings to be directly expressed as current density (A cm^{-2}).

The cathodic branch in the polarization curves corresponds to hydrogen evolution reaction, while the anodic branch features the most important information related to the corrosion resistance.

Figure 4.44 illustrates the typical polarization behavior ($\log i$ - E representation) for the discussed samples subjected to potentiodynamic electrochemical corrosion in 3.5 % NaCl solution (pH 7). It shows that the corrosion current density (i_{corr}) of the WC-Co-NiP brazed coating ($i_{\text{corr}} 10^{-5.3} \text{ A cm}^{-2}$) is lower than that of thermal sprayed WC-Co-Mo ($i_{\text{corr}} 10^{-5.0} \text{ A cm}^{-2}$) and WC-Co ($i_{\text{corr}} 10^{-4.7} \text{ A cm}^{-2}$). The corrosion potential (E_{corr}) of the brazed hardfacing is shifted to more positive potentials (-250 mV vs. SCE) in comparison to that of thermal sprayed coatings (approx. -660 mV vs. SCE), which is associated with the chemical composition of the samples. Both corrosion current density (i_{corr}) and corrosion potential (E_{corr}) lean toward a lower reaction rate

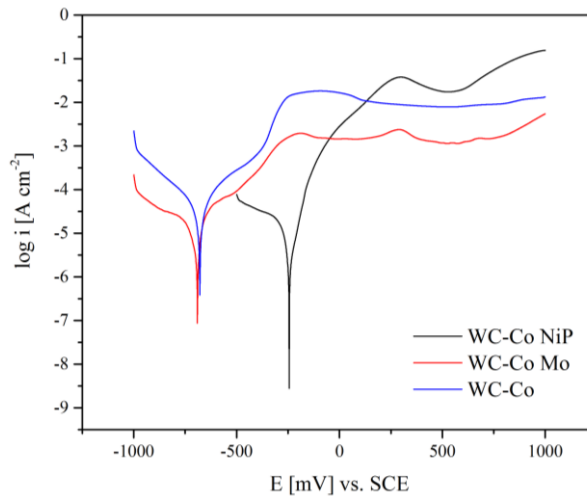


Figure 4.43 Polarization behavior of WC-Co-NiP, WC-Co-Mo and WC-Co in 3.5 % NaCl solution

Typical corrosion potential and corrosion current density of the analyzed samples obtained from the electrochemical polarization investigations performed in 3.5 wt.% NaCl aqueous solution are summarized in Table 4.8. The values indicate a slightly lower corrosion current density for the brazed coating in comparison the ones obtained from thermal sprayed coatings of similar chemical composition.

Table 4.8 Corrosion potential and corrosion current density values in 3.5% NaCl

Sample	E_{corr} [mV] vs. SCE	i_{corr} [A cm^{-2}]
WC-Co-NiP	-250	$10^{-5.3}$
WC-Co-Mo	-670	$10^{-5.0}$
WC-Co	-650	$10^{-4.7}$

Conclusively, the corrosion behavior of high temperature vacuum brazed WC-Co-NiP functional composite coatings, potentiodynamic polarized in 3.5% NaCl was found to be similar to the one observed in the case of thermal sprayed WC-Co-Mo and WC-Co respectively.

Additionally, during the experimental program, polarization studies were also performed in the potential interval between -750 mV and +1000 mV versus SCE for the 16MnCr5 material and from -500 mV to +1000 mV for the coated sample, both with a scan rate of 10 mV min⁻¹.

Figure 4.44 illustrates the polarization behavior for the discussed samples subjected to potentiodynamic electrochemical corrosion in 3.5 % NaCl solution (pH 7).

It is clear that the corrosion current density (i_{corr}) of the WC-Co-NiP brazed coating is substantially lower than that of 16MnCr5 steel. The corrosion potential (E_{corr}) of the hardfacing is shifted to more positive potentials (-250 mV) in comparison to the uncoated sample (-640 mV), which is due to the chemical composition.

The anodic Tafel slope (Figure 4.44) of the coating shows an inclination to passivate, due to the nickel based chemical composition of the brazing filler alloy. Adversely, the uncoated steel sample points no tendency towards passivation.

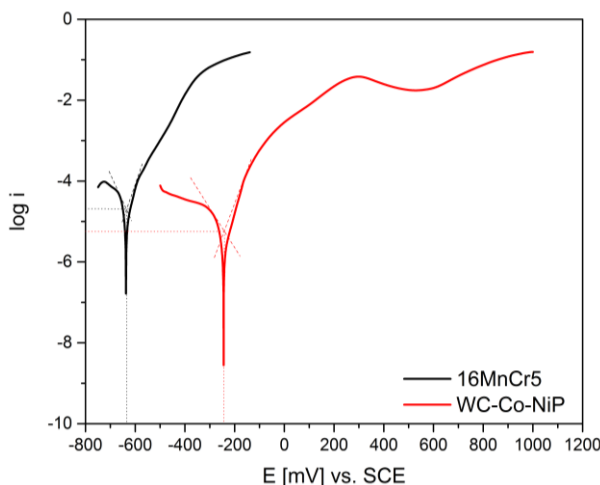


Figure 4.44 Polarization behavior of 16MnCr5 and WC-Co-NiP in 3.5 % NaCl solution

Both corrosion current density (i_{corr}) and corrosion potential (E_{corr}) lean toward a lower reaction rate, and consequently, better corrosion resistance of the coated sample compared to the uncoated one is to be expected.

The polarization curve of WC-Co-NiP coated samples showed passive plateau at values between 300 mV and 550 mV, indicating the formation of a passive film. Further increasing the potential in the anodic direction, the passive film previously formed on the surface of the sample, broke down and the nickel from the coating was dissolved at the same time.

Typical corrosion potential and corrosion current density of the analyzed samples obtained from the electrochemical polarization investigations performed in 3.5 wt.% NaCl aqueous solution are summarized in Table 4.9. The values indicate a corrosion current density around 10 times lower for the brazed coating in comparison to substrate material.

Table 4.9 Corrosion potential and corrosion current density values in 3.5% NaCl

Sample	E_{corr} [mV] vs. SCE	i_{corr} [A cm^{-2}]
16MnCr5	-640	$10^{-4.3}$
WC-Co-NiP	-250	$10^{-5.3}$

The micrographs illustrated in Figure 4.45 offer an overview (top-view) of the coatings' surface (testing area) a) before, and b) after the electrochemical investigation. It can be observed that the metallic binder is severely affected, while the reinforcing phase (WC) retains its structural integrity.

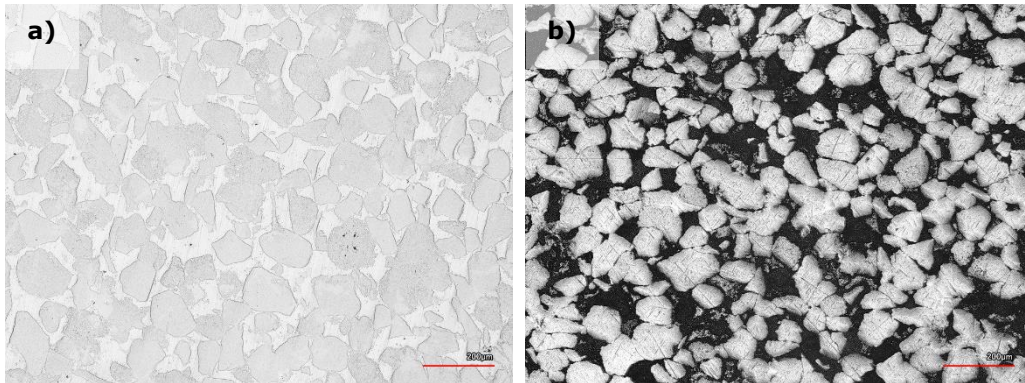


Figure 4.45 CLSM micrographs of: a) coating surface before electrochemical investigation, and b) after electrochemical investigation

Figure 4.46 illustrates the typical polarization behavior for the discussed samples subjected to potentiodynamic electrochemical corrosion in 0.5 M HCl solution (pH 0).

Similar to the electrochemical investigations performed in the 3.5 % NaCl solution, corrosion current density (i_{corr}) of the WC-Co-NiP brazed coating is substantially lower than that of 16MnCr5 steel in 0.5 M HCl solution. Likewise, the corrosion potential (E_{corr}) of the hardfacing is shifted to more positive potentials (-300 mV) compared to the substrate material (-500 mV). The anodic Tafel slope of the coating shows an inclination to passivate, due to the nickel based chemical composition of the brazing filler alloy. Adversely, the uncoated steel sample points no tendency towards passivation.

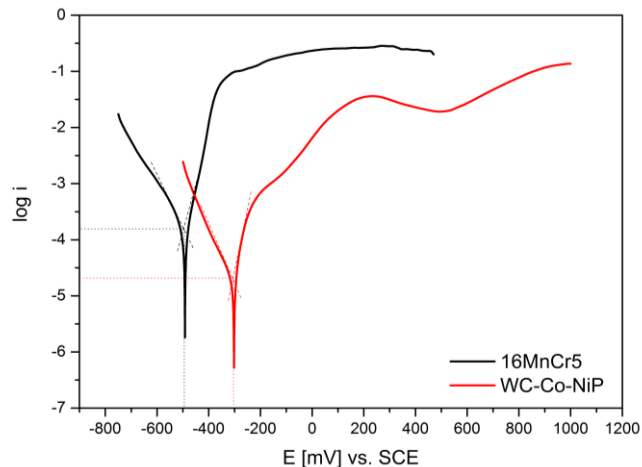


Figure 4.46 Polarization behavior of 16MnCr5 and WC-Co-NiP in 0.5 M HCl solution

Once again, both corrosion current density (i_{corr}) and corrosion potential lean toward a lower reaction rate, and consequently, better corrosion resistance of the coated sample compared to the uncoated one is to be expected.

The corrosion potential and corrosion current density of the analyzed samples obtained from the electrochemical polarization investigations performed in 0.5 M HCl aqueous solution are summarized in Table 4.10. Correspondingly, the corrosion current density of the coating is approx. 10 times lower than the values obtained for the base material.

Table 4.10 Corrosion potential and corrosion current density values in 0.5 M HCl

Sample	E_{corr} [mV] vs. SCE	i_{corr} [A cm^{-2}]
16MnCr5	-500	$10^{-3.8}$
WC-Co-NiP	-300	$10^{-4.7}$

Because transition metal carbides have high resistance to chlorine containing solutions, corrosion of WC-based composite coatings manifests through the dissolution of the metallic binder. This creates an area in which the metallic matrix is depleted, leaving behind only a skeleton of WC particles with severely affected properties, as shown in the BSE micrographs of Figure 4.47.

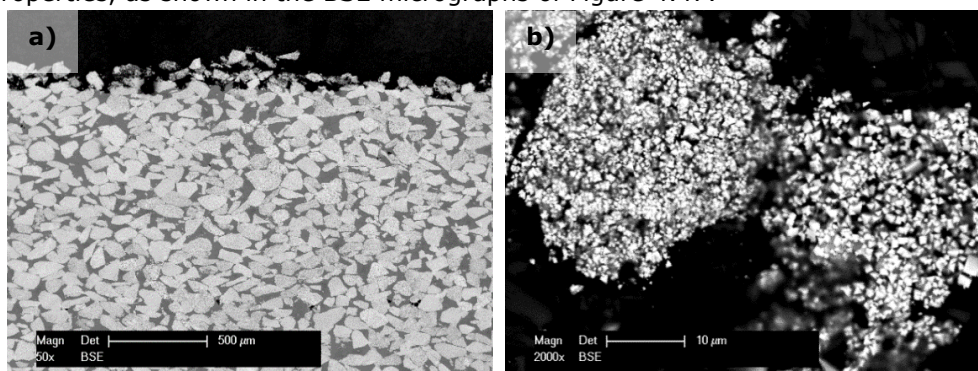


Figure 4.47 BSE micrographs after electrochemical corrosion: a) overview of coating, and b) detail of cemented WC particle

The superior corrosion resistance of WC-Co-NiP coatings compared to the 16MnCr5 case hardening steel substrate is attributed to the formation of the nickel passive layer. This film forms willingly in contrast to the development of the passive film of iron. Dissimilarities in the nature of the oxide layer grown on Fe and Ni are accountable for this phenomenon. The film thickness on Ni is between 0.9 nm and 1.2 nm, while the Fe oxide film is situated in the interval 1 nm and 4 nm. There are two theories regarding the morphology and chemical composition of the nickel passive film. One theory stipulates that the layer is completely NiO with a small quantity of nonstoichiometric nickel, giving rise to Ni^{3+} cation vacancies. In the case of the second one, it comprises of an inner film of NiO and an outer one of anhydrous $\text{Ni}(\text{OH})_2$. Once generated, the passive oxide film of nickel, neither cathodic treatment or chemical dissolution can easily remove it.

The passive film of nickel will not offer protection against corrosive attack in oxidizing medias such as nitric acid. Alloying with chromium will generate a denser, more stable film, increasing the corrosion resistance to a variety of oxidizing environments. However, these alloys are susceptible to attack in atmospheres containing chlorides or other halides, particularly if oxidizing compounds are present.

Corrosion will manifest mostly in the form of pitting and occasionally as stress corrosion cracking. Addition of molybdenum, titanium and/or tungsten should improve the behavior under all working conditions [109].

The EDX spectra of Figure 4.48 confirm the formation of Ni oxides and possibly W oxides as well as the dissolution of the metallic binder.

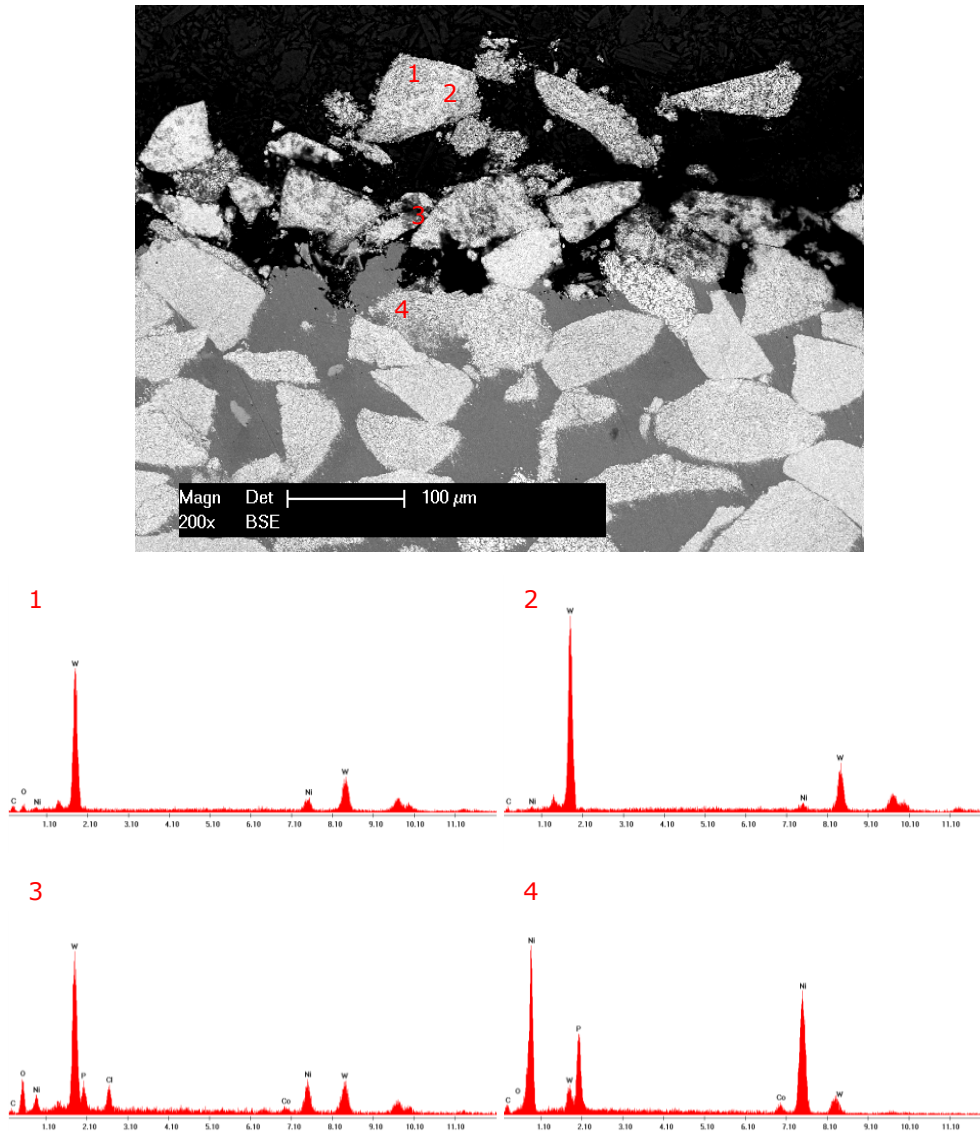


Figure 4.48 BSE cross-section micrograph and EDX spectra corresponding to the marked regions, after electrochemical corrosion

The corrosion behavior of the present high temperature vacuum brazed WC-Co-NiP functional coatings was found to be in good compliance with those of WC-based claddings tested under similar conditions by other researchers [69].

5 Conclusions

The original research described in the present work consists in a theoretical study on available literature data regarding functional coatings, fabrications methods and applications. The focus was directed to aspects concerning the production of high temperature vacuum brazed composite coatings, the optimization of deposition process parameters and characterization of such hardfacings.

In the current state of the art, tape brazing involves the use of flexible cloths rolled from mixtures of hard phase powders, filler metal powder and appropriate polymeric binders. The mats can easily be manufactured under diverse chemical compositions of base and filler metal powder, and formed to size and shape by cutting or stamping. After forming, the cloths are overlaid on top of the metallic substrate and fixed in place often with a small amount from the same polymeric binder. The coating process actually takes place at temperatures usually slightly above the liquidus temperature of the filler alloy, in vacuum or under protective atmosphere, with the aid of a furnace. During the brazing process, filler metal reaches liquid state and infiltrating the spaces between the hard phase particles wetting and enveloping them. Metallurgical interactions governed by diffusion and alloying appear among base powder and brazing alloy, as well as at the coating - metallic substrate interface, resulting in a strong metallurgical bond. No universal reference for the brazing temperatures and holding times exists, because the values depend strongly on the chemical composition of the substrate material, reinforcing powder and filler metal, their ratio in the mixture and the metallurgical interactions. Considering that the majority of substrate materials are iron, nickel, chromium or cobalt alloys, base powders are usually ceramics or cermets and the metal matrix consists typically of self-fluxing nickel base alloys the furnace brazing temperature is approximately 1100°C. Brazed overlays with a thickness range of 150 µm to 20 mm have been successfully deposited, with theoretical possibilities of an even greater thickness interval. Due to the common high amount of hard phases (up to 70% or more in some cases) Ni-base matrix alloy, and generally low porosity ($\approx 1\%$), these coatings can offer high wear and corrosion resistance under severe working conditions. The major limitation of this coating technique is the requirement to treat the whole substrate to the necessary high brazing temperature. This process can have a negative effect on the substrate material, leading to undesired grain growth or phase transformations. Another current disadvantage of the method is the use of potentially harmful chemical compounds in the polymeric binders, which need to be filtered, contained and neutralized.

Considering that WC is one of the most suitable materials for protection against wear and corrosion, due to its mechanical and chemical properties. The main attention was focused on utilizing this compound for its advantages, and simultaneously overcoming its limitations (low ductility and complex deposition processes), in order to obtain coatings with superior characteristics.

The present work dealt with the development of functional composite coatings based on cemented tungsten carbide reinforcement and nickel-based filler alloy using the high temperature vacuum brazing method. Cemented WC particles provide the hardness and low coefficient of friction, improving the wear resistance. Simultaneously, the Ni-based metallic matrix offers toughness and impact resistance

to the final coating. Moreover, the brazing process provides a compliant support for the WC-Co particles and strong adhesion between the coating and the metallic substrate, through a metallurgical bond.

This technique delivers a simple fabrication way for the functional overlays and guarantees low porosity of the coatings.

The **personal contributions** in this study refer to:

- utilizing vacuum brazing as a non-conventional coating method in order to obtain **WC-Co-NiP functional hardfacings** with superior wear and corrosion resistance;
- exploring the possibility of combining **recycled WC-Co powder** as reinforcing phase with **NiP brazing filler metal** as metallic matrix, to develop vacuum brazed composite coatings;
- careful selection of feedstock materials in order to favorably combine a manufacturing process as **accessible, economic, and environmentally friendly** as possible, with the production of coatings with superior characteristics;
- the successful employment of **water-base fugitive glue** as organic binder for the manufacturing of flexible cloths, which is safe to handle and harmless to the environment, and at the same time offers adequate flexibility and long shelf life;
- the usage of **BNi6** (NiP alloy) brazing filler metal **as metallic matrix**, in order to decrease the maximum temperature of the brazing process down to 1000°C, thus reducing production costs and thermal influence on the substrate material;
- studies on the deposition mechanism, as well as investigations on the influence of the thermal cycle parameters on the morphology of the coatings;
- **optimization** of the **brazing process parameters** for the studied chemical composition;
- investigations on the **coatings characteristics and properties** (including wear and corrosion resistance).

In this regard, several aspects can be highlighted:

- A careful selection of the brazing filler metal and reinforcing powders with specific chemical compositions, bonded together by certain organic binders, in order to produce superior coatings was performed;
- Commercially available WC-Co recycled material was utilized as reinforcing powder;
- Commercially available BNi6 brazing filler metal was selected for the role of metallic matrix;
- Water-based fugitive glue was utilized as organic binder;
- Flexible cloths were manufactured from both types of powders; The 1.7131 (16MnCr5) case hardening steel was utilized as substrate material due to availability and its importance as a structural material;
- As filler material, initially 6 types of Ni-based powder were proposed; due to its superior properties, the NiP based powder was selected to take the role of metallic matrix for the brazed coatings;
- NiP powder presents a dense and homogeneous microstructure, with occasional satellite type formations on the surface of some particles; moreover, it possesses the lowest melting temperature (900°C) due to the high P content (10 - 12 %);
- As tungsten carbide (WC) is well known for its exceptional hardness and wear/erosion resistance, it was chosen as hard phase material;

- The reinforcing material selected for this study was a commercially available WC-Co powder obtained from recycling of hard metal tools;
- WC-Co was found to be an ideal reinforcing material for the manufacturing of functional composite coatings due to its superior wear resistance, compressive strength, good elevated temperature and corrosion resistance;
- A water-based fugitive adhesive was used as binder for the manufacturing of the flexible tapes; its special formulation was found to offer a clean alternative to the conventionally used organic binders;
- Manufacturing the polymer bond hardfacing tapes involved mixing precise amounts from the selected powders and organic binder until the latter one fibrillated;
- A ratio of 75 wt.% WC-Co, 25 wt.% NiP and additional 2 wt.% organic binder was found to offer the optimum composition for preparing highly flexible composite tapes;
- The high temperature brazing process was carried out in a HITERM 80-200 cold wall vertical vacuum furnace at a stable pressure of $3.0 \cdot 10^{-4}$ mbar;
- 4 experimental brazing programs were tested in order to find the optimum process parameters;
- The brazing cycles were adjusted according to data provided by the thermal analysis correlated with the recommendations of the BMF manufacturer;
- It was found that Program 4, which was also the most complex, delivered the best results, regarding the required microstructure, morphology and low porosity observed from the SEM investigations;
- The optimized program was composed of 10 segments representing heating ramps, soaking times, cooling rates and intervals;
- The final brazing step performed at 1000°C for 30 min assured the high fluidity of the Ni-based alloy, necessary for wetting, infiltrating and filling the micro voids in order to obtain high quality coatings;
- As Program 3 and Program 4 differed only in the cooling stage, it can be mentioned that the additional cooling segment down to 870°C, with a lower rate, avoided the formation of microcracks in the coating;
- Results of the electron microscope investigations proved that the initial problem of high porosity, crack evolution and fracture occurrence was eliminated; the porosity degree decreased from an initial value of around 19 % to a final value of approx. 1 %;
- The high temperature vacuum brazed coatings displayed a dense structure, with uniform distribution of the cermet particles;
- Diffusion from the metallic matrix towards the cemented WC and substrate was highlighted using EDX line scan method; moreover, EDX mapping identified the elements and showed their distribution and relative proportion in the coating;
- The presence of Fe was limited to the substrate and also was found in smaller amounts in the interface region; W appeared to have diffused towards the interface; Co migrated towards the substrate and Ni replaced part of Co in the WC-Co cermet; P was concentrated in areas with high Ni concentrations;
- A phase composition consisting of 51 wt.% WC, 38 wt.% Ni₃P, 7 wt.% Ni₁₇W₃ and 4 wt.% Co₂W₄C was determined from the XRD patterns of the functional coating;

- Coating cross section microhardness ranged from a minimum of 647HV1 (metallic matrix) up to a maximum of 1132HV1 (cermet particles), with a mean of 896HV1;
- The adhesion of the coating to the substrate was determined from tensile adhesive strength tests; the coating itself reached a mean value of 150 MPa;
- Fracture occurred only through the coating, without any noticeable trace of delamination;
- A higher adhesive strength, compared to the cohesive one was confirmed, hence a superior metallurgical bond between coating and substrate;
- The coatings experienced a mean friction coefficient of 0.77 under dry sliding friction against a 100Cr6 ball with an average wear rate of $5.36 \cdot 10^{-4} \text{ mm}^3 \text{ N}^{-1} \text{ m}^{-1}$, value which was 170 times lower than that of the substrate material;
- The coatings experienced a mean friction coefficient of 0.33 under dry sliding friction against a WC-Co ball with an average wear rate of $1.55 \cdot 10^{-4} \text{ mm}^3 \text{ N}^{-1} \text{ m}^{-1}$, value which was around 7 times lower than that of the substrate material;
- The superior wear behavior was attributed to the presence of hard WC phase and self-lubricating Ni₃P;
- The corrosion behavior of high temperature vacuum brazed WC Co NiP functional composite coatings, potentiodynamic polarized in 3.5% NaCl was found to be similar to the one observed in the case of thermal sprayed WC Co Mo and WC Co respectively;
- The corrosion current density (i_{corr}) of the WC-Co-NiP brazed coating is lower than that of thermal sprayed WC-Co-Mo and WC-Co. The corrosion potential (E_{corr}) of the brazed hardfacing is shifted to more positive values in comparison to that of thermal sprayed coatings, which is associated with a lower reaction rate;
- The electrochemical polarization curves illustrated a 10 times lower corrosion current density in the case of WC-Co-NiP coatings compared to 16MnCr5 case hardening steel samples in both 3.5 % NaCl and 0.5 M HCl solutions;
- The superior corrosion resistance of WC-Co-NiP functional coatings is credited to the chemical composition of the metallic matrix, namely the Ni-P alloy (Ni₃P phase), which is able to readily generate a passive layer, stable up to the potential of around 600 mV vs. SCE;
- The corrosive attack of vacuum brazed WC-Co-NiP coatings is characterized by selective dissolution of the metallic matrix, compared to the general corrosion observed in the case of the substrate material.

Using the described method, high quality hardfacing coatings with low porosity, a good distribution of both large and small hard phases, excellent metallurgical bond and minimal dilution have been deposited. Simultaneously, the optimization process has eliminated the initial problem of cracks and fracture evolution and reduced by almost 20 percent the size and occurrence frequency of interconnected and individual pores. Moreover, significantly lower dry sliding wear rates of the WC-Co-NiP, compared to that of 16MnCr5 case hardened steel were found against both harder and softer materials. Furthermore, with the application of the functional coating the corrosion behavior was also ameliorated.

Accordingly, the present work highlights the crucial importance of optimizing the brazing process parameters for each chemical composition, thickness, and combination of flexible composite cloth and substrate material. At the same time, it proves once more the feasibility of using high temperature vacuum brazing as a practical technique of generating high quality WC-Co-NiP functional coatings.

Outlook

The theoretical and experimental study realized in the context of this thesis highlights current tendencies in the development and manufacturing of functional coatings deposited on metallic substrates.

Undoubtedly, numerous chemical compositions can be adopted and explored regarding the development of new functional coatings.

The virtually unlimited possibility of combining reinforcing materials that possess increased hardness and superior wear behavior, with tough and corrosion resistant matrix materials will lead to the fabrication of functional composite coatings with improved characteristics and extended service life.

In this regard, several further research directions can be outlined:

- further optimization of the brazing process parameters utilizing a statistical and numerical approach (Taguchi method);
- experimental coatings utilizing other reinforcing and matrix powdered materials;
- attempts to coat other substrate materials;
- attempts to deposit coatings on purely internal surfaces;
- attempts to coat actual components of greater size and more complex geometry
- assessment of the brazing process influence on the substrate material;
- further investigations regarding the stability and influence of the crystalline phases on the coatings' characteristics and properties;
- further investigations on the characteristics and properties of the coatings, namely determination of the modulus of elasticity, hardness of individual phases, tribological and corrosion behavior under different testing conditions.

References

- [1] R. Chattopadhyay, Green Tribology, Green Surface Engineering, and Global Warming, Ohio: ASM International, 2014.
- [2] A. Fischer and K. Bobzin, Friction, Wear and Wear Protection, Weinheim: WILEY-VCH Verlag GmbH & Co. KGaA, 2009.
- [3] T. Mang, K. Bobzin and T. Bartels, Industrial Tribology, Weinheim: wiley-VCH Verlag, 2010.
- [4] VTT TECHNICAL RESEARCH CENTRE OF FINLAND LTD, "<http://www.vttresearch.com/>," 15 1 2009. [Online]. Available: <http://www.vttresearch.com/media/news/vtt-new-friction-technology-translates-into-major-energy-and-cost-savings>. [Accessed 7 9 2016].
- [5] University of Southampton, "<http://www.southampton.ac.uk/>," [Online]. Available: http://www.southampton.ac.uk/engineering/research/impact/preventing_wear_and_tear.page?. [Accessed 10 12 2016].
- [6] G2MT Laboratories, "<http://www.g2mtlabs.com/>," G2MT Labos, [Online]. Available: <http://www.g2mtlabs.com/corrosion/cost-of-corrosion/>. [Accessed 18 2 2016].
- [7] NACE International, "International measures of Prevention, Application, and Economics of Corrosion Technologies Study," NACE International, Houston, 2016.
- [8] G. F. Hays, "<http://corrosion.org/>," [Online]. Available: http://corrosion.org/wco_media/nowisthetime.pdf. [Accessed 10 12 2016].
- [9] COR-PRO SYSTEMS , "www.cor-pro.com," COR-PRO SYSTEMS , [Online]. Available: <http://www.cor-pro.com/case-study-corrosions-economic-impact-across-multiple-industries/>. [Accessed 24 February 2017].
- [10] NACE International, "www.impact.nace.org," NACE International, [Online]. Available: <http://impact.nace.org/economic-impact.aspx>. [Accessed 24 February 2017].
- [11] L. Herring, "www.nasa.gov," National Aeronautics and Space Administration, 01 February 2006. [Online]. Available: <https://www.nasa.gov/centers/kennedy/news/corrosion.html>. [Accessed 07 March 2017].
- [12] J. R. Davis, Corrosion: Understanding the Basic, Ohio: ASM International, 2000.
- [13] MBRAUN, "www.mbraun.com," MBRAUN, [Online]. Available: <http://www.mbraun.com/solutions/functional-coatings>. [Accessed 1 03 2017].
- [14] N. Espallargas, Future Development of Thermal Spray Coatings, Woodhead Publishing Limited, 2015.

-
- [15] G. Straffelini, *Friction and Wear, Methodologies for Design and Control*, Springer, 2015.
- [16] B. G. Mellor, *Surface coatings for protection against wear*, Cambridge: Woodhead Publishing Limited, 2006.
- [17] M. Roy and J. P. Davim, *Thermal Sprayed Coatings and their Tribological Performances*, Hershey : Engineering Science Reference, 2015.
- [18] L. Pawlowsky, *The Science and Engineering of Thermal Spray Coatings*, Chichester: John Wiley & Sons Ltd, 2008.
- [19] D. Toma, W. Brandl and G. Marginean, "Wear and corrosion behavior of thermally sprayed cermet coatings," *Surface and Coatings Technology*, vol. 138, pp. 149-158, 2001.
- [20] A. Vencel, S. Arostegui, G. Favaro, F. Zivic, M. Mrdak, S. Mitrovic and V. Popovic, "Evaluation of adhesion/cohesion bond strength of the thick plasma spray coatings by scratch testing on coatings cross-section," *Tribology International*, vol. 44, pp. 1281-1288, 2011.
- [21] M. Kasparova, F. Zahalka and S. Houdkova, "Evaluation of the bond strength of the thermally sprayed coatings," in *Metal 2010*, Roznov pod Radhostern, 2010.
- [22] T. Y. Cho, J. H. Yoon, J. Y. Cho, Y. K. Joo, J. H. Kang, S. Zhang, H. G. Chun, S. Y. Hwang and S. C. Kwon, "Surface properties and tensile bond strength of HVOF thermal spray coatings of WC-Co powder onto the surface of 420J2 steel and the bond coats of Ni, NiCr and Ni/NiCr," *Surface and Coatings Technology*, vol. 203, pp. 3250-3253, 2009.
- [23] D. Utu, G. Marginean, W. Brandl and I. Cartis, "Improvement of the oxidation behaviour of electron beam remelted MCrAlY coatings," *Solid State Sciences*, vol. 7, no. 1, pp. 459-464, 2005.
- [24] D. Utu, W. Brandl, G. Marginean, I. Cartis and V. A. Serban, "Morphology and phase modification of HVOF-sprayed MCrAlY-coatings remelted by electron beam irradiation," *Vacuum*, vol. 77, no. 4, pp. 451-455, 2005.
- [25] P. Gavendova, J. Cizek, J. Cupera, M. Hasegawa and I. Dlouhy, "Microstructure modification of CGDS and HVOF sprayed CoNiCrAlY bond coat remelted by electron beam," *Procedia Materials Science*, vol. 12, pp. 89-94, 2016.
- [26] G. Marginean and D. Utu, "Cyclic oxidation behaviour of different treated CoNiCrAlY coatings," *Applied Surface Science*, vol. 258, pp. 8307 - 8311, 2012.
- [27] C. M. Cotell, J. A. Sprague and F. A. Smidt, "Porcelain Enameling," in *Surface Engineering*, USA, ASM International, 1994, pp. 1343-1384.
- [28] M. Roy, *Surface Engineering for Enhanced Performance against Wear*, Wien: Springer-Verlag, 2013.
- [29] K. Funatani and G. E. Totten, *Heat Treating*, Missouri: ASM International, 2001.
- [30] K. Bobzin, *Oberflächentechnik für den Maschinenbau*, Weinheim: Wiley-VCH Verlag, 2013.
- [31] V. Popov, *Contact Mechanics and Friction*, Berlin: Springer-Verlag, 2010.
- [32] P. J. Blau, *Friction Science and Technology*, New York: CRC Press, 2009.

- [33] I. F. Secosan, *Morphology, Wear and Corrosion Behaviour of HVOF Cermet Coatings Sprayed on Inner Cylindrical Surfaces*, Timisoara: Editura Politehnica, 2012.
- [34] P. Blau, *Friction, Lubrication, and Wear Technology*, USA: ASM International, 1992.
- [35] G. Straffelini, *Friction and Wear, Methodologies for Design and Control*, Springer, 2015.
- [36] J. Archard, "Contact and Rubbing of Flat Surfaces," *Journal of Applied Physics*, vol. 24, no. 8, p. 24, 1953.
- [37] H. Czichos and K. H. Habig, *Tribologie-Handbuch*, Auflage 4, Wiesbaden: Springer Vieweg, 2015.
- [38] N. Perez, *Electrochemistry and Corrosion Science*, New York: Kluwer Academic Publishers, 2004.
- [39] S. D. Cramer and B. S. Covino, *Corrosion: Fundamentals, Testing, and protection*, ASM International, 2003.
- [40] American Welding Society, *Standard Welding Terms and Definitions, Including Terms for Adhesive Bonding, Brazing, Soldering, and Thermal Spraying*, Miami: American Welding Society (AWS), 2001.
- [41] American Welding Society, *Brazing Handbook*, Miami: American Welding Society (AWS), 2007.
- [42] D. L. Olsen, T. A. Siewert, S. Liu and G. R. Edwards, *Welding, Brazing, and Soldering*, USA: ASM International, 1993.
- [43] H. Mehler, *Diffusion in Solids Fundamentals, Methods, Materials, Diffusion-Controlled Processes*, Springer, 2017.
- [44] V. A. Serban and A. Raduta, *Stiinta si Ingineria Materialelor*, Editia a III-a, Timisoara: Editura Politehnica, 2014.
- [45] M. M. Schwartz, *Brazing*, Ohio: ASM International, 2003.
- [46] ASM International, *Alloy Phase Diagrams*, USA: ASM International, 1992.
- [47] Oerlikon Metco, "www.oerlikon.com," September 2014. [Online]. Available: <https://www.oerlikon.com/metco/en/products-services/coating-materials/braze/>. [Accessed 12 December 2016].
- [48] C. M. Fernandes and A. M. R. Senos, "Cemented carbide phase diagrams: A review," *Int. Journal of Refractory Metals and Hard Materials*, vol. 29, pp. 405-418, 2011.
- [49] A. F. Guillermet, "Thermodynamic Properties of the Co-W-C System," *Metalurgical Transactions*, vol. 20A, pp. 935-956, 1989.
- [50] Computational Thermodynamics Inc., "http://www.calphad.com," [Online]. Available: <http://www.calphad.com/tungsten-cobalt-carbon.html>. [Accessed 10 January 2017].
- [51] J. Brailey, D. Worden, E. Bretonne and J. Wolf, "Coating metallic substrate with powdered filler and molten metal". USA Patent 3743556, 3 July 1973.
- [52] Kennametal, "www.kennametal.com," Kennametal, [Online]. Available: <http://www.kennametal.com/en/products/engineered-wear-solutions/cladding-welding-and-thermal-spray/conforma-clad-and-ultraflex-brazed-cladding.html>. [Accessed 4 January 2017].

- [53] M. R. Dustoor and L. N. Moskowitz, "A New Process for Customized Coatings," *Thin Solid Films*, vol. 180, pp. 29-37, 1983.
- [54] E. J. Breton, J. D. Wolf and D. Worden, "Process for producing sintered articles from flexible preforms containing polytetrafluoroethylene and at least about 85 volume percent of sinterable particulate material". USA Patent 3864124, 4 February 1975.
- [55] D. A. Purser, "Recent Developments in Understanding the Toxicity of PTFE Thermal Decomposition Products," *Fire and Materials*, vol. 16, pp. 67-75, 1992.
- [56] W. C. Hasz and D. E. Budinger, "Turbine engine components having wear coating and method for coating a turbine engine component". USA Patent 6451454, 17 September 2002.
- [57] Y. Kitahara, S. Takahashi and T. Fujii, "Thermal analysis of polyethylene glycol: Evolved gas analysis with ion attachment mass spectrometry," *Chemosphere*, vol. 88, pp. 663-669, 2012.
- [58] The Toxin and Toxin Target Database, "<http://www.t3db.ca/>," [Online]. Available: http://www.t3db.ca/toxins/T3D3469#toxicity_profile. [Accessed 05 January 2017].
- [59] D. T. Pascal, V. A. Serban and G. Marginean, "Optimization of Process Parameters for the Manufacturing of High Temperature Vacuum Brazed WC-NiCrBSi Coatings," *Solid State Phenomena*, vol. 254, pp. 164-169, 2016.
- [60] J. Grogan, S. C. DeVito, R. Pearlman and K. R. Korzekwa, "Modeling Cyanide Release from Nitriles: Prediction of Cytochrome P450Mediated Acute Nitrile Toxicity," *Chem. Res. Toxicol.*, vol. 5, pp. 548-552, 1992.
- [61] H. Krappitz, "Coating techniques using brazing," in *Advances in brazing*, Suffolk, Woodhead Publishing Limited, 2013, pp. 472-497.
- [62] C. Gill, "www.conformaclad.com," Kennametal, February 2004. [Online]. Available: <http://www.conformaclad.com/extruderwearparts.html>. [Accessed 06 January 2017].
- [63] D. W. Bucholz and C. B. Harley, "Erosion Resistant, Infiltration Brazed Tungsten Carbide Coatings used in Fly Ash Conveyance Systems," in *20th ASM Heat Treating Society Conference*, St. Louis, 2000.
- [64] D. W. Bucholz and G. A. Saltzman, "Corrosion, Wear and Erosion Resistant Brazed Coatings of Tungsten Carbide," in *20th ASM Heat Treating Society Conference*, St. Louis, 2000.
- [65] S. M. Uddin, H. Krappitz, D. Esslingen, J. Barnikel, D. Mülheim and I. Reinkensmeier, "www.innobraze.de," [Online]. Available: <http://innobraze.de/wp-content/uploads/2016/06/515-Repair-brazing-and-protection-of-Titanium-turbine-components-using-polymer-bonded-tapes.pdf>. [Accessed 06 January 2017].
- [66] V. Mammadov, K. Tacon, B. Davies and N. S. Ahmedov, "Coatings help to improve centrifugal pump reliability," in *12th European Fluid Machinery Congress*, Edinburgh, 2014.
- [67] C. Juliot and D. W. Bucholz, "Erosion Resistance of Infiltration Brazed Tungsten Cladings," Kennametal, [Online]. Available: <http://www.conformaclad.com/PulpandPaper/>. [Accessed 06 January 2017].

110 References

- [68] L. X. Gao, T. Liu and D. Q. Zhang, "Preparation of NiCrBSi-WC brazed coating and its microstructure characteristics," *Surface and Interface Analysis*, 8 August 2012.
- [69] D. Q. Zhang, T. Liu, H. G. Joo, L. X. Gao and K. Y. Lee, "Microstructure and corrosion resistance of the brazed WC composite coatings in aerated acidic chloride media," *International Journal of Refractory Metals and Hard Materials*, vol. 35, pp. 246-250, 2012.
- [70] G. B. Stachowiak and G. W. Stachowiak, "Tribological characteristics of WC-based claddings using a ball-cratering method," *International Journal of Refractory Metals and Hard Materials*, vol. 28, pp. 95-105, 2010.
- [71] K. D. Vernon-Parry, "Scanning Electron Microscopy: an introduction," *Elsevier Science*, vol. 13, no. 4, pp. 40-44, 2000.
- [72] J. Goldstein, D. Newbury, D. Joy and C. Lyman, *Scanning Electron Microscopy and X-Ray Microanalysis*, 3rd Edition: Springer, 2013.
- [73] FEI, *An Introduction to Electron Microscopy*, ISBN 978-0-578-06276-1, 2010.
- [74] P. W. Hawkes, *Scanning Electron Microscopy: Physics of Image Formation and Microanalysis*, Springer, 2013.
- [75] J. J. Friel, *X-Ray and Image Analysis in Electron Microscopy*, Princeton Gamma Tech, 2003.
- [76] N. Yao and Z. L. Wang, *Handbook of microscopy for nanotechnology*, New York: Kluwer Academic Publishers, 2005.
- [77] KEYENCE CORPORATION, "www.keyence.com," [Online]. Available: <http://www.keyence.com/ss/products/microscope/vkx/>. [Accessed 06 February 2017].
- [78] M. Lee, *X-Ray Diffraction for Materials Research*, Oakville: Apple Academic Press, 2016.
- [79] Philips Analytical, *X'Pert - MPD Service Manual 940501*, The Netherlands: Philips Analytical X-Ray, 1994.
- [80] B. Cullity and S. R. Stock, *Elements of X-Ray Diffraction*, Essex: Pearson Education Limited, 2014.
- [81] M. Lita, *METODE DE INVESTIGATIE IN STIINTA MATERIALELOR*, Timisoara: Editura Politehnica, 2009.
- [82] "www.csun.edu," California State University Northridge, [Online]. Available: http://www.csun.edu/~bavarian/Courses/MSE%20528/microindentation_hardness_testing.pdf. [Accessed 23 01 2017].
- [83] P. Roberts, *Industrial Brazing Practice*, Boca Raton: CRC Press Taylor & Francis Group, 2013.
- [84] "www.hoganas.com," Höganäs AB, [Online]. Available: <https://www.hoganas.com/en/products/>. [Accessed 10 December 2016].
- [85] O. Mars and E. Hryha, "Vacuum Levels Influence on the Properties of Various High Temperature Brazing Alloys," in *IBSC*, Long Beach, 2015.
- [86] Höganäs AB, "www.hoganas.com," Höganäs AB, [Online]. Available: <https://www.hoganas.com/en/products/>. [Accessed 10 December 2016].
- [87] A. S. Kurlov and A. I. Gusev, *Tungsten Carbides Structure, Properties and Application in Hardmetals*, Springer, 2013.

- [88] V. P. Astakhov, *Drills: Science and Technology of Advanced Operations*, CRC Press, Taylor & Francis Group, 2014.
- [89] R. Parkinson, "Properties and applications of electroless nickel," Nickel Development Institute, 1995.
- [90] W. Sade, R. T. Proenca, T. D. O. Moura and J. R. T. Branco, "Electroless Ni-P Coatings: Preparation and Evaluation of Fracture Toughness and Scratch Hardness," *ISRN Materials Science*, no. doi:10.5402/2011/693046, 2011.
- [91] C. Yanahai, C. Hengyang, Z. Zhencai, Z. Yong and P. Yuxing, "Tribological Behavior of Ni-P Deposits on Dry Condition," *Rare Metal Materials and Engineering*, vol. 43, no. 1, pp. 11-16, 2014.
- [92] A. Farzaneh, M. Ehteshamzadeh and M. Mohammadi, "Corrosion performance of electroless Ni-P coatings prepared in different conditions and optimized by the Taguchi method," *J. Appl. Electrochem.*, vol. 41, pp. 19-27, 2011.
- [93] R. Jenkins and R. L. Snyder, *Introduction to X-Ray Powder Diffractometry*, John Wiley & Sons, Inc., 1996.
- [94] N. Kazamer, D. T. Pascal, G. Marginean, V. A. Şerban, C. Codrean and I. D. Uţu, "A Comparison between Hardness, Corrosion and Wear Performance of APS Sprayed WC-CoMo and WC-Co Coatings," *Solid State Phenomena*, vol. 254, pp. 71-76, 2016.
- [95] M. J. Azizpour, H. Mohammadi, M. Jalai and H. Fasihi, "Adhesion Strength Evaluation Methods in Thermally Sprayed Coatings," *International Journal of Mechanical, Aerospace, Industrial, Mechatronic and Manufacturing Engineering*, vol. 6, no. 1, pp. 1129-1131, 2012.
- [96] J. Lasage and D. Chicot, "Models for Hardness and Adhesion of Coatings," *Surface Engineering*, vol. 15, no. 6, pp. 447-453, 1999.
- [97] J. Lasage, "Interface Indentation Test to Determine Adhesion of Coatings," *Revue de Metallurgie*, vol. 90, no. 12, pp. 1655-1663, 1993.
- [98] D. Chiot, P. Demarecaux and J. Lasage, "Apparent interface toughness of substrate and coating couples for indentation tests," *Thin Solid Films*, vol. 283, pp. 151-157, 1996.
- [99] S. P. Lu and O. Y. Kwon, "Microstructure and bonding strength of WC reinforced Ni-base alloy brazed composite coating," *Surface and Coatings Technology*, vol. 153, pp. 40-48, 2002.
- [100] S. P. Lu, Y. Guo and L. S. Chen, "Preparation and its wear resistance of WC-Co/NiCrBSi metallurgical bonded composite coatings," *Acta Metallurgica Sinica*, vol. 13, no. 3, pp. 857-861, 2000.
- [101] S. Lu, Y. Guo and L. Chen, "Microstructure and Properties of WC-Co/NiCrBSi Brazing coating," *J. Mater. Sci. Technol.*, vol. 15, no. 3, pp. 283-285, 1999.
- [102] O. Y. K. Y. G. S. P. Lu, "Wear behavior of brazed WC/NiCrBSi(Co) composite coatings," *Wear*, vol. 254, pp. 421-428, 2003.
- [103] ASM International, *Surface Engineering*, ASM International, 1994.
- [104] J. Bao, J. W. Newkirk and S. Bao, "Wear-resistant WC composite coatings by brazing," *Journal of Materials Engineering and Performance*, vol. 13, pp. 358-388, 2004.
- [105] ASTM International, *ASTM G40-15 Standard Terminology Related to Wear and Erosion*, ASTM International, 2015.

112 References

- [106] J. R. Davis, *Surface Engineering for Corrosion and Wear Resistance*, ASM International, 2001.
- [107] International Union of Pure and Applied Chemistry, *Compendium of Chemical Terminology*, Blackwell Scientific Publications, 2014.
- [108] Federal Carbide Company, "Corrosion resistance of Tungsten Carbide Grades," [Online]. Available: http://www.federalcarbide.com/corrosion_resistant_tungsten_carbide_grades.html. [Accessed 15 April 2017].
- [109] P. A. Schweitzer, *Fundamentals of Metallic Corrosion*, Boca Raton: CRC Press Taylor & Francis Group, 2007.

APPENDIX 1



Safety Data Sheet



1. COMPANY AND PRODUCT IDENTIFICATION

iLoveToCreate
A Duncan Enterprises Company
5673 East Shields Avenue
Fresno, CA 93727
559-291-4444
559-291-9444 (Fax)
www.ilovetocreate.com

EMERGENCY TELEPHONE NUMBERS

Health Emergencies:
559-291-4444 7:00 am – 3:30 pm Pacific Std. Time
Spill and Off-Hour Health Emergencies:
800-424-9300 U.S. and Canada
703-527-3887 Outside U.S. and Canada (Collect)

Product Name: Aleene's Tack-It Over and Over
Product Use/Description: Water-based adhesive
Not intended for: No data.

2. HAZARDS IDENTIFICATION

Classification:	This mixture does not meet the criteria for classification.
Health & Physical Hazard Statement:	No data.
Other Hazards not classified:	No data.
Signal Word:	None
Precautionary Statement:	None
Pictogram(s) by GHS:	None

3. COMPOSITION / INFORMATION ON INGREDIENTS

Detailed formulation is submitted by the client and it is proprietary information.

Products are made by physical manipulation and chemical reaction from the ingredients. These ingredient chemicals may not exist as its original formula in final products. None of these ingredients are hazardous substances.

Reportable ingredients (if applicable): This mixture does not meet the criteria for classification. Low hazards present under normal conditions.

4. FIRST AID MEASURES

General Advice:	No data.
On Inhalation:	Health injuries are not known or expected under normal use.
On Skin Contact:	Health injuries are not known or expected under normal use.
On Eye Contact:	Direct contact with eyes may cause temporary irritation.
On Ingestion:	Health injuries are not known or expected under normal use.
Acute/Delayed Symptoms:	Low hazards under normal conditions.
Medical Advice:	This is not hazardous according to OSHA 29 CFR 1910.1200.
Note to Physician:	No data.

5. FIRE FIGHTING MEASURES

Extinguishing Media	
Suitable extinguishing media:	No unusual fire or explosion hazard noted. Use fire-extinguishing media appropriate for surrounding materials.
Unsuitable extinguishing media:	No data.
Protection of Firefighters	
Specific hazards arising from the chemical:	Carbon oxides.
Protective equipment for firefighters:	See section 8 of this SDS for Personal Protective Equipment.
Special precautions/ protective equipment for firefighters:	No special precautions.
Will hazardous combustion occur?:	Will not occur.

6. ACCIDENTAL RELEASE MEASURES

Emergency Containment procedures:	No data.
Environmental Precautions, if any?:	Avoid discharge into drains, water courses or onto the ground.
Methods for Cleaning Up:	Absorb spillage with suitable absorbent material. Clean up in accordance with all applicable regulations.
Personal Protective Equipment:	See section 8 of this SDS for Personal Protective Equipment.

7. HANDLING AND STORAGE

Safe Storage:	Store in closed original container in a dry place. Store away from incompatible materials. Storage temperature: between 40°F and 100°F. Protect from freezing.
Safe Handling:	No specific usage precautions noted.
Known Incompatibilities:	No data.

8. EXPOSURE CONTROL AND PERSONAL PROTECTION

Occupational Exposure Limits: No specific usage precautions noted.

Appropriate Engineering Controls: No special requirements under ordinary conditions of use and with adequate ventilation.

Individual Protection measures, such as PPE (Personal Protective Equipment):

Personal Protection Equipment:	
Respiratory Protection:	Under normal conditions, respirator is not normally required.
Eye Protection:	Wear safety glasses. If splash potential exists, wear full face shield or chemical goggles.
Hand Protection:	No special precautions.
Skin Protection:	No special precautions.
Thermal Protection:	No data.
General Safety and Hygiene Measures:	No specific hygiene procedures noted, but good personal hygiene practices are always advisable, especially when working with chemicals.
Further Information:	No data.

9. PHYSICAL AND CHEMICAL PROPERTIES

Physical State/Appearance:	Liquid
Color:	White
Odor:	Slightly sweet.
Odor Threshold:	N/A
pH:	4
Boiling Point/Range:	> 212°F (>100°C)
Melting Point/Range:	32°F (0°C)
Flash Point:	> 212°F (>100°C)
Evaporation Rate:	1 Water=1
Vapor Density:	0.62 (Air=1)
Solubility(ies):	Miscible in water.
Vapor Pressure:	17.5 mm Hg at 20°C
Relative Density:	No data.
Viscosity:	No data.
Partition Coefficient (n-octanol/water), if applicable:	N/A
Explosive Properties:	No data.
Flammability: (Solid, gas)	N/A
Flammability Limit in Air:	N/A
Upper/Lower	
Autoignition temperature:	N/A
Decomposition temperature:	N/A

10. STABILITY AND REACTIVITY

Chemical Stability:	Stable under normal temperature conditions.
Conditions to Avoid:	Heat and direct sunlight.
Incompatible Materials:	Strong oxidizing agents. Alkalies.
Hazardous Decomposition Products:	Carbon oxides.
Possibility of Hazardous Reactions/Polymerization:	Will not occur.

11. TOXICOLOGICAL INFORMATION

Information on likely routes of exposure:

Eye Contact – Serious Eye Damage or Irritation	
Skin Contact – Skin Corrosion, Sensitization or Irritation:	Not a skin sensitizer.
Ingestion – Carcinogenicity/Aspiration Hazard:	This product is not considered to be a carcinogen by IARC, ACGIH, NTP or OSHA.
Inhalation – Respiratory Sensitization/Toxicity:	Not a skin sensitizer.
Symptoms of exposure:	No data.
Information on toxicological effects:	No data.
Delayed or Immediate effects:	No data.
Germ Cell Mutagenicity:	No data.
Specific target organ toxicity (single exposure):	No data.
Specific target organ toxicity (repeated exposure):	No data.
Chemicals listed on NTP, IARC or OSHA as a Carcinogen?:	This product is not considered to be a carcinogen by IARC, ACGIH, NTP or OSHA.

Chemical Name: None	Oral LD50 -	Dermal LD50 -	Inhalation LC50 -	Percentage -
-------------------------------	-----------------------	-------------------------	-----------------------------	------------------------

*Estimates for product may be based on additional component data not shown.

12. ECOLOGICAL INFORMATION (NON-MANDATORY)

Ecotoxicity:	Not expected to be harmful to aquatic organisms.
Persistence and degradability:	No data.
Bioaccumulative potential:	No data.
Mobility in soil:	The product is insoluble in water and will sediment in water systems.
Other adverse effects:	No data.

13. DISPOSAL CONSIDERATIONS (NON-MANDATORY)

Local Disposal instructions/Contaminated packaging disposal instructions:	Disposal recommendations are based on material as supplied. Disposal must be in accordance with current applicable laws and regulations, and material characteristics at time of disposal. Do not discharge into drains, water courses or onto the ground.
--	--

14. TRANSPORTATION INFORMATION (NON-MANDATORY)

	DOT	IMDG	IATA
UN/ID number:	Not regulated	Not regulated	Not regulated.
Proper shipping name:	-	-	-
Transport hazard class:	-	-	-
Packing group (if applicable):	-	-	-
Environmental Provisions:	-	-	-
Special Precautions in transport:	No data.		
Transport in bulk according to Annex II of MARPOL 73/78 and IBC Code	No data.		
Emergency Response Guide Number:	No data.	EmS-No:	No data.

Pictograms		
US: None	IATA: IMDG: None	Marine Pollutant: None

15. REGULATORY INFORMATION (NON-MANDATORY)

US Federal Regulations:	
TSCA Section 12(b) Export Notification (40 CFR 707, Subpt. D):	This product is manufactured in compliance with all provisions of the Toxic Substance Control Act, 15 U.S. C.2601 et. Seq.
CERCLA (Superfund) reportable quantity (lbs.) (40 CFR 302.4)	No data.
OSHA Specifically Regulated Substances (29 CFR 1910.1001-1050):	No data.
Section 302 Extremely Hazardous Substance (40 CFR 355, Appendix A):	No data.

Chemical Name:	CAS Number:	Reportable Quantity:	Threshold planning quantity:	Threshold planning quantity, lower value:	Threshold planning quantity, upper value:
None	X	X	X	X	X
Superfund Amendments and Reauthorization Act of 1986 (SARA)					
SARA/Title III:	This product does not contain any substances at or above the reported threshold under Section 313, based on available data.				
SARA 304 Emergency release notification:	No regulated.				
SARA 311/312 (40 CFR 370) Hazardous Chemical:	Not regulated.				
SARA 313 (TRI reporting):	<u>Chemical Name:</u> None	<u>CAS Number:</u> -	<u>% by wt.</u> -		
Drug Enforcement Administration (DEA) (21 CFR 1308.11-15):	Not controlled.				
Clean Air Act (CAA) Section 112 Hazardous Air Pollutants (Haps) List:	No data.				
Clean Air Act (CAA) Section 112(r) Accidental Release Prevention (40 CFR 68.130):	No data.				
Safe Drinking Water Act (SDWA):	No data.				
Canadian Domestic Substances List (DSL):	No data.				
FDA:	No data.				
Conforms to Non-Toxic ASTM-4236:	Products are certified in a program of toxicological evaluation by a nationally recognized toxicologist to contain no materials in sufficient quantities to be toxic or injurious to humans or to cause acute or chronic health problems. These products are certified to be labeled in accordance with the voluntary chronic hazard labeling standard ASTM D-4236. In addition, there is no physical hazard as defined within 29 CFR Part 1910.1200(c).				
California Proposition 65 Warning:	This product contains the following chemicals that are known to the State of California to cause cancer, birth defects, or other reproductive harm: None				
EPA Clean Air / Water Act:	No data.				
EPA Hazardous Wastes:	No data.				
HMIS III Rating:	Health: 1; Flammability: 1; Physical Hazard: 0				
Unless a concentration is specified in Section 2 of the SDS, the above chemicals(s) are present in trace amounts.					
*A "Yes" indicates that all components of this product comply with the inventory requirements administered by the governing country(s).					

16. OTHER INFORMATION

These recommendations and information contained in this MSDS have been compiled from sources believed to represent the most current information available when the MSDS was prepared. However, the manufacturer / distributor of this product does not provide any warranty, guaranty of representation as to the correctness or sufficient of this information. If this material is used in large amounts and/or an unusual manner, the user is obliged to determine what safety measures are appropriate, including the applicable and relevant workplace and environmental regulations pertaining to handling, use and disposal.

Table of Abbreviations			
ACGIH:	American Conference of Governmental Industrial Hygienists	LD:	Lethal Dose
ANSI:	American National Standards Institute	MARPOL:	Marine Pollution
ASTM:	American Society for Testing Materials	mg / kg:	Milligram per Kilogram
°C:	Degrees Centigrade	mm:	Millimeter
CAA:	Clean Air Act	MSHA:	Mine Safety and Health Administration
CAS:	Chemical Abstract Service	N/A:	Not Applicable
CERCLA:	Comprehensive Environmental Response, Compensation & Liability Act	NFPA:	National Fire Protections Association
CFR:	Code of Federal Regulations	NIOSH:	National Institute for Occupational Safety and Health
CPR:	Controlled Products Regulations	NTP:	National Toxicology Program
DEA:	Drug Enforcement Act	OEL:	Over Exposure Limit
DOT:	Department of Transportation	OSHA:	Occupational Safety and Health Administration
DSL:	Canadian Domestic Substances List	PEL:	Permissible Exposure Limits
EMS:	Emergency Medical Goods Services	ppm	Parts Per Million
EPA:	Environmental Protection Agency	SARA	Superfund Amendment and Reauthorization Act
F:	Degrees Fahrenheit	STEL	Short-Term Exposure Limit
FDA:	Food & Drug Administration	SDS:	Safety Data Sheet
g/l:	Grams per Liter	SDWA:	Safe Drinking Water Act
HAPs:	Hazardous Air Pollutants	TLV:	Threshold Limit Value
Hg:	Mercury	TRI:	Toxics Release Inventory
HMIS:	Hazardous Materials Identification System	TSCA	Toxic Substances Control Act
HNOC:	Hazard(s) Not otherwise classified	TWA	Time - Weighted Average
IARC:	International Agency for Research on Cancer	U.N.	United Nations
IATA:	International Air Transport Association	WHMIS	Workplace Hazardous Materials Information System
ID:	Identification / Identity	>	Greater Than
IDLH:	Immediate Danger to Life or Health	<	Less Than
IMDG:	International Maritime Dangerous Goods	73/78:	1973 & 1978
LC:	Lethal Concentration		

Creation Date:	Version: 2	Revision date:
8/8/2011-FP	1	
	2	5/10/2016-JL

END SAFETY DATA SHEET

APPENDIX 2

		Date	10.01.2017
Material data sheet			
Material Number	1.7131		
Country	Germany		
Designations	16MnCr5		
Standards	DIN EN 10084 (06/2008)	Case hardening steels.	
	DIN EN 10132-2 (05/2000)	Cold rolled narrow steel strip for heat-treatment. Case hardening steels.	
	DIN EN 10263-3 (02/2002)	Steel rod, bars and wire for cold heading and cold extrusion. Technical delivery conditions for case hardening steels.	
	DIN EN 10297-1 (06/2003)	Seamless circular steel tubes for mechanical and general engineering purposes. Non-alloy and alloy steel tubes. Steels for case hardening (appendix)	
Steelgroup	Alloy special structural steels: Structural steels, Cr-Si-, Cr-Mn-, Cr-Mn-B- and Cr-Si-Mn-steels		
Range of application	<p>Case hardening steels: Small cog wheels, arbors, cardan joints, parts of control</p> <p>Steels for cold extrusion: High-grade mass produced structural parts in general engineering, construction of apparatus, motor and vehicle construction, in a sequence of working processes (upset forging, cold extrusion, pressing, bulging, drawing with intermediate surface and annealing treatment) parts of different shapes can be manufactured, possessing high density, a favorable fibering for stress, a very good surface condition and a high dimensional accuracy. Because when cold extruded, as a result of the strengthening by cold working, hardness, breaking strength and yield point increase, and through this, the working properties of the finished parts can be improved. Also, according to circumstances, it is possible, to accomplish very high requirements with unalloyed steels, that by conventional production of the parts through machining and heat treatment only could be reached with alloyed steel grades. In connection with the high internal stress of the cold work hardened surface zone, the smooth surface leads to an increased fatigue and vibratory strength. In addition to that, this surface is endowed with very favorable sliding properties and good resistance wear band, due to its firmly adhering phosphate coating. Through the possibility to adapt the fibering to the shape of the structural component, a deteriorating notch effect can be avoided. Through the deformation under the effect of pressure in steel tools, the enormity of the deformation as well as the quality of steel is limited through the maximum admissible surface pressing between the work piece and the tool. The choice of material mainly depends on the shape of the structural components, the necessary cold deformation and mechanical quality values of the finished part. Depending on the steel quality, cold deformed work pieces can also be heat treated, hardened and tempered or case hardened.</p>		
© 2010 Verlag Stahlschlüssel Wegst GmbH, Germany (www.stahlschluessel.de)		Page 1 of 57	

Material data sheet			Date
Material Number	1.7131		10.01.2017
Country	Germany		
Designations	16MnCr5		
Chemical composition			
Element	min/max	Others	Footnote
C	0,14 - 0,19		
Si	<=0,40		
Mn	1,00 - 1,30		
P	<=0,025		
S	<=0,035		
Cr	0,80 - 1,10		
-			657)
657) DIN EN 10263-2+3 Si <= 0,30%; P <= 0,025%; S <= 0,025%; Cu <= 0,25%			
© 2010 Verlag Stahlschlüssel Wegst GmbH, Germany (www.stahlschluessel.de)			Page 2 of 57

						Date	10.01.2017
Material data sheet							
Material Number	1.7131						
Country	Germany						
Designations	16MnCr5						
Mechanical properties							
dimension	value	specimen	at temperature	cooling	duration		
DIN EN 10084 (06/2008)							
Case hardening steels.							
treated to hardness range							
Hardness [HBW]	156 - 207 HBW						
treated to ferrite-pearlite microstructure and hardness range							
Hardness [HBW]	140 - 187 HBW						
normalised							
Hardness [HBW]	138 - 187 HBW						
soft annealed							
Hardness [HBW]	<=207 HBW						
quenched							
Jominy test piece (+H)							
- 1,5 mm	39 - 47 HRC						
- 3 mm	36 - 46 HRC						
- 5 mm	31 - 44 HRC						
- 7 mm	28 - 41 HRC						
- 9 mm	24 - 39 HRC						
- 11 mm	21 - 37 HRC						
- 13 mm	<=35 HRC						
- 15 mm	<=33 HRC						
- 20 mm	<=31 HRC						
- 25 mm	<=30 HRC						
- 30 mm	<=29 HRC						
- 35 mm	<=28 HRC						
- 40 mm	<=27 HRC						
Jominy test piece (+HH)							
- 1,5 mm	42 - 47 HRC						
- 3 mm	39 - 46 HRC						
- 5 mm	35 - 44 HRC						
- 7 mm	32 - 41 HRC						
- 9 mm	29 - 39 HRC						
- 11 mm	26 - 37 HRC						
- 13 mm	24 - 35 HRC						
- 15 mm	22 - 33 HRC						
- 20 mm	20 - 31 HRC						
- 25 mm	<=30 HRC						
- 30 mm	<=29 HRC						
- 35 mm	<=28 HRC						
- 40 mm	<=27 HRC						
© 2010 Verlag Stahlschlüssel Wegst GmbH, Germany (www.stahlschluessel.de)							
Page 3 of 57							

Material data sheet		Date	10.01.2017
Material Number	1.7131		
Country	Germany		
Designations	16MnCr5		
quenched			
Jominy test piece (+HL)			
- 1,5 mm	39 - 44 HRC		
- 3 mm	36 - 43 HRC		
- 5 mm	31 - 40 HRC		
- 7 mm	28 - 37 HRC		
- 9 mm	24 - 34 HRC		
- 11 mm	21 - 32 HRC		
- 13 mm	<=30 HRC		
- 15 mm	<=28 HRC		
- 20 mm	<=26 HRC		
- 25 mm	<=25 HRC		
- 30 mm	<=24 HRC		
- 35 mm	<=23 HRC		
- 40 mm	<=22 HRC		
quenched and tempered bei ~ 200 °C			
Tensile strength			
<=16 mm	>=1000 MPa		3)
16 - 40 mm	>=900 MPa		3)
40 - 100 mm	>=700 MPa		3)
treated to capacity for shearing			
Hardness [HBW]			
			4)
3) Informative			
4) Under suitable circumstances shearable in untreated condition			
© 2010 Verlag Stahlschlüssel Wegst GmbH, Germany (www.stahlschluessel.de)		Page 4 of 57	

LIST OF PUBLICATIONS AND CONFERENCES

- R. Muntean, *D.T. Pascal*, G. Mărginean, N. Vaszilcsin – „**Carbon nanofibers decorated with Pt-Co nanoparticles as catalysts for electrochemical cell applications. I. Synthesis and structural characterization**” – International Journal of Electrochemical Science, 12 (2017) 4597-4609, doi:10.20964/2017.05.25.
- *D.T. Pascal*, R. Muntean, N. Kazamer, G. Mărginean, W. Brandl, V. A. Şerban, - „**Characteristics of High Temperature Vacuum Brazed WC-Co-NiCrBSi Functional Composite Coatings**”, NANOCON 2016, 19-21 October, Brno, Czech Republic, Conference Proceedings, pp. 775-781, ISBN 978-80-87294-71-0
- N. Kazamer, *D.T. Pascal*, G. Mărginean, V. A. Şerban, W. Brandl, P.C. Vălean, - „**Aspects concerning the wear and corrosion behavior of WC-CoCr coatings and respectively DLC/WC-CoCr systems**”, NANOCON 2016, 19-21 October, Brno, Czech Republic, Conference Proceedings, pp. 383-389, ISBN 978-80-87294-71-0
- R. Muntean, U. Rost, *D.T. Pascal*, G. Mărginean, N. Vaszilcsin, - „**Determination of the electrochemical surface area for CNF/Pt electrocatalyst using cyclic voltammetry**”, Chemical Bulletin of Politehnica University of Timișoara, Romania, Vol. 61 (75), 2, 2016
- *D. T. Pascal*, V. A. Şerban, G. Marginean, - „**Optimization of Process Parameters for the Manufacturing of High Temperature Vacuum Brazed WC-NiCrBSi Coatings**”, Solid State Phenomena, Vol. 254, pp. 164-169, 2016 (10.4028/www.scientific.net/SSP.254.164)
- N. Kazamer, *D. T. Pascal*, G. Marginean, V. A. Şerban, C. Codrean, I. D. Uțu, - „**A Comparison between Hardness, Corrosion and Wear Performance of APS Sprayed WC-CoMo and WC-Co Coatings**”, Solid State Phenomena, Vol. 254, pp. 71-76, 2016 (10.4028/www.scientific.net/SSP.254.71)
- N. Kazamer, *D. T. Pascal*, D Uțu, - „**Short review regarding the HVOF thermal spraying technology, material usage and future developments**”, Scientific Bulletin of the Politehnica University of Timișoara (Transactions on Mechanics), Timișoara, Romania, Vol. 58(72), 1, ISSN 1224 – 6077, 2015
- *D.T. Pascal*, R. Muntean, N. Kazamer, G. Mărginean, W. Brandl, V. A. Şerban, Characteristics of High Temperature Vacuum Brazed WC-Co-NiCrBSi Functional Composite Coatings, NANOCON 2016, 19 – 21 October, Brno, Czech Republic, 2016.
- *D.T. Pascal*, W. Brandl, G. Marginean Corrosion Behavior of High Temperature Vacuum Brazed Composite Coatings, KoopKaffee Workshop, 6 Mai, Gelsenkirchen, Germany, 2016.
- *D.T. Pascal*, V. A. Şerban, G. Mărginean, Optimization of Process Parameters for the Manufacturing of High Temperature Vacuum Brazed WC-NiCrBSi Coatings, AMS 2015, 16 – 17 October, Timisoara, Romania, 2015.
- *D.T. Pascal*, W. Brandl, G. Marginean Sliding Wear Behavior of High Temperature Vacuum Brazed Composite Coatings, KoopKaffee Workshop, 27 April, Gelsenkirchen, Germany, 2015.

- *D.T. Pascal, V. A. Șerban, W. Brandl, G. Mărginean, Optimization of Process Parameters for Hardfacing Brazing in Vacuum, BraMat 2015, 5 – 7 March, Brasov, Romania, 2015.*
- *D.T. Pascal, W. Brandl, G. Marginean, Optimization of vacuum furnace hardfacing brazing process parameters, Junior Euromat 2014, The Federation of European Materials Societies, 21-25 July, Lausanne, Switzerland, 2014.*
- *D.T. Pascal, W. Brandl, G. Marginean Optimization of Vacuum Furnace Hardfacing Brazing Process Parameters, KoopKaffee Workshop, 24 April, Gelsenkirchen, Germany, 2014.*

CURRICULUM VITAE

PERSONAL INFORMATION:

Name: Dragos Toader Pascal
Nationality: Romanian
Date of Birth: 10 April 1988
Email: dragos.pascal@student.upt.ro
dragos.pascal@w-hs.de

EDUCATION:

October 2013 – present: PhD Student

- Materials Engineering - Faculty of Mechanical Engineering - Politehnica University of Timisoara, Romania;
- Department of Materials Science and Testing - Westphalian University of Applied Sciences, Gelsenkirchen, Germany;
- Research activities in the field of materials science and engineering;
- Main topic: *Development of High Temperature Vacuum Brazed WC-Co-NiP Functional Composite Coatings*

10.2011 – 07.2013: Master Degree (M. Sc.)

- Department of Materials and Manufacturing Engineering - Faculty of Mechanical Engineering - Politehnica University of Timisoara, Romania;
- Final thesis: *Properties of DLC/ WC-CoCr Multilayer Coatings*

10.2007 – 09.2011: Bachelor Degree (B. Sc.)

- Department of Materials and Manufacturing Engineering - Faculty of Mechanical Engineering - Politehnica University of Timisoara, Romania;
- Final thesis: *Corrosion behavior of thermally sprayed coatings used in the food processing industry*

Languages: English, German.